Chapter 3

RESULTS

3.1 Syntheses of ligands

In this work, there are two ligands to be synthesized, 2-(phenylazo)pyridine (azpy) and 2,6-(diphenylazo)pyridine (diazpy).

The azpy and diazpy ligands were synthesized by coupling reactions of 2-aminopyridine and 2,6-diaminopyridine with nitrosobenzene, respectively. Purification was done by column chromatography as described previously. The reactions are shown in equation (1) and (2).

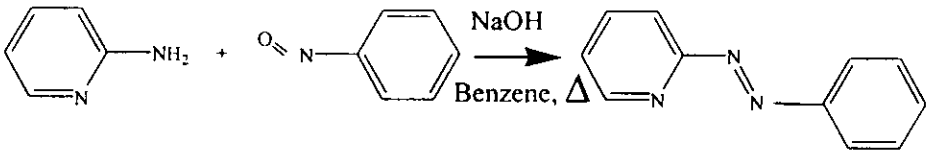

(1)

2-aminopyridine nitrosobenzene 2-(phenylazo)pyridine (azpy)

35% yield

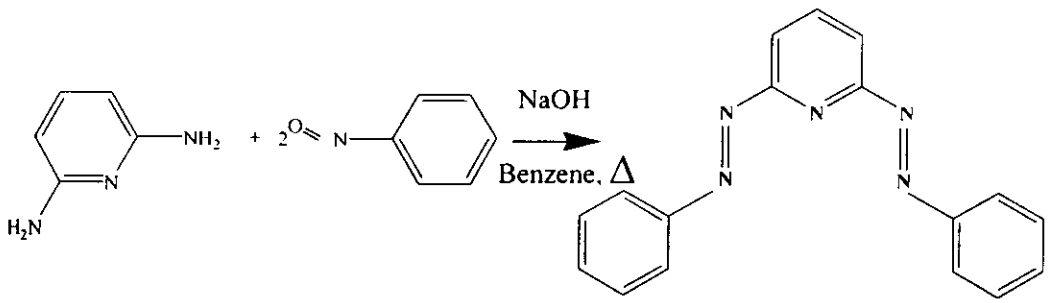

(2)

2,6-diaminopyridine nitrosobenzene 2,6-(diphenylazo)pyridin (diazpy)

45% yield

The yields of the azpy and diazpy ligands were 30-50%. The physical properties of ligands are shown in Table1.

Table 1 The physical properties of ligands

Ligands	Physical properties		
	Appearance	Color	Melting point (^{O} C)
azpy	Liquid	Orange	32-34[a]
diazpy	Solid	Red-orange	104-105

[a]Results from Krause and Krause (1980)

The solubility of 0.0015 g of both ligands were tested in 10 mL of various solvents (water, methanol, ethanol, acetonitrile, acetone, ethyl acetate, dichloromethane and hexane). Those ligands were very soluble in most solvents, but diazpy insoluble in water.

3.2 Characterization of ligands

The chemistries of ligands were determined by using these techniques:

3.2.1 Elemental analysis

3.2.2 Fast-atom bombardment (FAB) mass spectrometry

3.2.3 UV-Visible absorption spectroscopy

3.2.4 Infrared spectroscopy

3.2.5 Nuclear Magnetic Resonance spectroscopy (1D and 2D)

3.2.6 Cyclic Voltammetry

3.2.7 X-ray Diffractometer

3.2.1 Elemental analysis

Elemental analysis is a principle method to study composition of elements in compound. Therefore, the elements in the diazpy ligand were confirmed by this method.

Table 2 Elemental analysis data of the diazpy ligand

Ligand	%C		%N		%H	
	Calc.	Found	Calc.	Found	Calc.	Found
diazpy	71.07	71.61	24.37	23.93	4.56	4.59

3.2.2 Fast-atom bombardment (FAB) mass spectrometry

The FAB mass spectrum of the diazpy ligand is shown in Figure 3. From the data, the maximum peak, which gave 100% relative abundance at m/z 288 corresponded to the molecular weight of diazpy with one protonation. The expected structure will be confirmed by this method. The results of this technique are shown in Table 3.

Table 3 FAB mass spectroscopic data of the diazpy ligand

m/z	Stoichiometry	Equivalent species	Rel. Abun. (%)
288	$[diazpy+H]^+$	$[L+H]^+$	100
310	$[diazpy+Na]^+$	$[L+Na]^+$	30

MW. of diazpy (L) = 287.32 g/mol

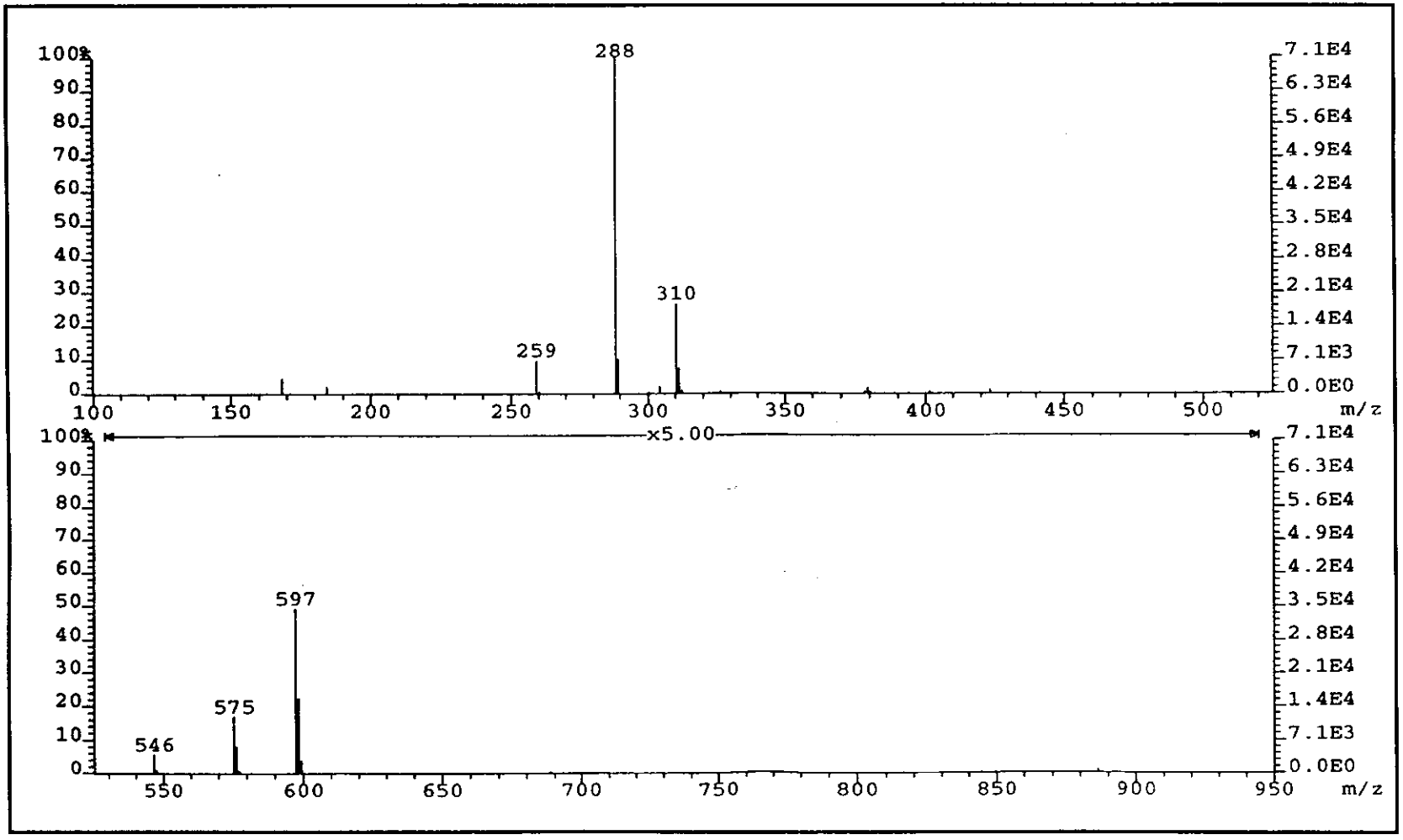

Figure 3 FAB mass spectrum of diazpy.

3.2.3 UV-Visible absorption spectroscopy

UV-Visible absorption spectroscopy is the method to study the electronic transitions of the ligands. The UV-Visible absorption spectra data of diazpy, azpy, bpy and phen exhibited in the range 200-800 nm in CH_3CN, EtOH, MeOH, DMSO and CH_2Cl_2 solvents. In addition, the absorption spectra of all ligands in CH_3CN solution are shown in Figure 4 to 7. The spectroscopic data are summarized in Table 4.

Table 4 UV-visible absorption spectroscopic data of diazpy, azpy, bpy and phen ligands

Ligands	λ_{max} nm, ($\varepsilon^a \times 10^{-4}$ M^{-1} cm^{-1})				
	CH_2Cl_2	CH_3CN	DMSO	EtOH	MeOH
diazpy	321 (3.12) 445 (0.13)	321 (2.82) 440 (0.14)	290 (3.20) 326 (2.56) 440 (0.11)	279 (3.80) 443 (0.12)	295 (2.90) 441 (0.12)
azpy	317 (1.7) 446 (0.05)	314 (1.5) 442 (0.06)	319 (1.7) 449 (0.05)	315 (1.7) 445 (0.04)	318 (1.9) 441 (0.04)
bpy	237 (1.3) 280 (1.9)	236 (1.2) 280 (1.5)	n	236 (1.2) 280 (1.9)	235 (2.1) 280 (3.0)
Phen	264 (3.1)	229 (8.1) 263 (6.7)	n	229 (4.6) 264 (3.8)	228 (4.9) 263 (6.7)

[a]Molar extinction coefficient, n = cannot be observed

The absorption spectra of the diazpy and azpy ligands displayed intense bands in the region 200-400 nm. The absorption occurring in UV region ($\varepsilon \sim$ 25000–6000

$M^{-1}cm^{-1}$) were assigned to $\pi \rightarrow \pi^*$ transitions. While, both ligands showed weak absorption bands ($\varepsilon \sim$ 400–1400 $M^{-1}cm^{-1}$) in visible region which assigned to $n \rightarrow \pi^*$ transitions. However, the absorption spectra of the bpy and phen showed only two $\pi \rightarrow \pi^*$ transitions in UV region.

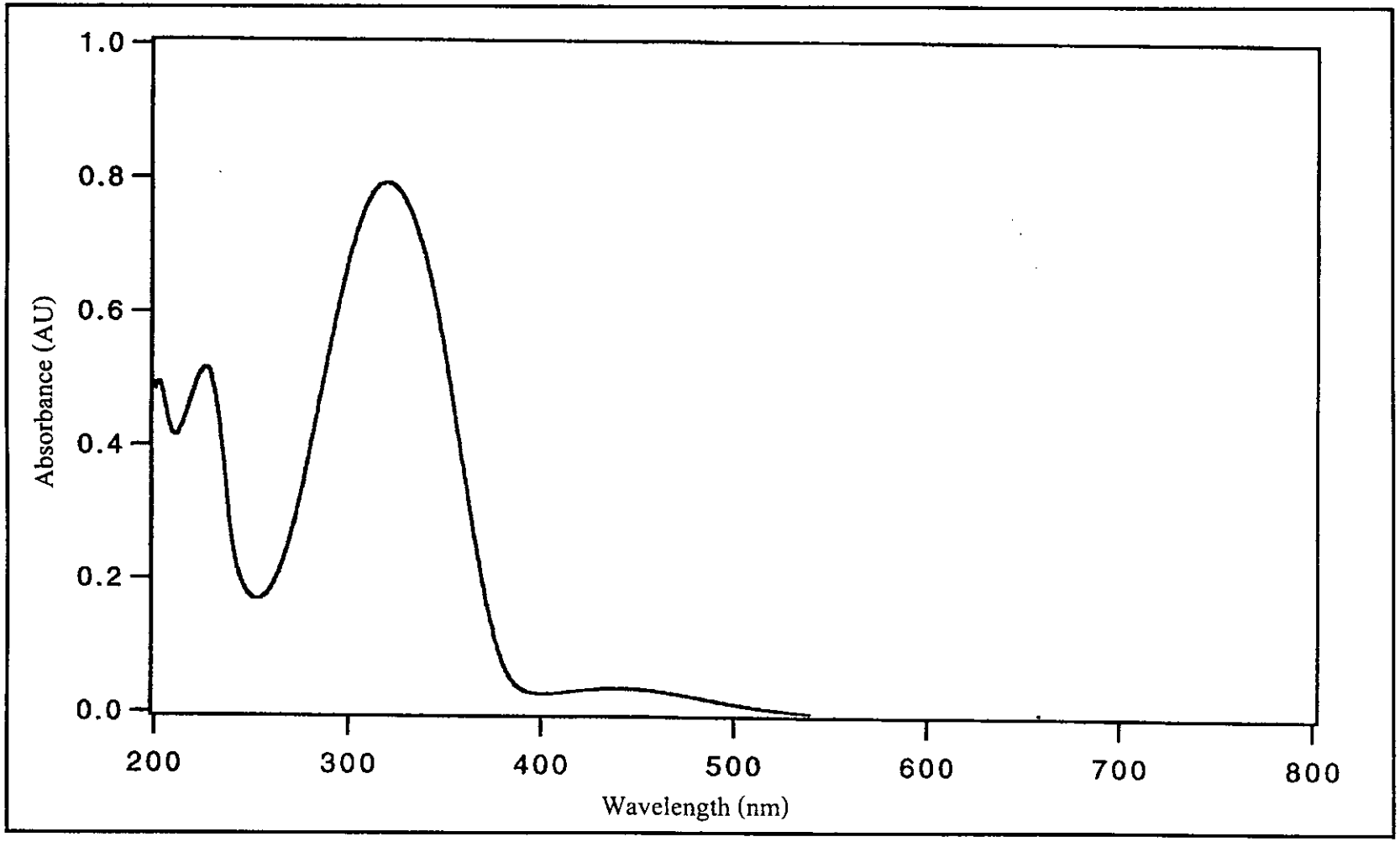

Figure 4 UV-Visible absorption spectrum of diazpy in CH_3CN.

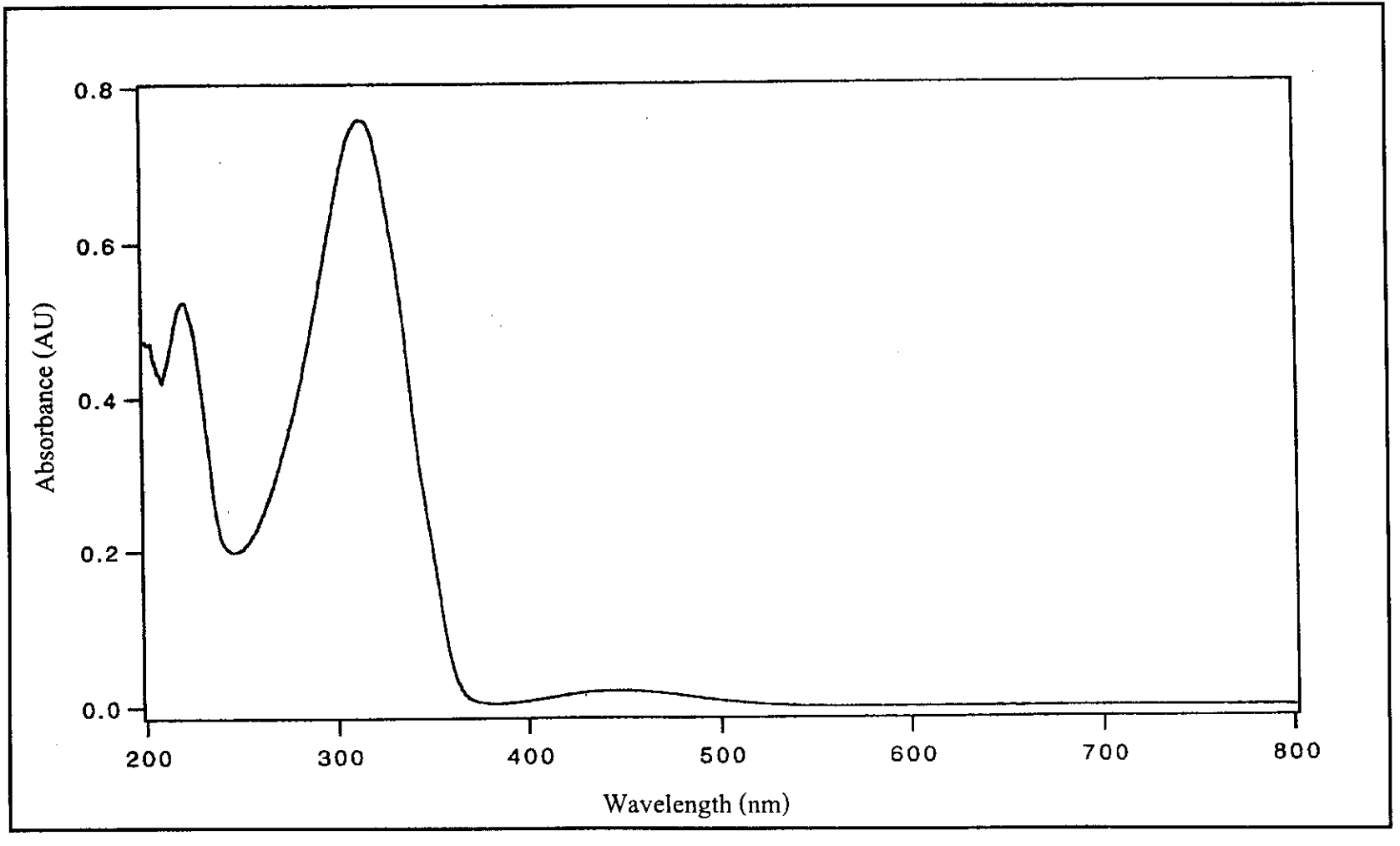

Figure 5 UV-Visible absorption spectrum of azpy in CH_3CN.

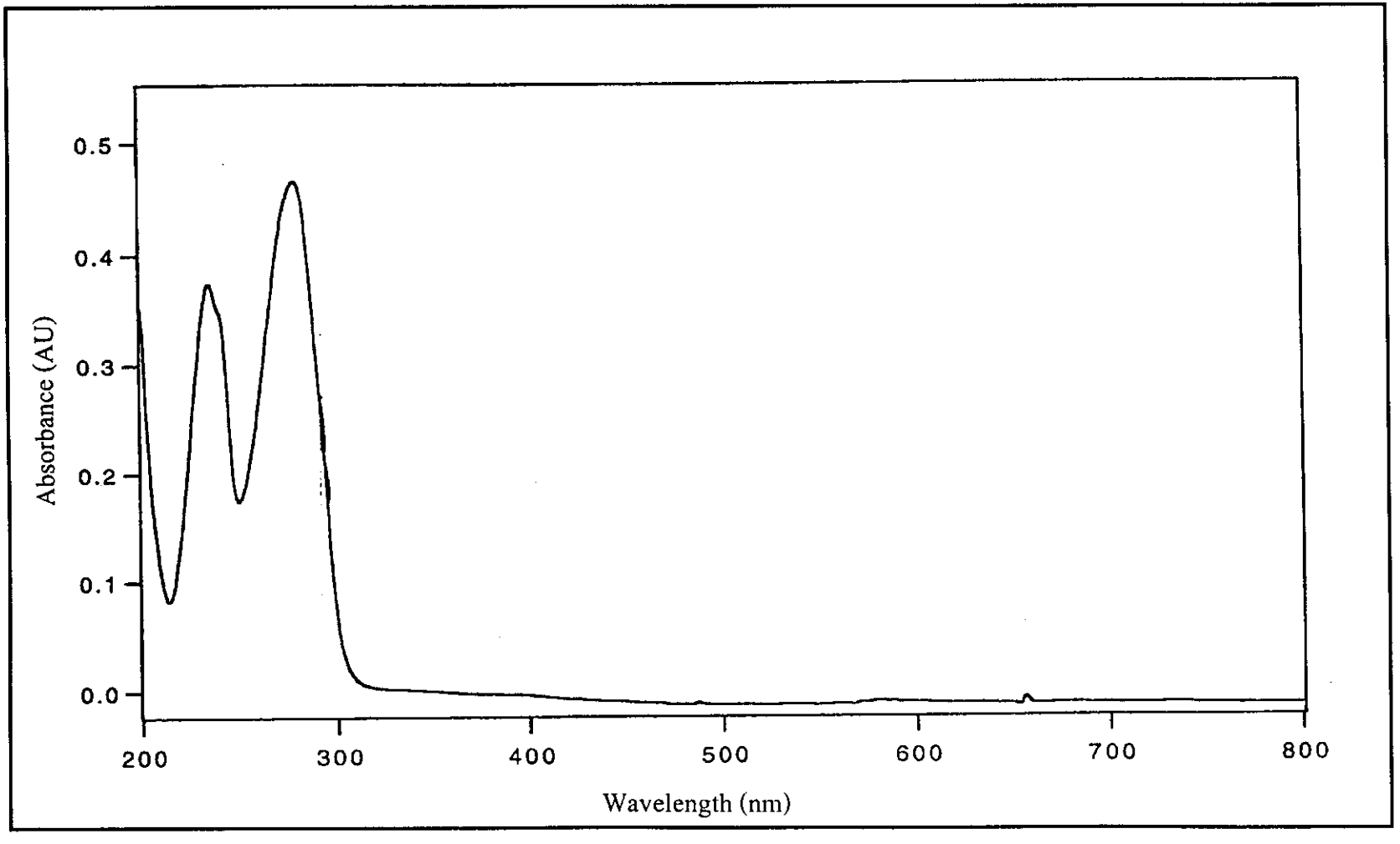

Figure 6 UV-Visible absorption spectrum of bpy in CH_3CN.

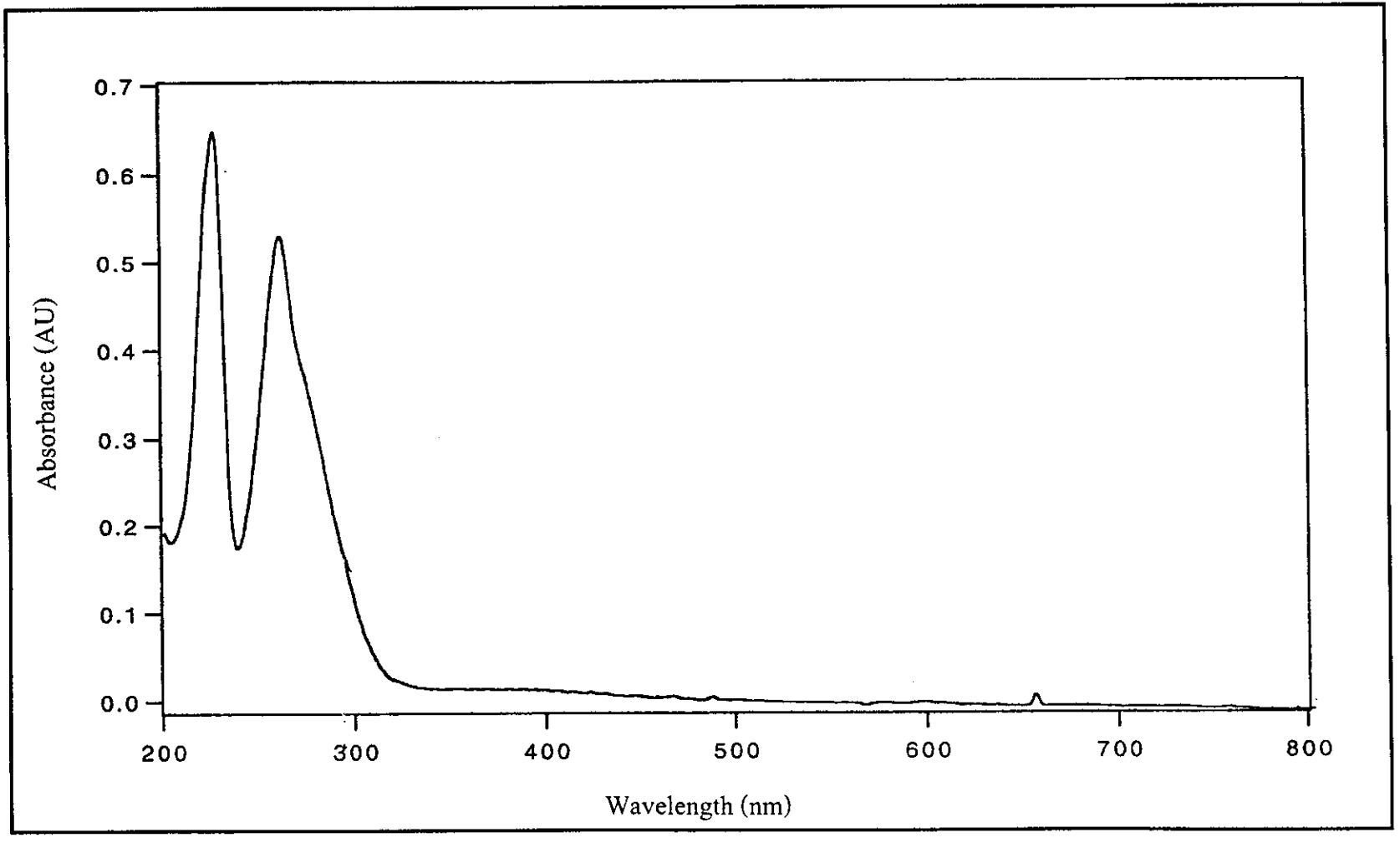

Figure 7 UV-Visible absorption spectrum of phen in CH_3CN.

3.2.4 Infrared spectroscopy

The functional groups of ligands were studied by infrared spectroscopy technique. Infrared spectra of diazpy and azpy ligands were recorded in the range 4000-370 cm^{-1} and their infrared spectra are shown in Figure 8 and Figure 9. The interesting intense vibration frequencies of ligands were C=C, C=N, N=N (azo) stretching vibration and C-H bending of monosubstituted benzene. The infrared spectroscopic data of diazpy compared with results of azpy are listed in Table 5.

Table 5 Infrared spectroscopic data of diazpy and azpy ligands

Vibration modes	Frequencies (cm^{-1})	
	diazpy	azpy
C=N, C=C stretching	1568 (s) 1487 (m) 1475 (m)	1580 (s) 1491 (m) 1476 (m) 1464 (m)
N=N stretching	1420 (s) 1447 (m)	1421 (s)
C-H bending of monosubstituted benzene	823 (s) 764 (s) 683 (s)	790 (s) 738 (s) 688 (s)

s = strong, m = medium

Infrared spectra of diazpy and azpy ligands showed many vibrations of different intensities below 1,600 cm^{-1}. They were C=C, C=N stretching of pyridine and phenyl rings and C-H bending of monosubstituted benzene. The most important peak was N=N stretching which used to consider the π-acid property in azo complexes. The N=N stretching of azpy showed the intense peak at 1421 cm^{-1}. Whereas, the N=N stretching of diazpy showed two intense peaks, at 1420 cm^{-1} and 1447 cm^{-1}. This corresponded to the vibration energies of both N=N (azo) in diazpy molecule. The vibration energies of both N=N (azo) were different frequencies. This may be due to nonplanarity in diazpy molecule.

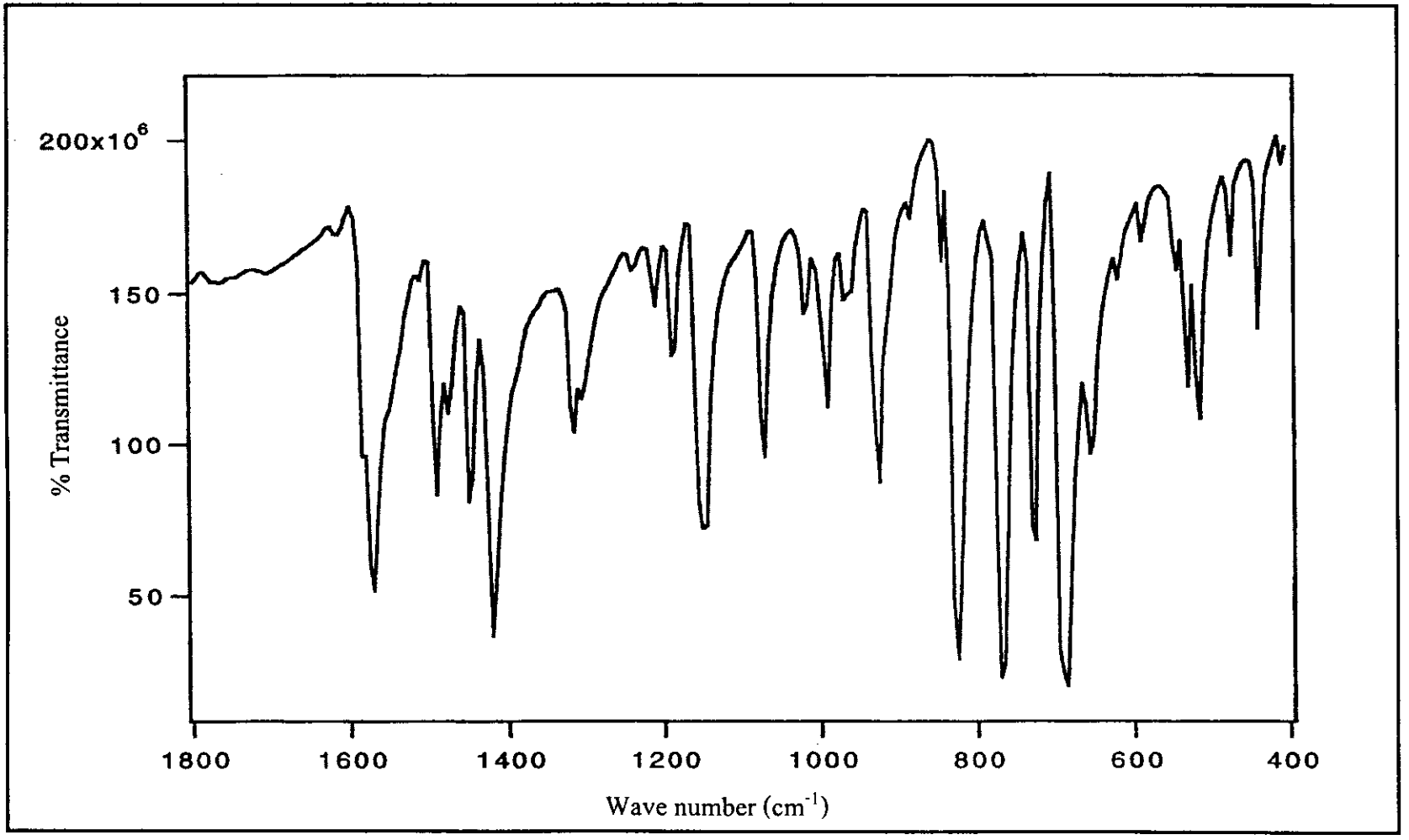

Figure 8 IR spectrum of diazpy.

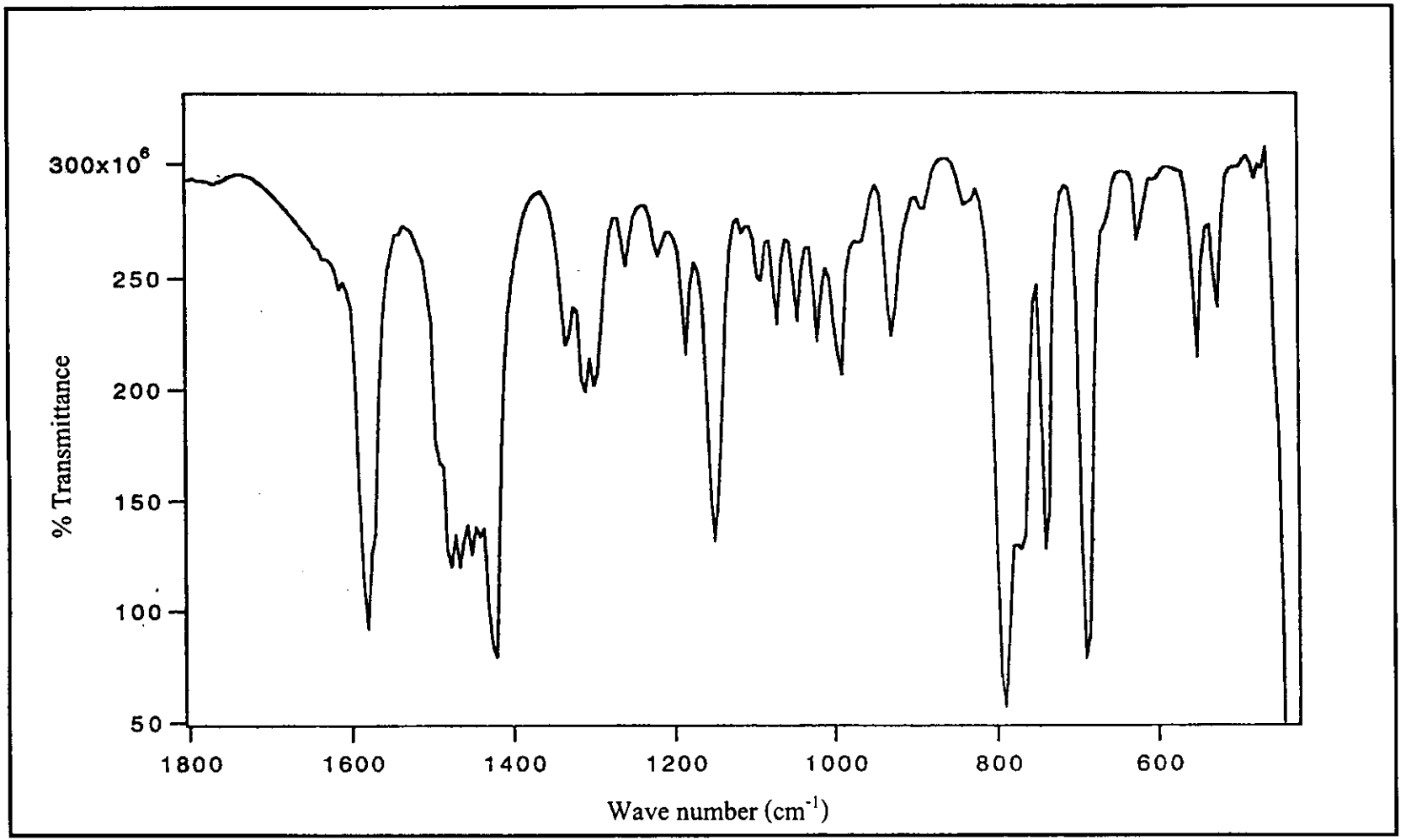

Figure 9 IR spectrum of azpy.

3.2.5 Nuclear Magnetic Resonance spectroscopy

Nuclear Magnetic Resonance (NMR) spectroscopy is an important technique to determine molecular structure. In this work, The structures of ligands and complexes were explained by using 1D and 2D NMR spectroscopic techniques (^{1}H NMR, ^{1}H-^{1}H COSY NMR, ^{13}C NMR, DEPT NMR, ^{1}H-^{13}C HMQC NMR). The NMR spectra of the azpy, bpy and phen ligands were recorded in acetone-d_6 on UNITY SNOVA 500 MHz. While, the spectra of the diazpy ligand were recorded on Bruker AVANCE 300 MHz. The tetramethylsilane (TMS, $(CH_3)_4Si$) was used as an internal reference. The chemical shift and proton, carbon assignments of diazpy, azpy, bpy and phen ligands are summarized in Table 6 to 9, respectively.

Table 6 ^{1}H and ^{13}C NMR spectroscopic data of the diazpy ligand

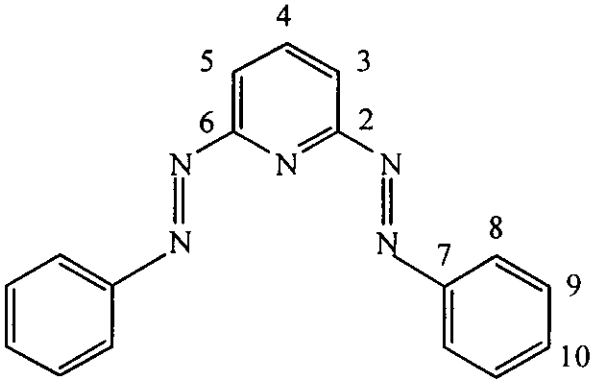

H-Position	^{1}H NMR			^{13}C NMR
	δ (ppm)	*J* (Hz)	Number of H	δ (ppm)
4	8.27 (t)	7.8, 7.8	1	141.79
8	8.07 (dd)	7.2, 2	4	124.18
3 (5)	7.92 (d)	7.8	2	115.38

Table 6 (continued)

H-Position	^{1}H NMR			^{13}C NMR
	δ (ppm)	*J* (Hz)	Number of H	δ (ppm)
9	7.65 (m)	-	6	130.35
10				133.41
Quaternary carbon				163.93 155.31

m = multiplet, d = doublet, dd = doublet of doublet, t = triplet

The diazpy ligand had five equivalent protons on molecule. The ^{1}H NMR data of diazpy appeared five signals (Figure 10).

The proton H4 was effected from resonance results. Therefore, the chemical shift of proton H4 occurred at most downfield. This signal was splitted by proton H3 (J = 7.8 Hz), H5 (J = 7.8 Hz) and appeared as triplet peak at 8.27 ppm.

The chemical shift of proton H3 (H5) occurred at higher field than proton H4, because it was less effected from resonance results than proton H4. The resonance occurred as doublet at 7.92 ppm. It was splitted by proton H4 (J = 7.8).

The proton H8 were two equivalent protons on both phenyl rings located closed to azo nitrogen. The resonance occurred as doublet of doublet at 8.07 ppm. The splitting of doublet of doublet peaks was observed for coupling with proton H9 (J = 7.2 Hz) and H10 (J = 2.0 Hz).

The signal of proton H9 showed multiplet peaks, which resonated at the same position with signal of proton H10 (7.65 ppm).

In addition, also the peak assignment was done using simple correlation ^{1}H-^{1}H COSY spectroscopy. The ^{1}H-^{1}H COSY NMR signals of ^{1}H-^{1}H COSY NMR are

shown in Figure 11.

The ^{13}C NMR (Figure 12) results corresponded to the results of DEPT NMR (Figure 13), which showed only methine carbon signals. The ^{13}C NMR spectrum of diazpy ligand appeared 7 signals for 17 carbons. The signal at the most downfield (163.93 ppm) was signal of two equivalent quaternary carbons (C2 and C6). The signal at 153.31 ppm belonged to two equivalent quaternary carbons (C7 of both phenyl rings). The signals of two equivalent carbon C3 (C5) and carbon C4 on pyridine ring occurred at 115.38 and 141.79 ppm, respectively. The ^{13}C NMR spectrum at 130.35, 124.18 and 133.41 ppm were attributed to four equivalent carbons of carbon C8 and carbon C9 and two equivalent carbons of carbon C10, respectively.

Moreover, the ^{13}C NMR signals assignments were based on the ^{1}H-^{13}C HMQC NMR spectrum (Figure 14), which exhibited correlation between ^{1}H NMR spectrum and ^{13}C NMR spectrum.

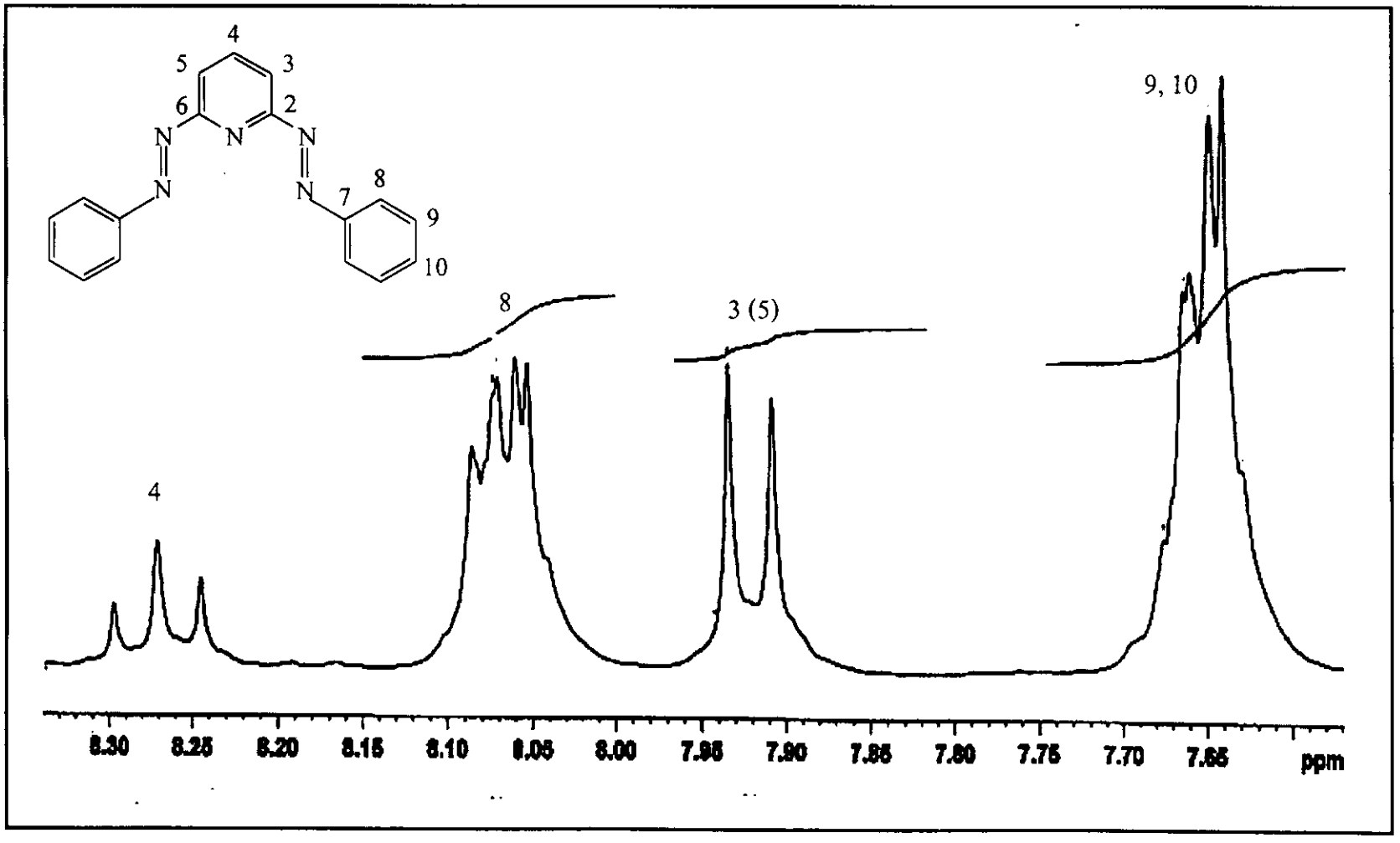

Figure 10 ^{1}H NMR spectrum of diazpy in acetone-d_6 (300 MHz).

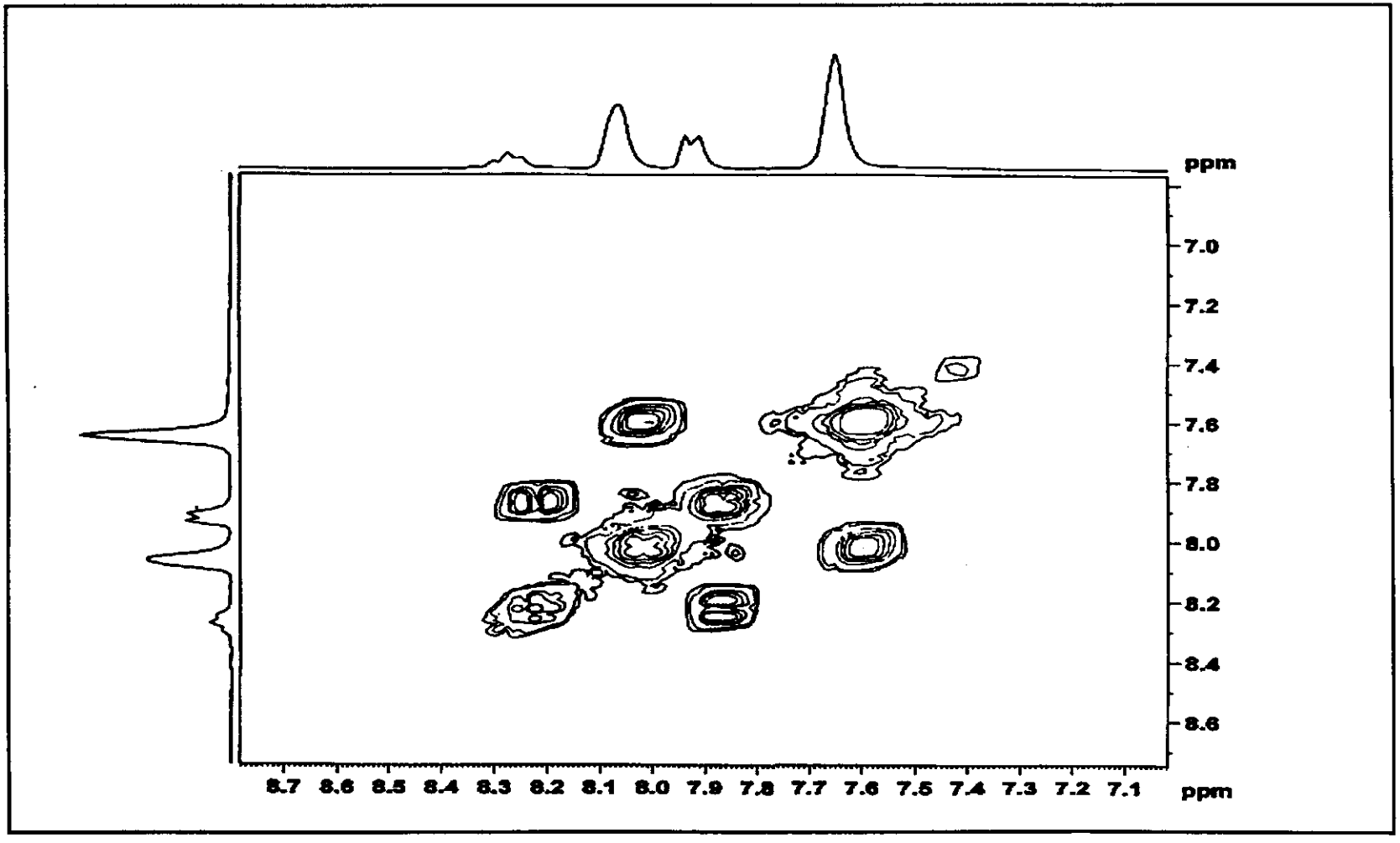

Figure 11 ^{1}H- ^{1}H COSY NMR spectrum of diazpy in acetone-d_6 (300 MHz).

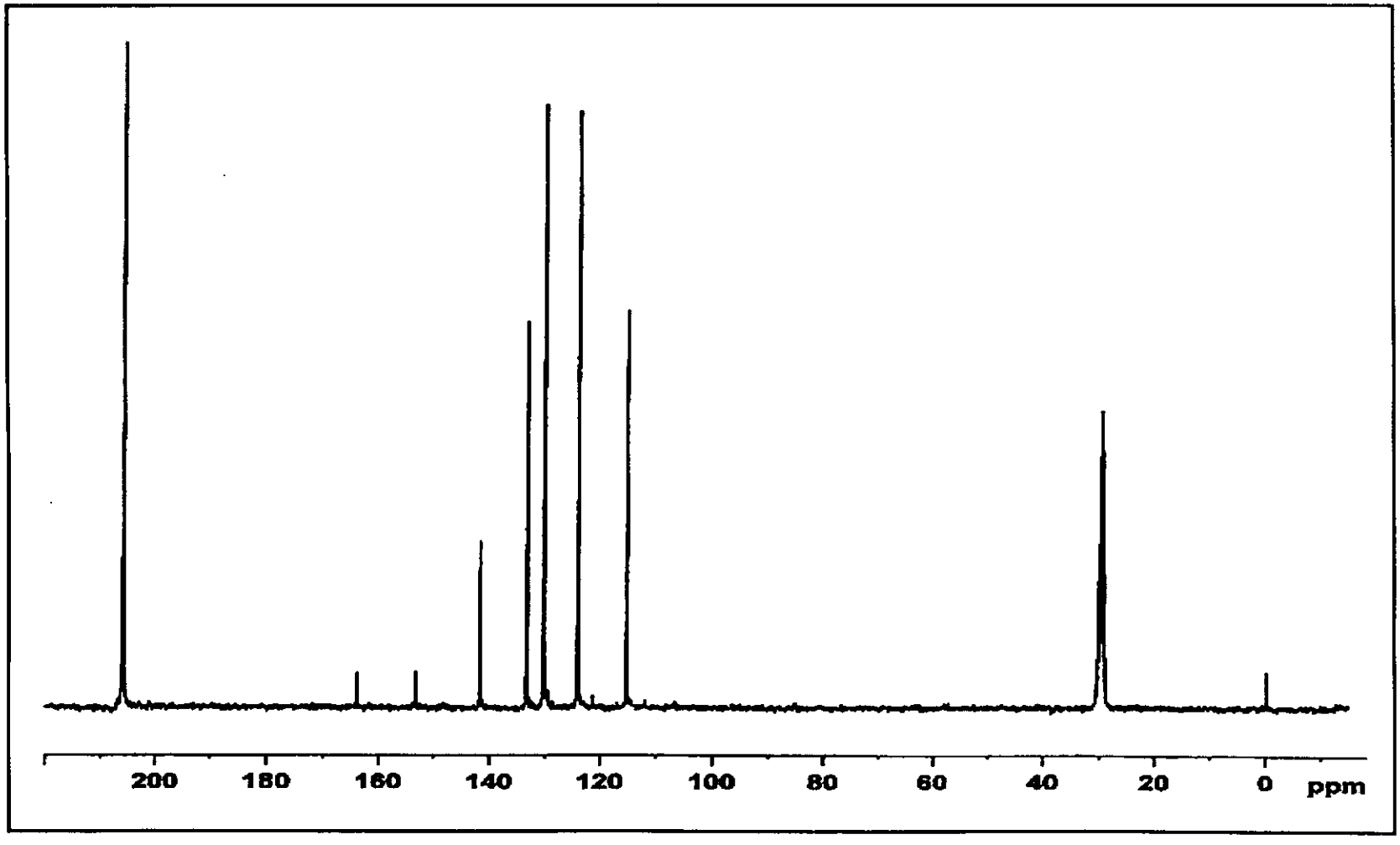

Figure 12 ^{13}C NMR spectrum of diazpy in acetone-d_6 (300 MHz).

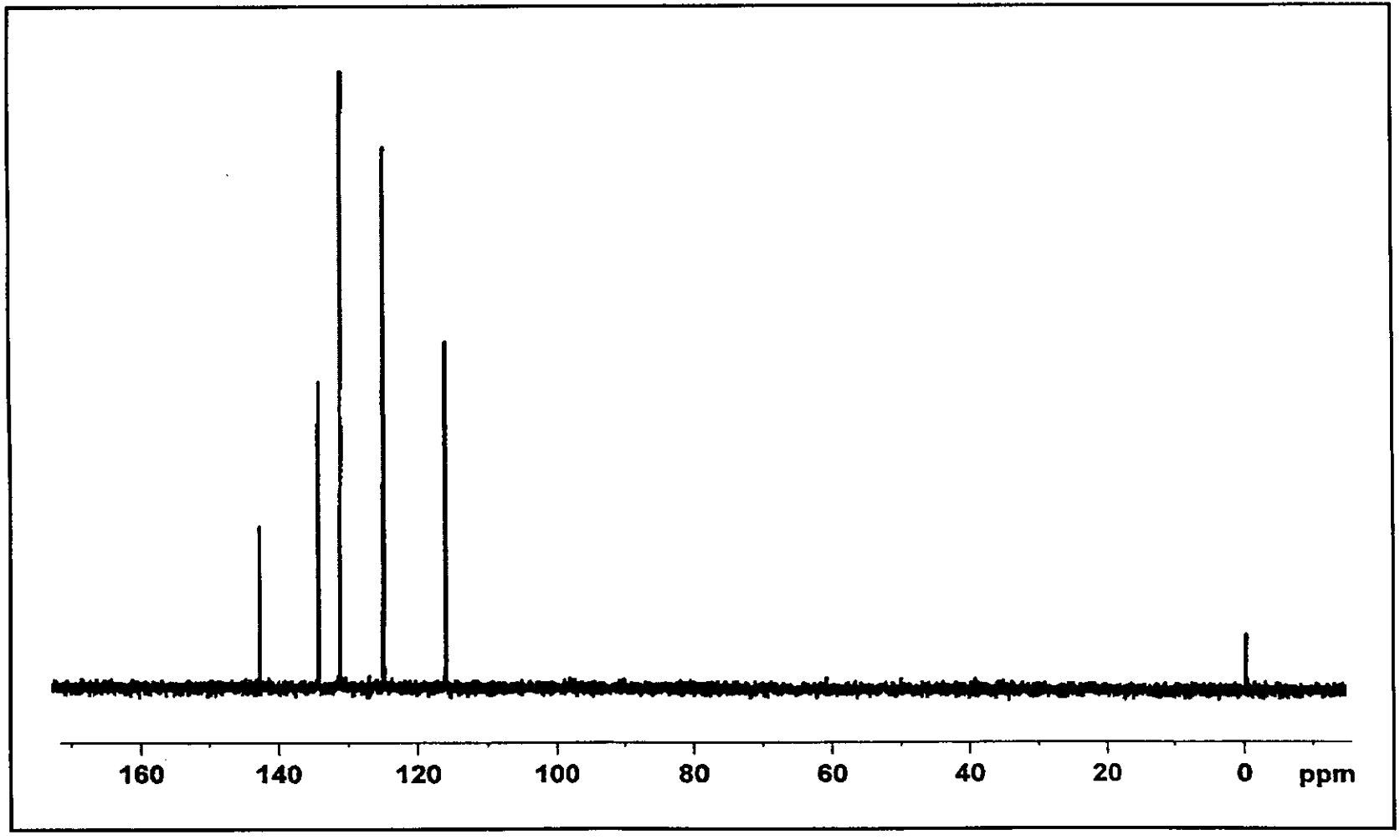

Figure 13 DEPT NMR spectrum of diazpy in acetone-d_6 (300 MHz).

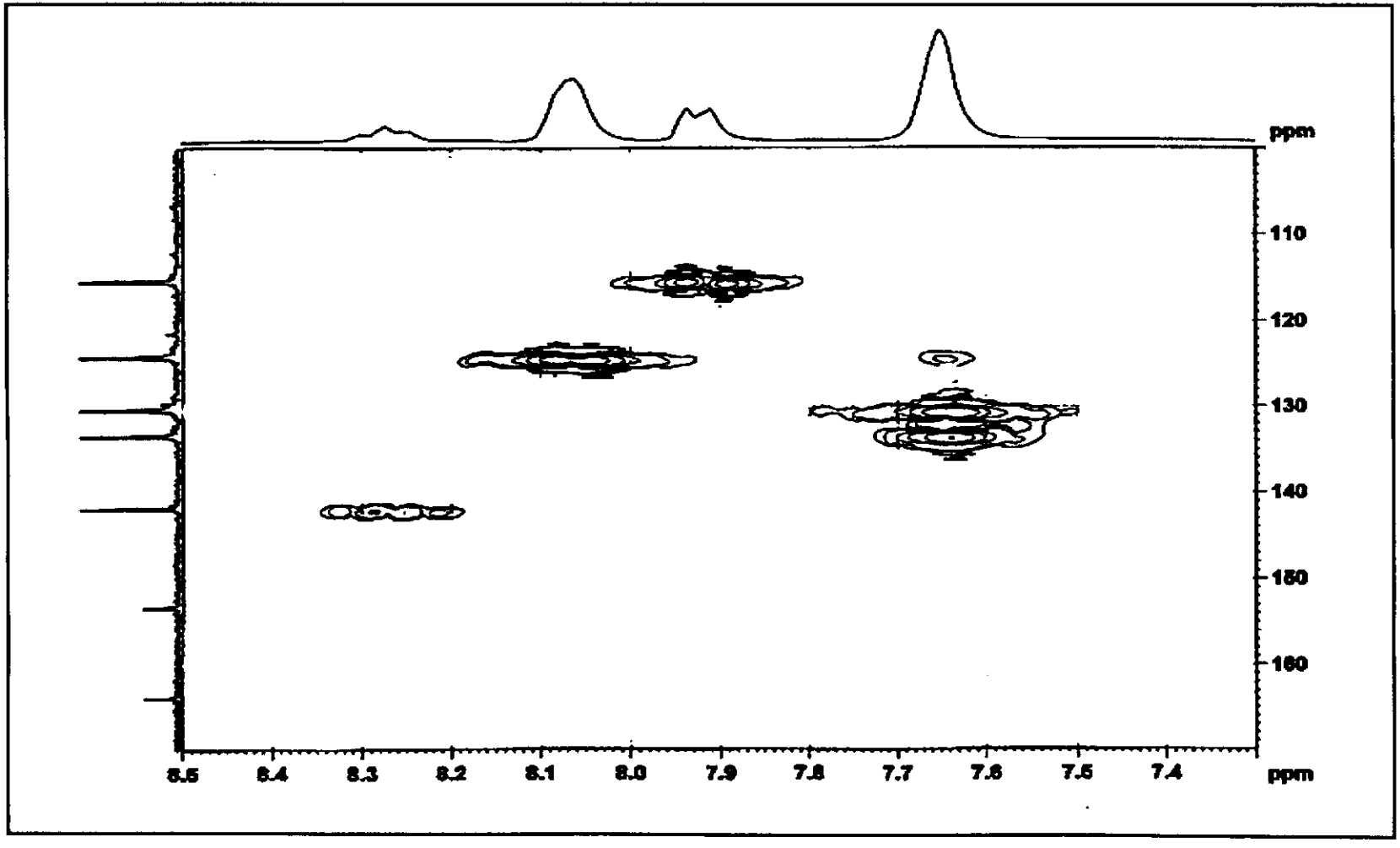

Figure 14 ^{1}H-^{13}C HMQC NMR spectrum of diazpy in acetone-d_6 (300 MHz).

Table 7 The NMR spectroscopic data of the azpy ligand in acetone-d_6

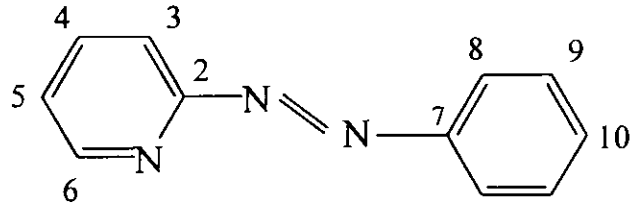

H-Position	^{1}H NMR			^{13}C NMR
	δ (ppm)	*J* (Hz)	Number of H	δ (ppm)
6	8.76 (dd)	5.0, 1.5	1	150.13
4	8.06 (ddd)	7.5, 7.5, 1.5	1	139.32
8	8.04 (dd)	7.5, 2.0	2	123.88
3	7.80 (d)	8.0	1	114.04
9, 10	7.64 (m)	-	3	132.97 130.10
5	7.57 (ddd)	7.5, 5.0, 1.0	1	126.25
Quaternary carbon				164.05 153.09

m = multiplet, d = doublet, dd = doublet of doublet and

ddd = doublet of doublet of doublet

The structure of the azpy ligand was supported by ^{1}H NMR, ^{1}H-^{1}H COSY NMR, ^{13}C NMR, ^{1}H-^{13}C HMQC NMR techniques. It was recorded on UNITY SNOVA 500 MHz. The ^{1}H NMR spectrum of the azpy ligand (Figure 15) showed 6 resonances for 9 protons.

The proton H3 on the pyridine ring was splitted by the proton H4 (J = 8.0 Hz), resulting in doublet signal at 7.80 ppm. Since, it located near proton H4 and effected by nitrogen of azo function. Therefore, it showed the signal shifted to lower field than proton H5 but higher field than proton H4 and H6.

The proton H4 was coupled with proton H3 (J = 7.5 Hz), H5 (J = 7.5 Hz) and H6 (J = 1.5), giving doublet of doublet of doublet (ddd) signal at 8.04 ppm.

The proton H5 appeared at the most high field (7.57 ppm) and was splitted by proton H6 (J = 5.0 Hz), H4 (J = 7.5 Hz) and H3 (J = 1.0 Hz).

The signal of proton H6 was observed at the most downfield, 8.76 ppm. The signal appeared as doublet of doublet (dd), due to the coupling with proton H5 (J = 5.0 Hz) and H4 (J = 1.5 Hz).

The signal of proton H8 closed to the azo function appeared at lower field than H9 and H10. This signal was doublet of doublet peak with splitted by proton H9 and proton H10 (J = 7.5, 2.0 Hz).

The proton H9 showed chemical shift like proton H10. The splitting of both protons in the azpy ligand appeared as multiplet peak at 7.64 ppm.

The ^{13}C NMR signal assignments (Figure 17) were based on the ^{1}H-^{13}C HMQC NMR spectrum (Figure 18). The ^{13}C NMR spectrum of azpy showed 9 signals. There were two quaternary carbons, showed downfield resonance at 164.05 ppm, which was assigned to quaternary carbon (C2). The intense peak at 153.09 ppm belonged to the quaternary carbon (C7). The carbon C3 signal occurred at 114.04 ppm which higher field than carbon C8 (123.88 ppm). The carbon C6 and carbon C4 signal were observed at 150.13 and 139.32 ppm, respectively. The peak at 132.97 and 130.10 ppm referred to carbon C9 and carbon C10, respectively.

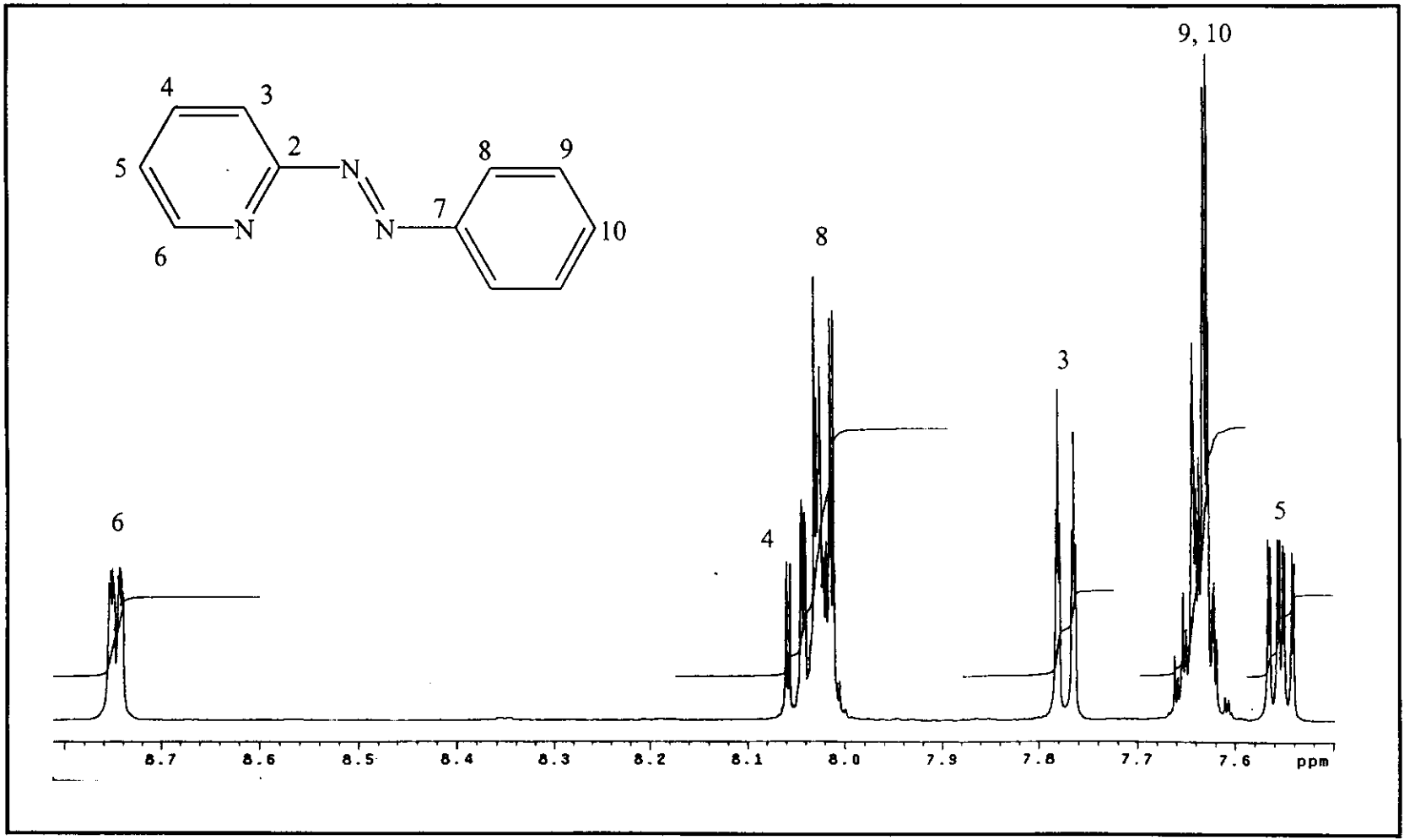

Figure 15 ^{1}H NMR spectrum of azpy in acetone-d_6 (500 MHz) .

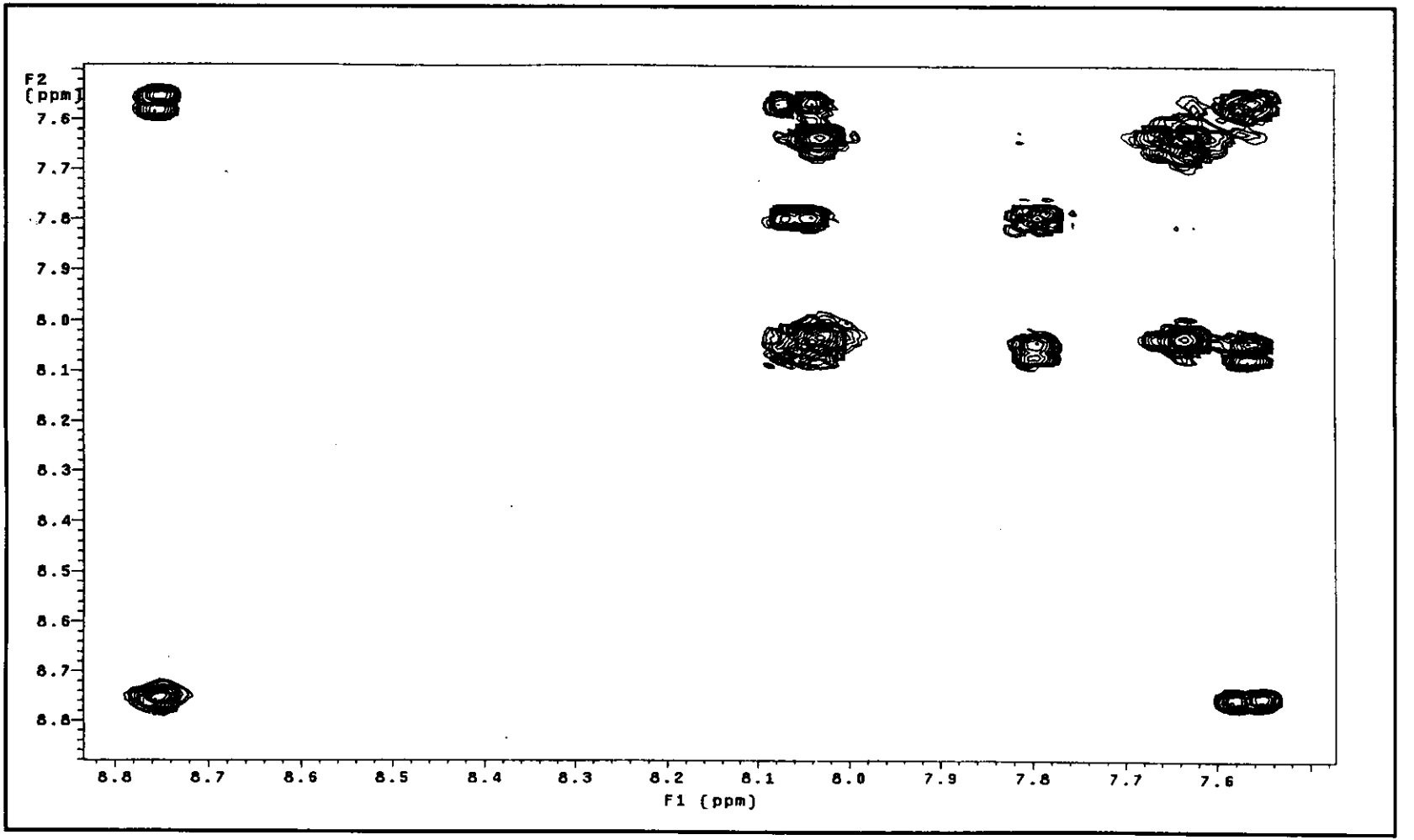

Figure 16 ^{1}H- ^{1}H COSY NMR spectrum of azpy in acetone-d_6 (500 MHz) .

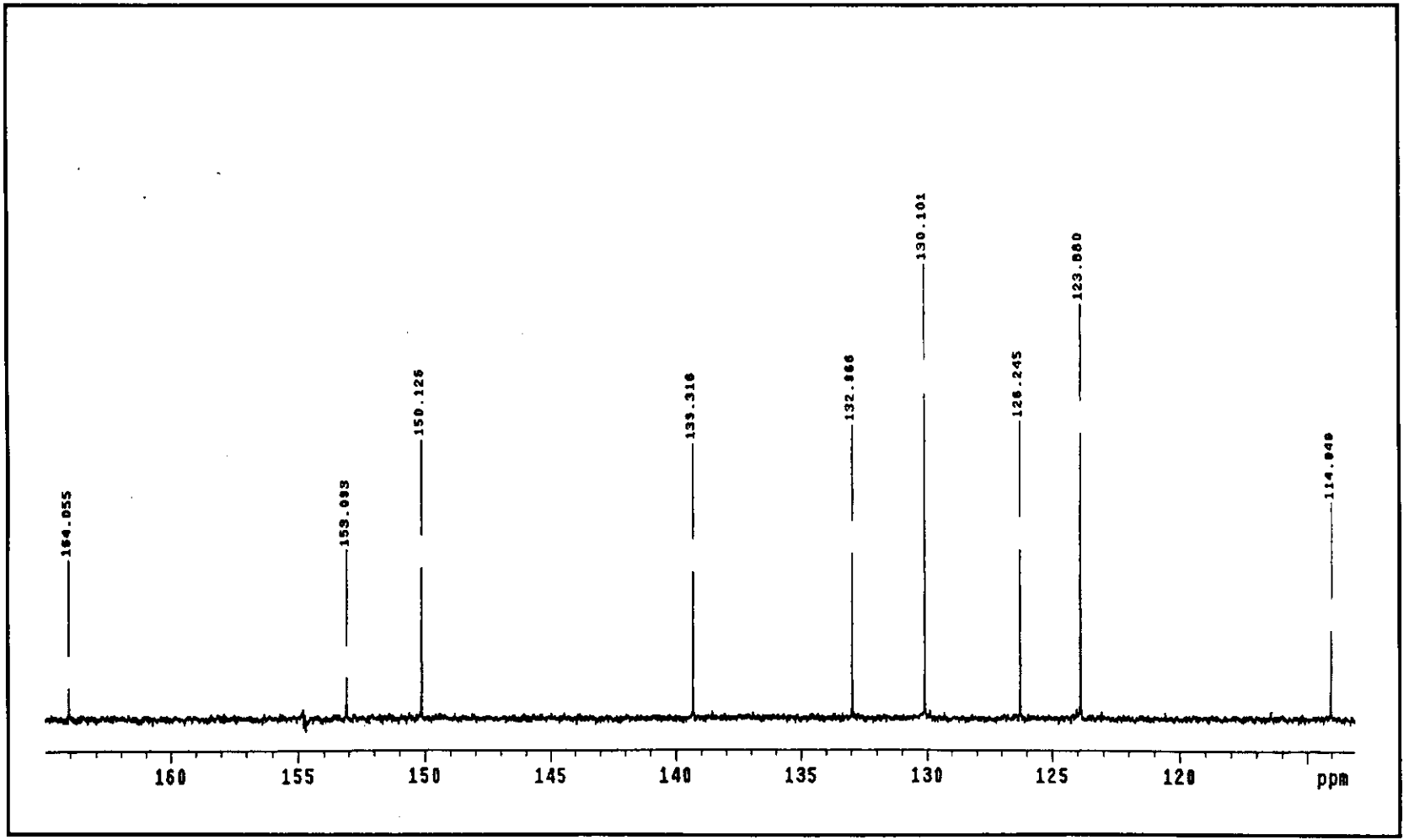

Figure 17 ^{13}C NMR spectrum of azpy in acetone-d_6 (500 MHz).

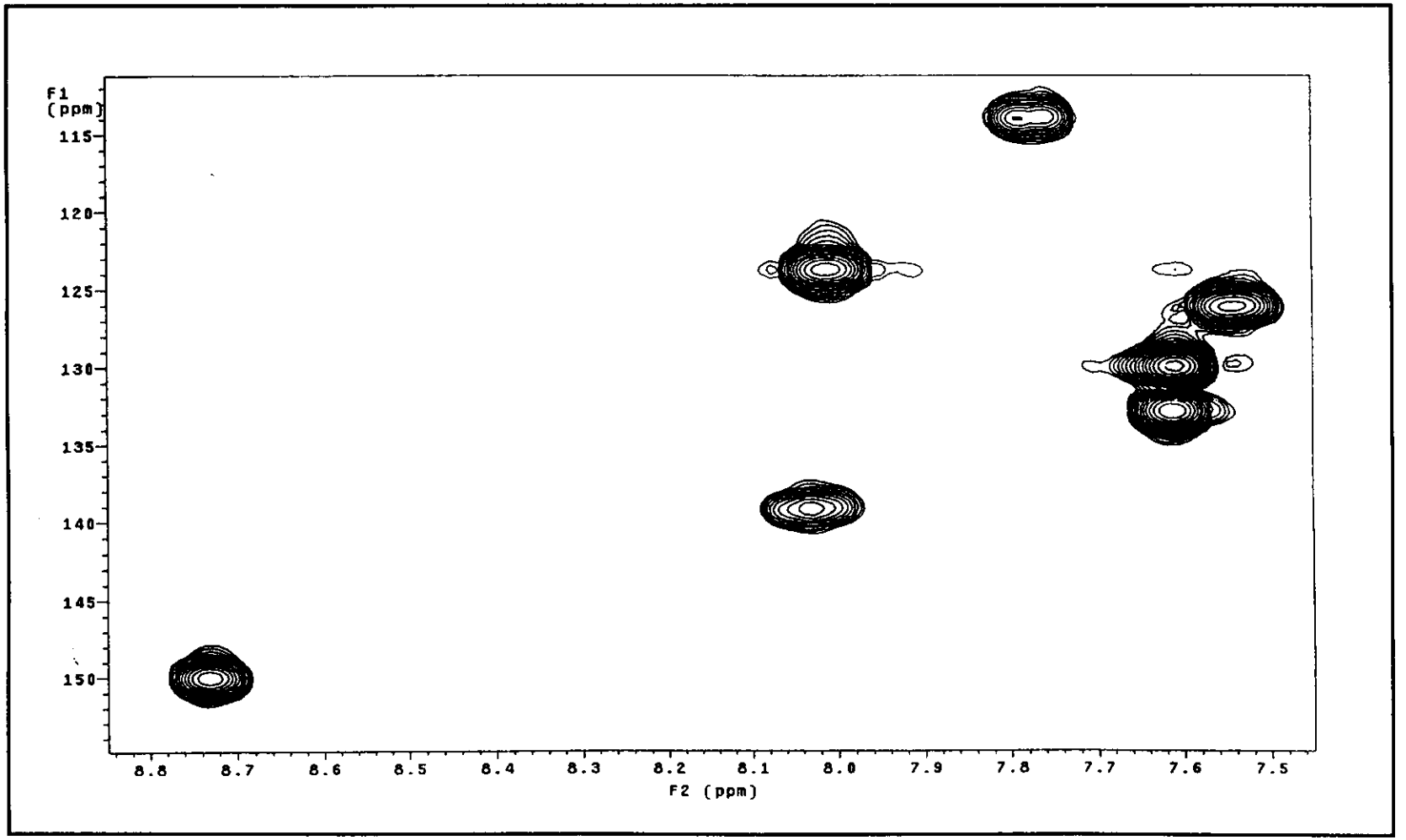

Figure 18 ^{1}H-^{13}C HMQC NMR spectrum of azpy in acetone-d_6 (500 MHz).

Table 8 The NMR spectroscopic data of the bpy ligand in acetone-d_6

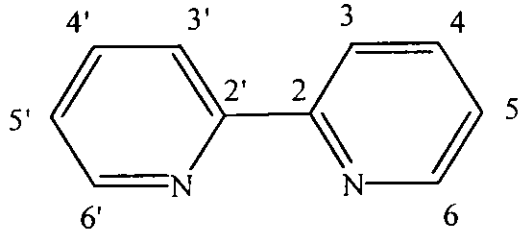

H-Position	^{1}H NMR			^{13}C NMR
	δ (ppm)	*J* (Hz)	Number of H	δ (ppm)
6, 6′	8.69 (ddd)	4.8, 2.0, 1.0	2	149.94
3, 3′	8.49 (ddd)	8.0, 1.0, 1.0	2	137.69
4, 4′	7.94 (ddd)	7.5, 8.0, 1.5	2	124.68
5, 5′	7.43 (ddd)	8.0, 5.0, 1.0	2	121.34
Quaternary carbon				156.65

ddd = doublet of doublet of doublet

The ^{1}H NMR signals of the bpy ligand showed only four signals for 8 protons (Figure 19). This is due to the symmetric structure of bpy. The protons of the H6 (H6′), H3 (H3′), H4 (H4′) and H5 (H5′) occurred at 8.69 (ddd), 8.49 (ddd), 7.94 (ddd) and 7.43 (ddd) ppm, respectively. The ^{1}H NMR assignments were based on the ^{1}H-^{1}H COSY NMR spectroscopic data (Figure 20).

Since, proton H6 was located next to the nitrogen atom. Therefore, the chemical shift of proton H6 occurred at lower field than other protons. The signal of proton H3 appeared at lower field than proton H4 and H5 but higher field than proton H6. It showed as doublet of doublet of doublet (ddd) with *J*-coupling 8.0 (H4), 1.0 (H5), 1.0 (H6) Hz at 8.49 ppm.

The ^{13}C NMR signal assignments (Figure 21) were based on the ^{1}H-^{13}C HMQC NMR spectroscopic data (Figure 22). The ^{13}C NMR spectrum of the bpy ligand displayed 4 equivalent resonance signals in aromatic region. The downfield resonance at 156.65 ppm was assigned to the quaternary carbon (C2, C2′). The methine carbons occurred at 149.94, 137.69, 124.68 and 121.34 ppm assigned to signals of carbon C6 (6′), carbon C3 (3′), carbon C4 (4′) and carbon C5 (5′), respectively.

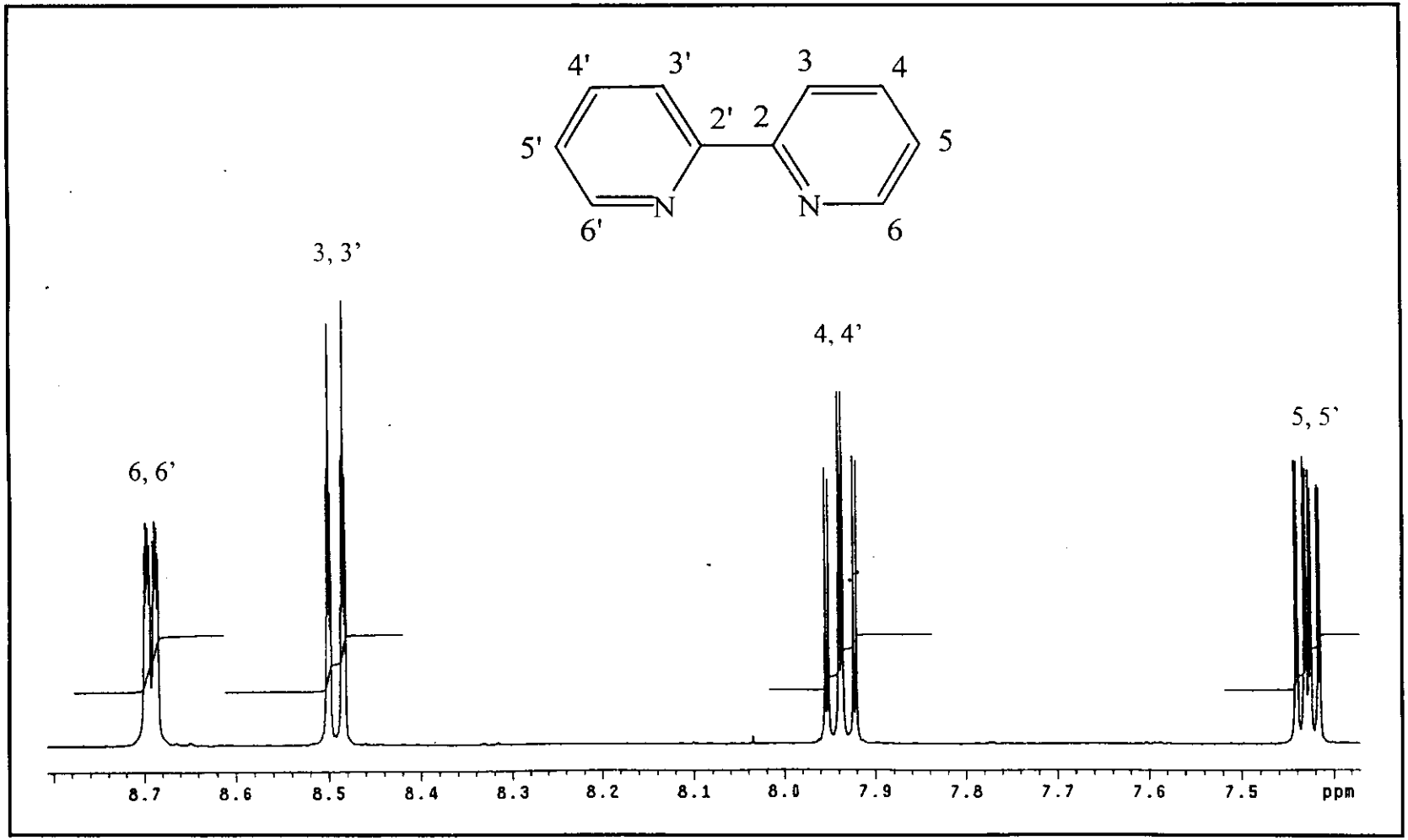

Figure 19 ^{1}H NMR spectrum of bpy in acetone-d_6 (500 MHz).

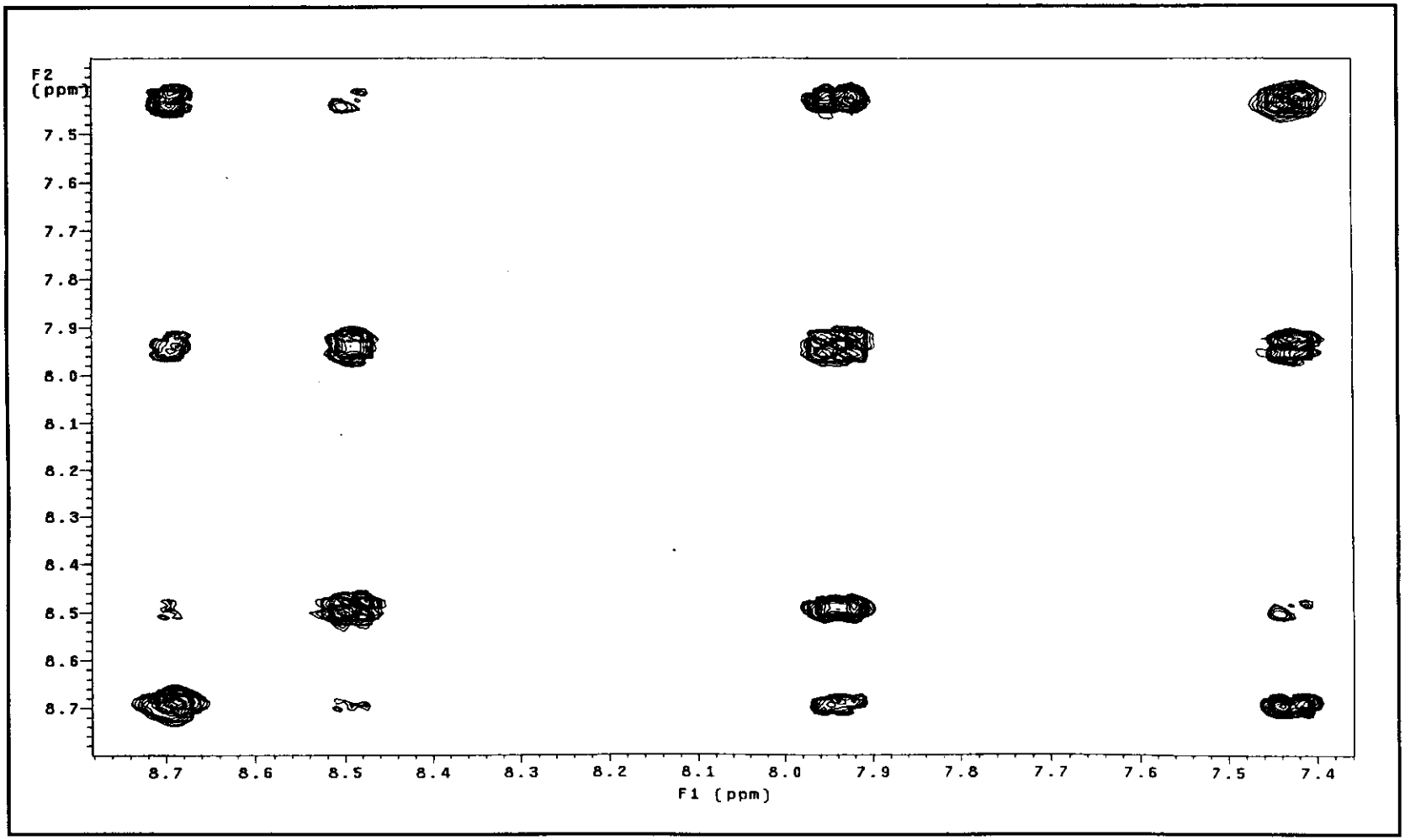

Figure 20 ^{1}H-^{1}H COSY NMR spectrum of bpy in acetone-d_6 (500 MHz).

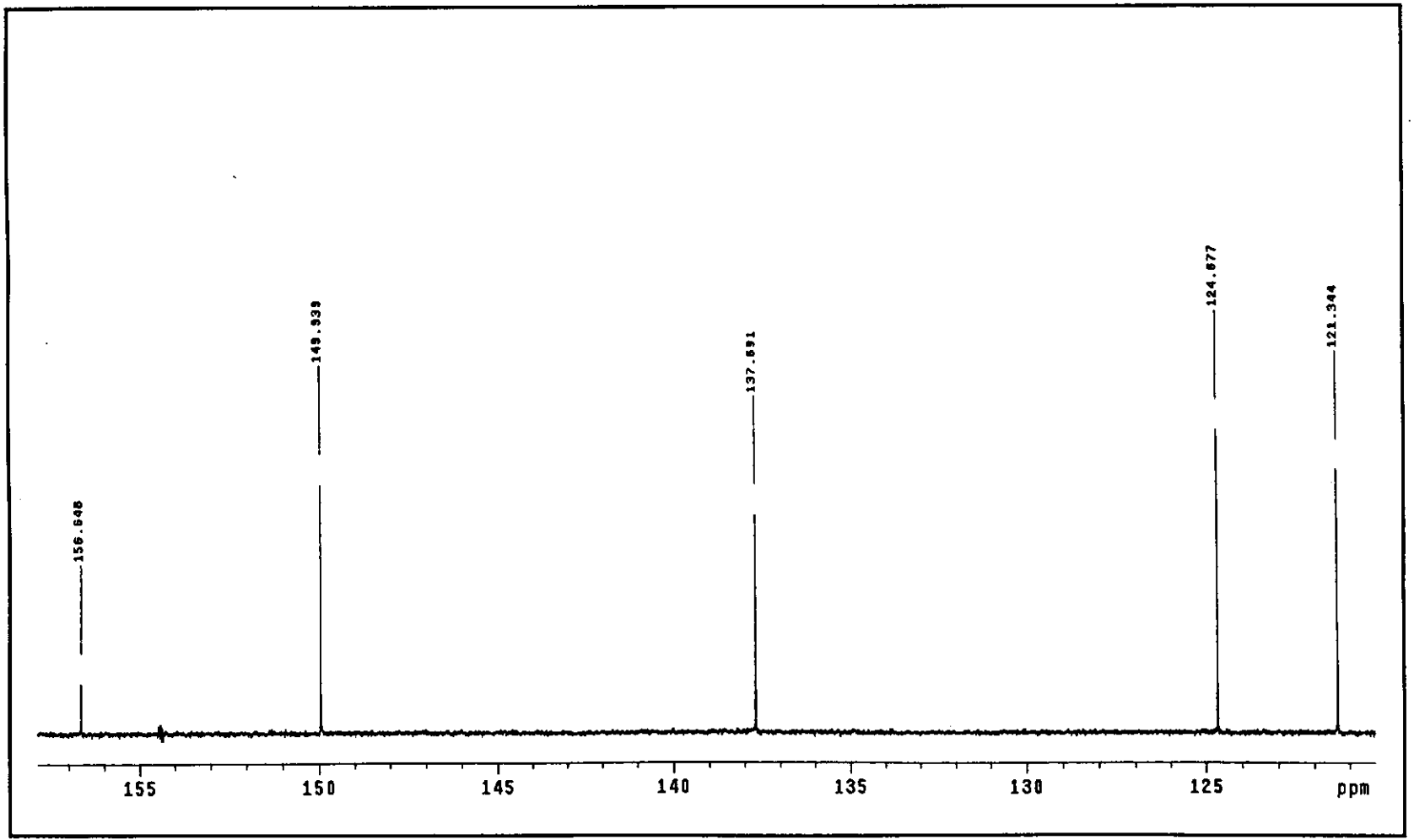

Figure 21 ^{13}C NMR spectrum of bpy in acetone-d_6 (500 MHz).

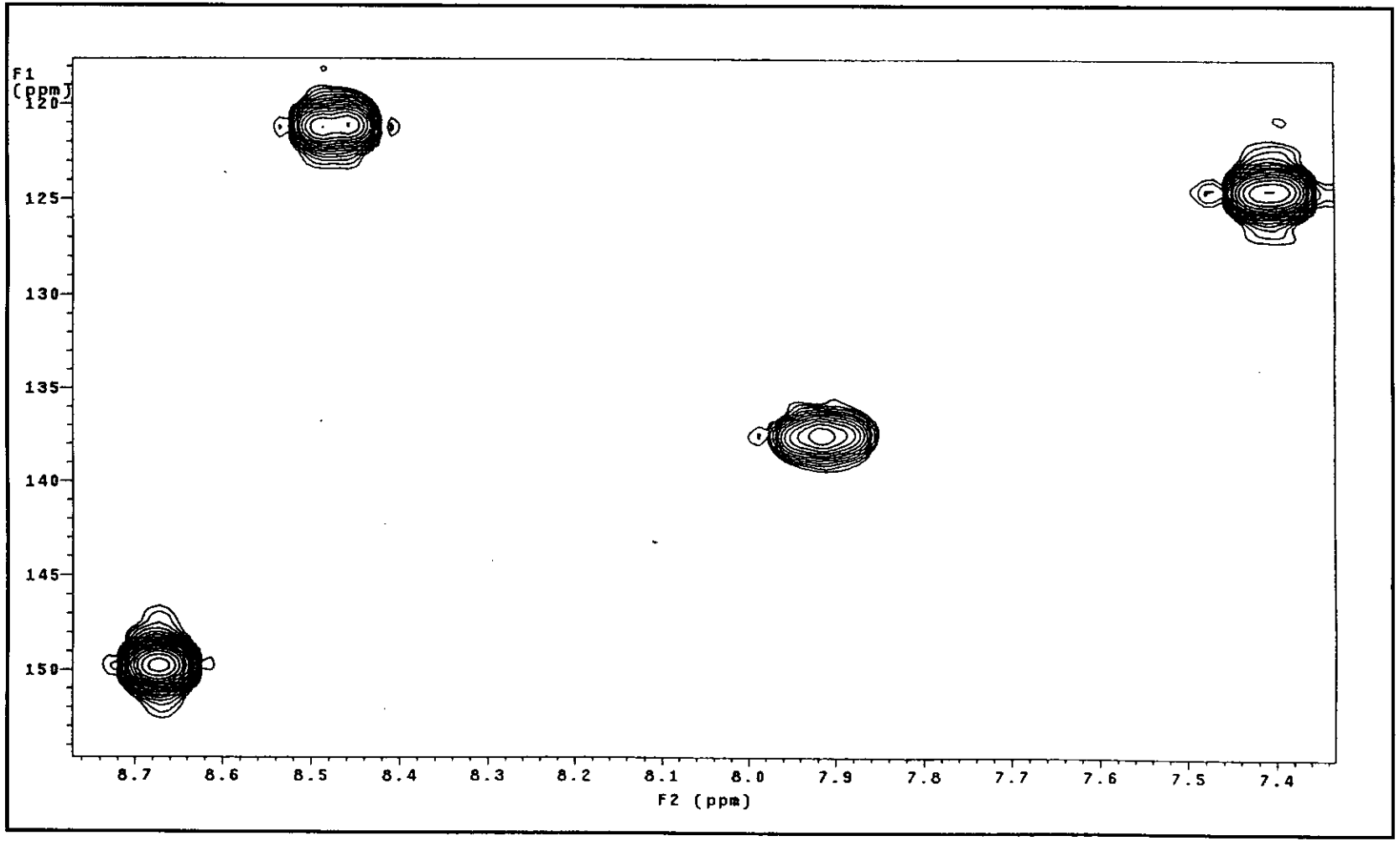

Figure 22 ^{1}H-^{13}C HMQC NMR spectrum of bpy in acetone-d_6 (500 MHz).

Table 9 The NMR spectroscopic data of the phen ligand in acetone-d_6

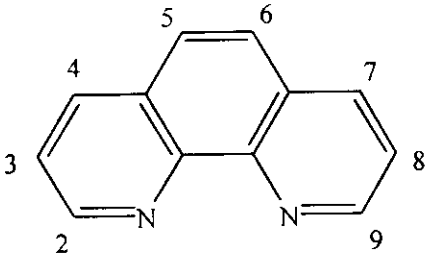

H-Position	^{1}H NMR			^{13}C NMR
	δ (ppm)	*J* (Hz)	Number of H	δ (ppm)
2, 9	9.18 (dd)	4.5, 1.5	2	150.76
4, 7	8.48 (dd)	8.5, 1.5	2	136.94
5, 6	7.98 (s)	-	2	127.40
3, 8	7.78 (dd)	8.0, 4.5	2	123.96
Quaternary carbon				146.76 129.53

dd = doublet of doublet and s =singlet

The ^{1}H NMR spectrum of the phen ligand (Figure 23) showed again the presence of four signals. The phen ligand had four equivalent protons on molecule. In addition, the assignment of signals was based on the used of ^{1}H-^{1}H COSY NMR spectra (Figure 24).

The chemical shift of proton H2 occurred at the most downfield. The signal of this proton was doublet of doublet which splitted by proton H3 (J = 4.5 Hz) and H4 (J = 1.5Hz) at 9.18 ppm. The proton H3 was located between proton H2 and H4 and gave the coupling constant J = 4.5 and 8.0 Hz, respectively.

The proton H4 occurred downfield than proton H5, which coupled with proton H3 (J = 8.5 Hz) and proton H2 (J = 1.5 Hz). The chemical shift of proton H5 occurred at 7.98 ppm.

The ^{13}C NMR signal assignments (Figure 25) were based on the ^{1}H-^{13}C HMQC NMR spectra (Figure 26). The ^{13}C NMR spectrum of the phen ligand displayed 4 resonance signals in aromatic region. The downfield resonance at 146.76 ppm was assigned to quaternary carbon, which was located near one of nitrogen. The signal at 129.53 ppm was assigned to quaternary carbon, which was not closed to nitrogen atom. The signals at 150.76, 136.94, 127.40 and 123.96 ppm were assigned to C2 (2′), C4 (4′), C5 (5′) and C3 (3′), respectively.

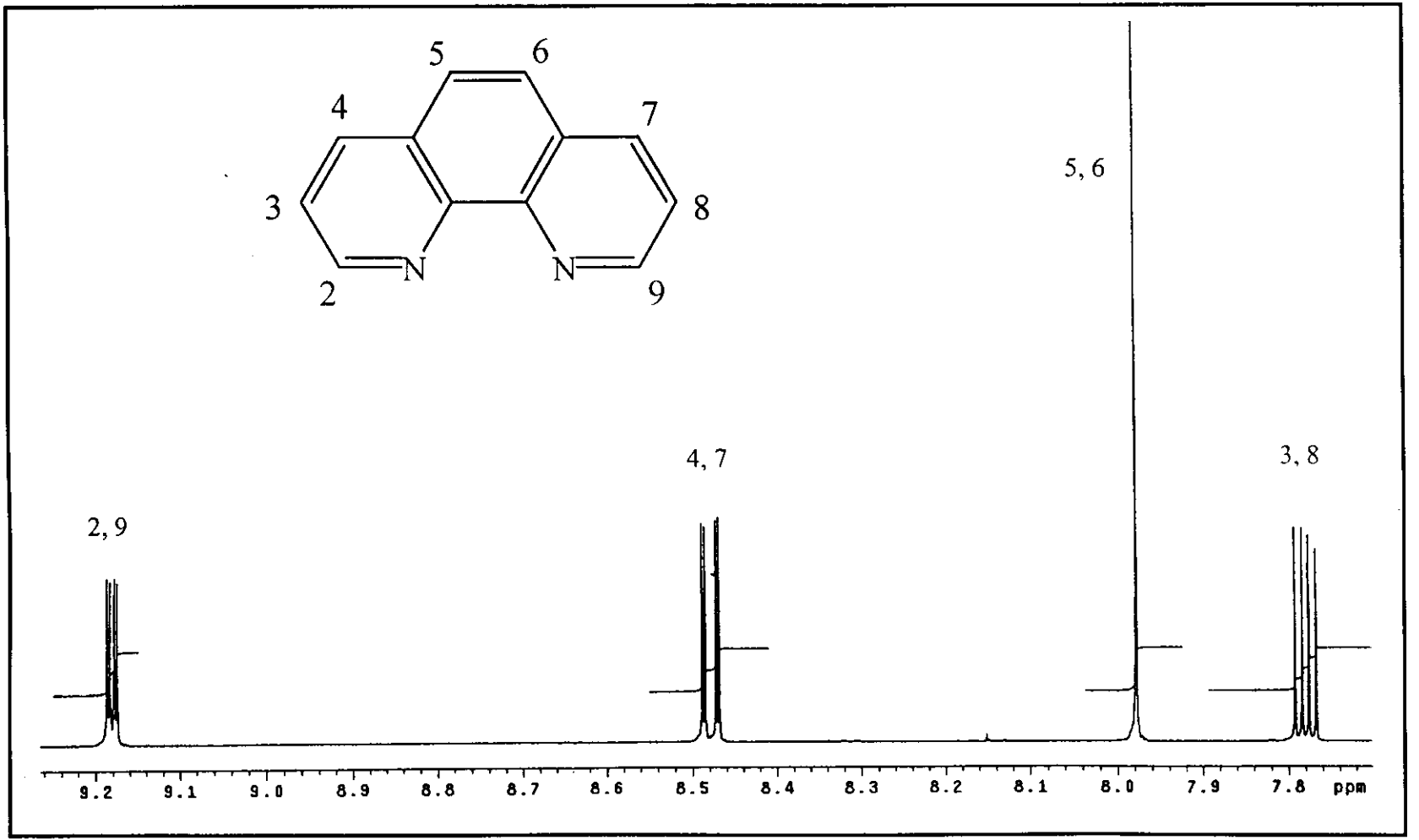

Figure 23 ^{1}H NMR spectrum of phen in acetone-d_6 (500 MHz).

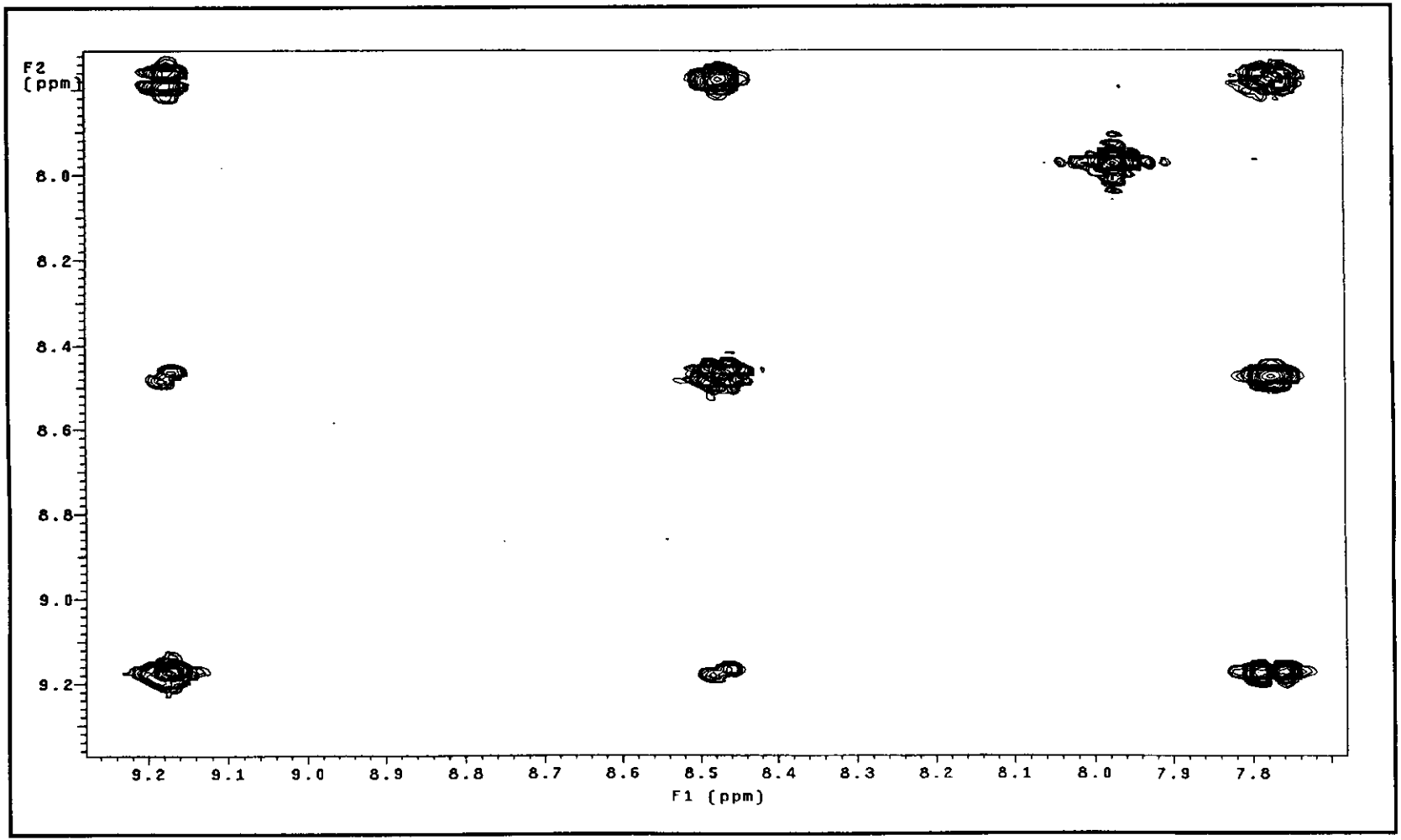

Figure 24 ^{1}H-^{1}H COSY NMR spectrum of phen in acetone-d_6 (500 MHz)

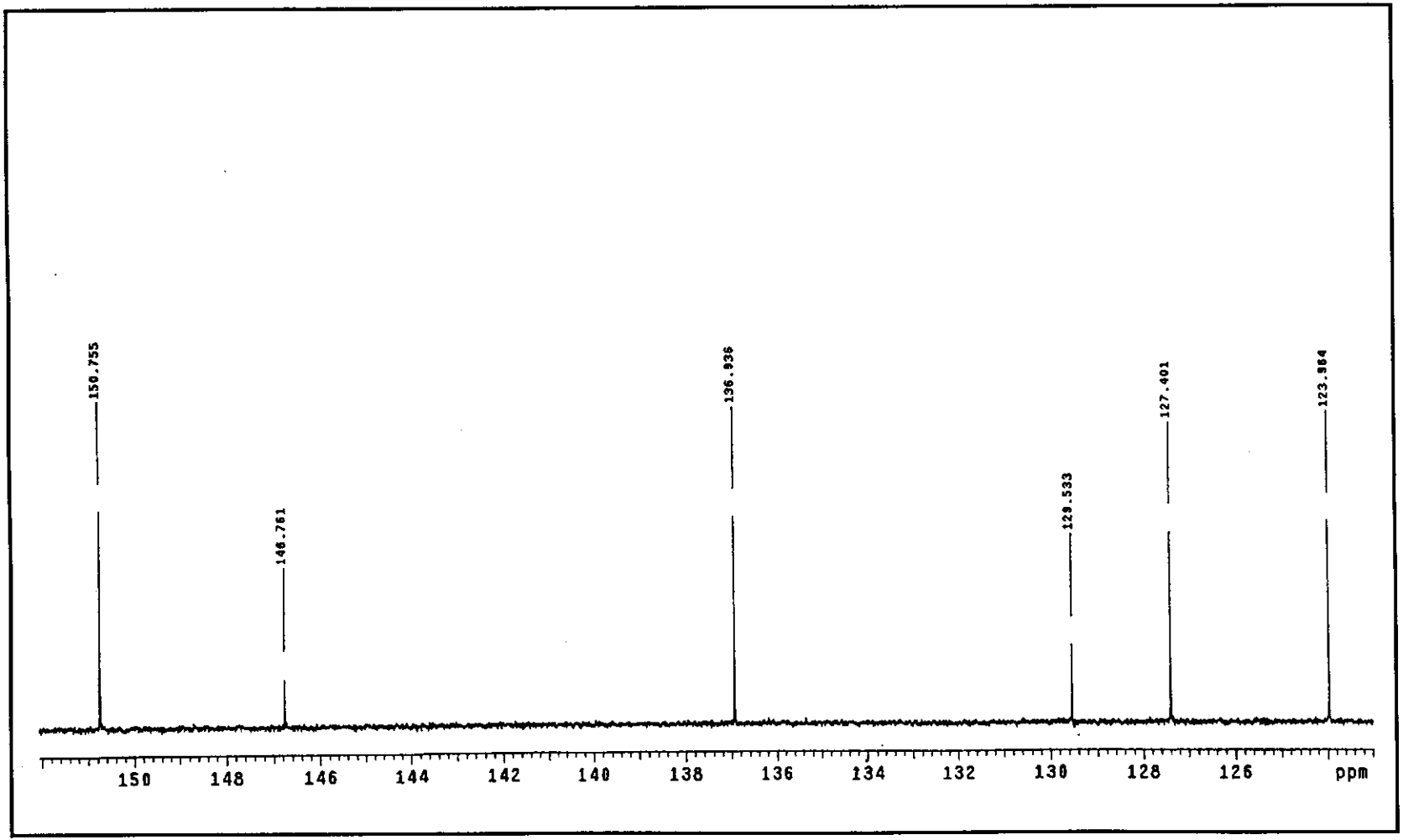

Figure 25 ^{13}C NMR spectrum of phen in acetone-d_6 (500 MHz).

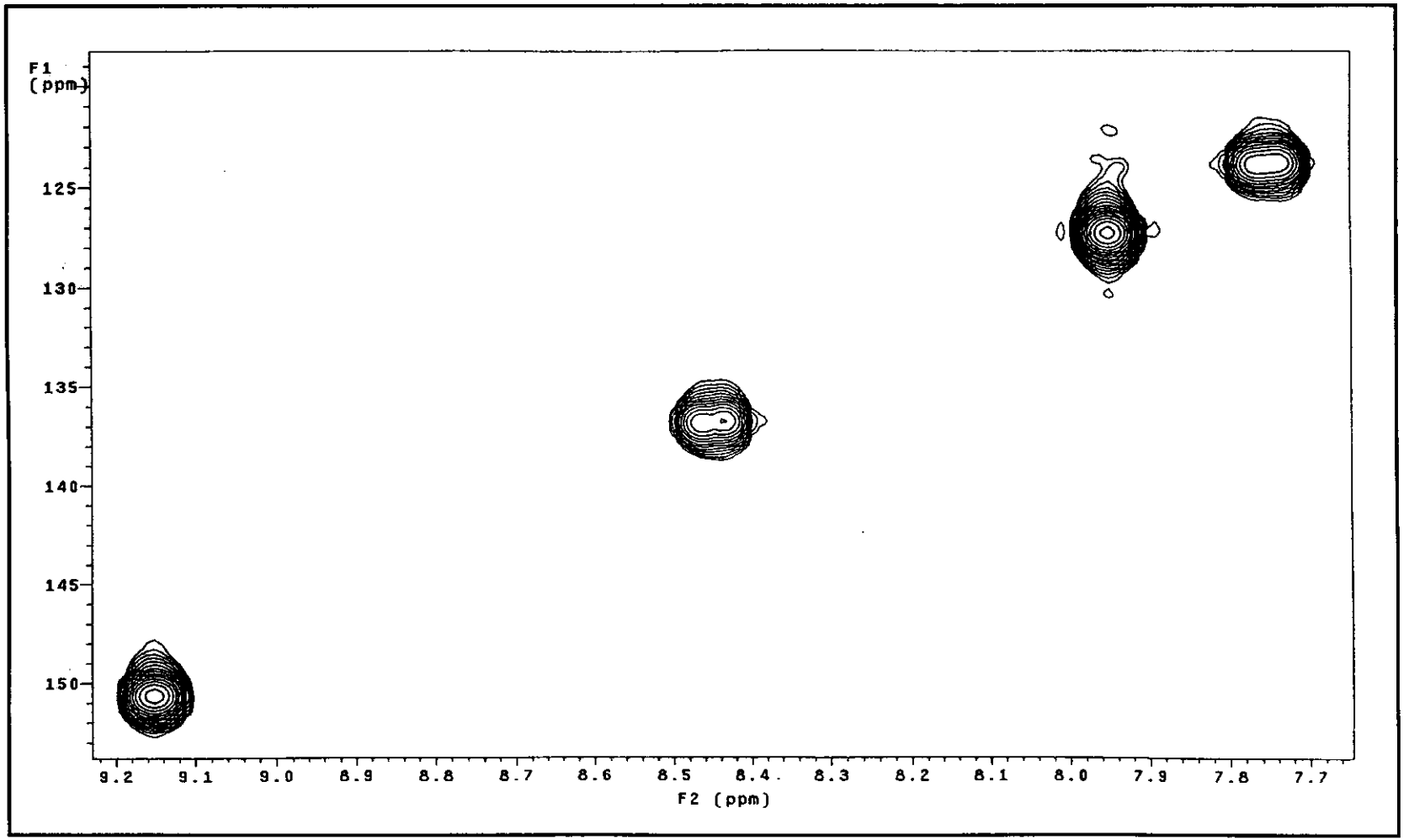

Figure 26 ^{1}H-^{13}C HMQC NMR spectrum of phen in acetone-d_6 (500 MHz).

3.2.6 Cyclic Voltammetry

Cyclic Voltammetry is a technique to study the electrochemistry of ligands. The cyclic voltammograms in acetonitrile solution of diazpy and azpy ligands are shown in Figure 27 to 28, respectively. The potentials were compared with the potential of ferrocene couple.

In this experiment, the different scan rates were used to check the couple or the redox reaction. The couple having equal anodic and cathodic current was referred to reversible couple. On the other hand, the unequal currents were referred to the unequally transfer of the electron in reduction and oxidation. This led to irreversible couple. The cyclic voltammetric data of both ligands are summarized in Table 10.

Table 10 Cyclic voltammetric data of the azpy and diazpy ligands in 0.1 M TBAH acetonitrile at scan rate 50 mV/s (ferrocene as an internal standard)

Ligands	$E_{1/2}$, V (ΔE_p, mV)			
	Oxidation		Reduction	
	E_{pa}, V	E_{pc}, V	E_{pa}, V	E_{pc}, V
azpy	-	-	-1.47	-1.61
diazpy	-	-	-1.31	-1.43 -1.65

E_{pa} = anodic peak and Ep_c = cathodic peak

ΔE_p of ferrocene (diazpy) = 75 mV

ΔE_p of ferrocene (azpy) = 65 mV

Reduction range

Reduction potentials of the ligands were studied in the range 0.00 to –2.00 V. An electrochemistry behavior of the diazpy was different from that of azpy. The two irreversible peaks were observed. While, azpy showed only one irreversible peak in this range. However, the first Ep_c of the diazpy ligand occurred at nearly potentials with those of azpy.

Oxidation range

The cyclic voltammograms of the azpy and diazpy ligands showed no signal in the potential range 0.00 to +1.30 V.

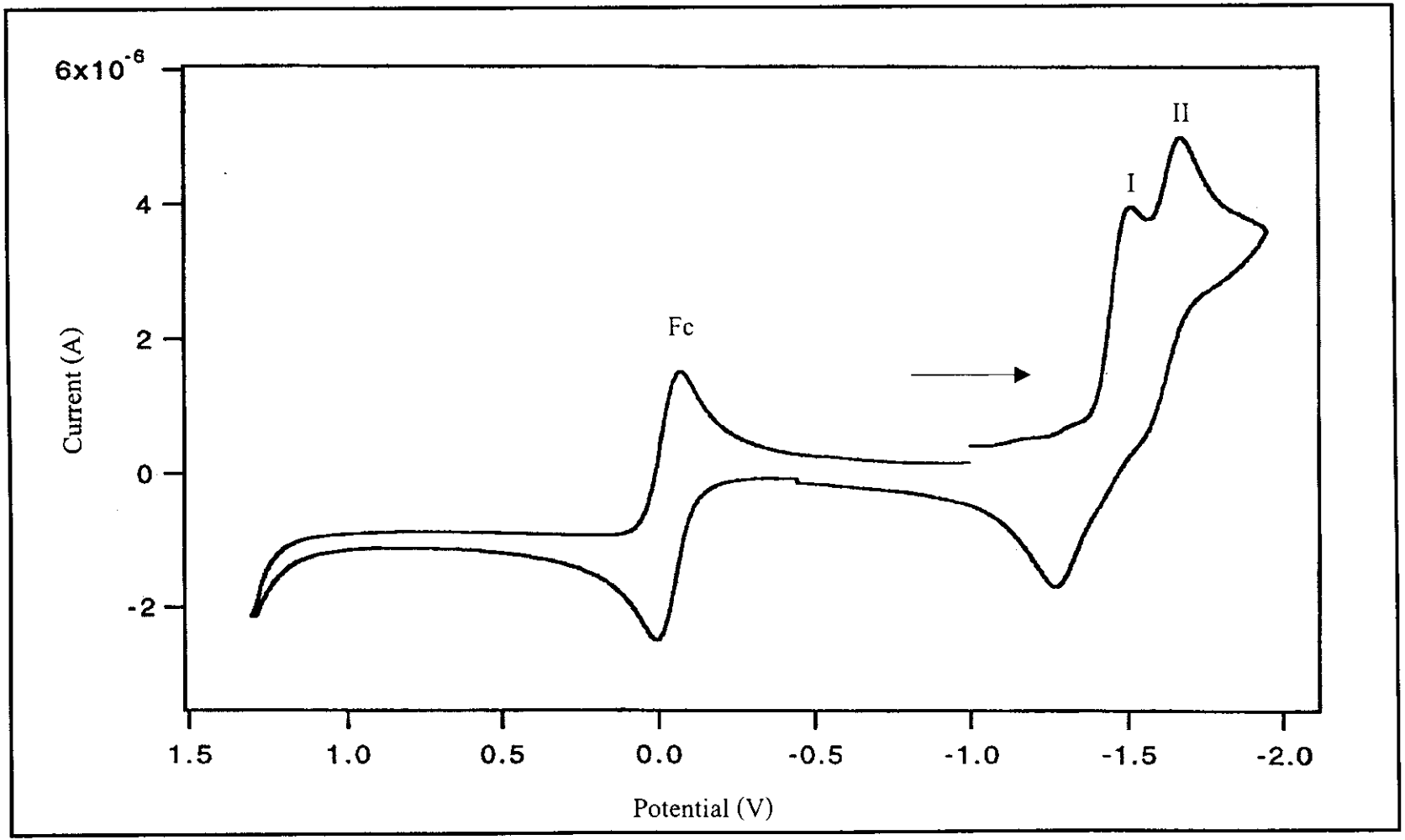

Figure 27 Cyclic voltammogram of diazpy in 0.1 M TBAH CH_3CN at scan rate 50 mV/s.

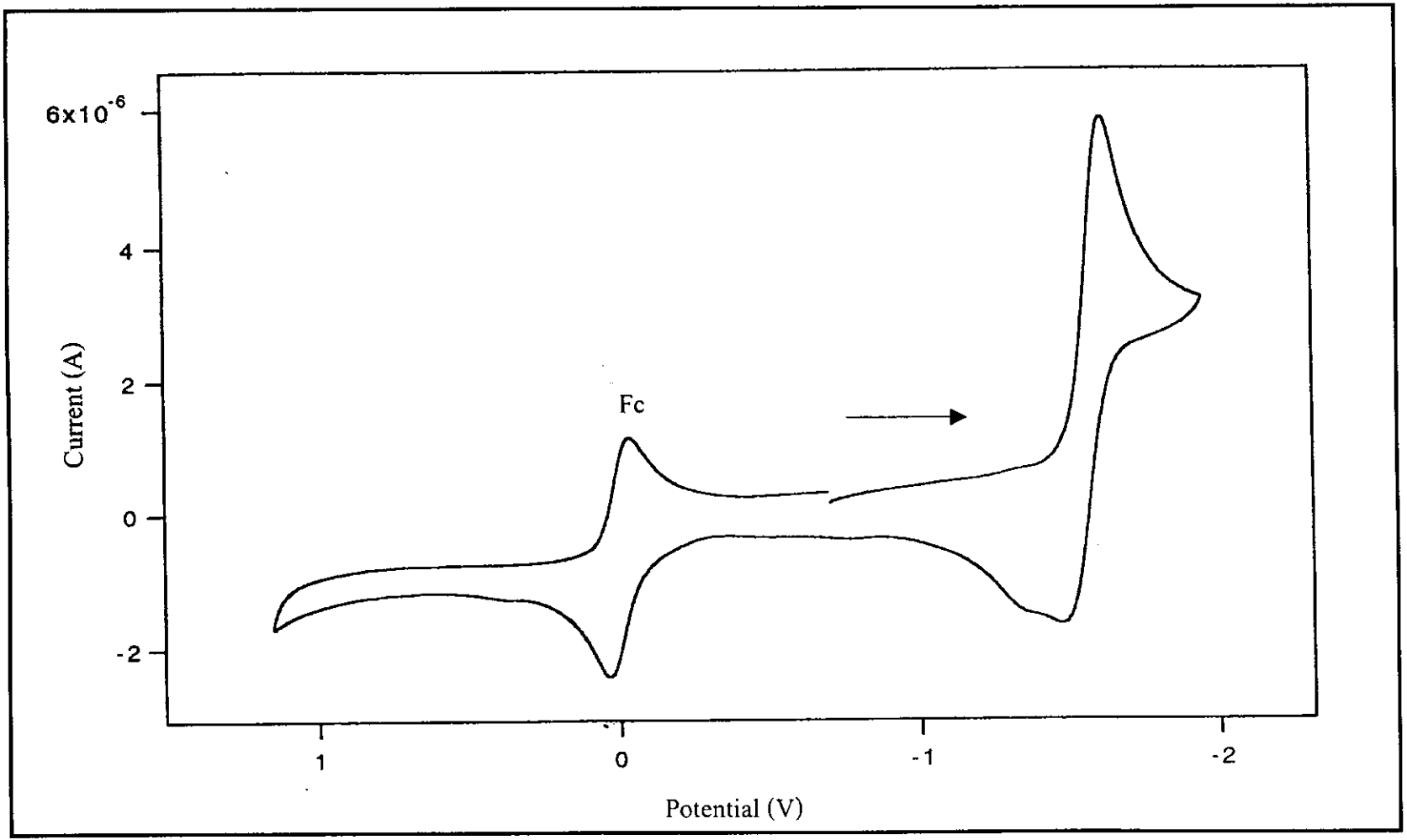

Figure 28 Cyclic voltammogram of azpy in 0.1 M TBAH CH_3CN at scan rate 50 mV/s.

3.2.7 X-ray Diffractometer

The X-ray crystallography is the most important technique to identify the geometries of ligand. The single crystal of 2,6-(diphenylazo)pyridine (diazpy) was grown by slowly diffusion of hexane into the dichloromethane solution. The crystallographic data are listed in Table 11 to 12. The crystal structure of diazpy is shown in Figure 29.

Table 11 Crystal and experimental data of the 2,6-(diphenylazo)pyridine ligand

Empirical formular	$C_{17}H_{13}N_5$
Formular weight	287.32
Crystal system	Triclinic
Space group	$P\bar{1}$
Unit cell dimention	a = 11.5978(8), α = 66.402(1)°
	b = 12.0235(9), β = 89.233(1)°
	c = 12.2389(9), γ = 75.760(1)°
Volume	1508.9(2) Å^3
Z	4
Temperature	293(2) K
Wavelength	0.71073
Density	0.632 mg/m^3
Absorption coefficient	0.040 nm^{-1}
Goodness-of-fit on F2	0.938
Final R indices [$I>2\sigma(I)$]	$R1$ = 0.0644, $wR2$ = 0.1438
R indices (all data)	$R1$ = 0.1281, $wR2$ = 0.1731

Table 12 The selected bond distances (Å) and angles (°) and their estimated standard deviations for 2,6-(diphenylazo)pyridine

		Distances	
N(1A)-N(2A)	1.246(2)	N(2A)-C(7A)	1.437(2)
N(4A)-N(5A)	1.240(2)	N(4A)-C(11A)	1.432(2)
N(1A)-C(1A)	1.422(3)	N(5A)-C(12A)	1.433(3)
		Angles	
C(1A)-N(1A)-N(2A)	114.46(18)	N(3A)-C(11A)-N(4A)	112.21(16)
N(1A)-N(2A)-C(7A)	112.84(17)	C(11A)-N(4A)-N(5A)	113.24(17)
N(2A)-C(7A)-N(3A)	112.04(16)	N(4A)-N(5A)-C(12A)	114.87(18)

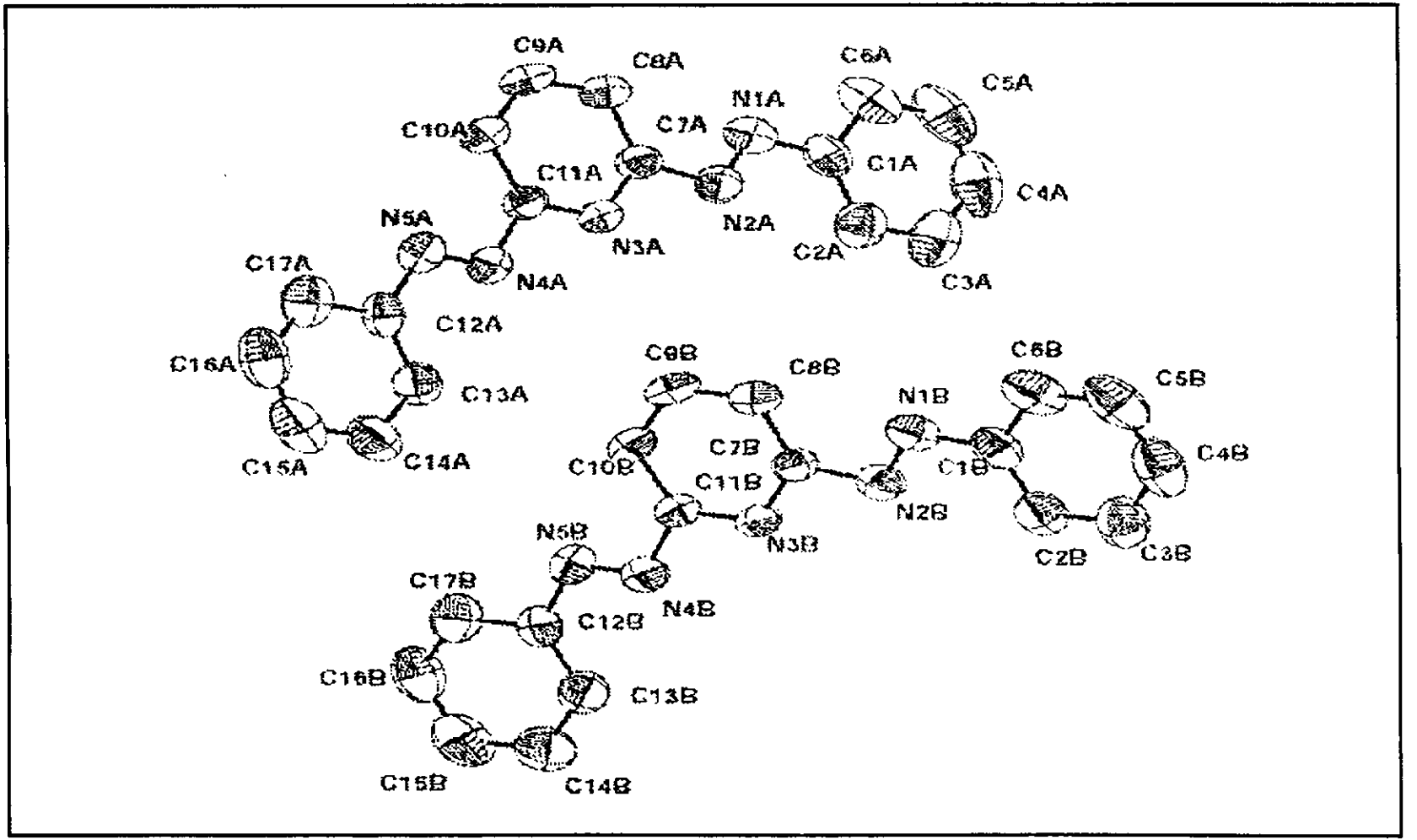

Figure 29 The structure of 2,6-(diphenylazo)pyridine.

3.3 Synthesis of the [Ru(diazpy)Cl_2] complex

The [Ru(diazpy)Cl_2] complex was obtained from reaction between $RuCl_3.3H_2O$ and diazpy in refluxing ethanol. It was purified by column chromatography on siliga gel with 2:1 toluene/acetonitrile as the eluent. The [Ru(diazpy)Cl_2] complex was used as precursor for synthesis the [Ru(diazpy)$(L)_2]^{2+}$ complexes. The physical properties of [Ru(diazpy)Cl_2] complex are summarized in Table 13.

Table 13 The physical properties of [Ru(diazpy)Cl_2] complex

Complex	Physical properties		
	Appearance	Color	Melting point (^{o}C)
[Ru(diazpy)Cl_2]	Solid	Black	More than 400

The solubility of 0.0015 g of [Ru(diazpy)Cl_2] complex was tested in 10 mL of water, methanol, ethanol, acetonitrile, acetone, ethyl acetate, dichloromethane and hexane solvents. This complex was slightly soluble in MeOH, EtOH and ethyl acetate and it was more soluble in acetonitrile and acetone. It was well soluble in dichloromethane but it was insoluble in water and hexane.

3.4 Characterization of the [Ru(diazpy)Cl_2] complex

Chemistry of the [Ru(diazpy)Cl_2] complex was characterized by using Elemental analysis, Electrospray mass spectrometry, Infrared spectroscopy, UV-Visible absorption spectroscopy, Nuclear Magnetic Resonance spectroscopy (1D and

2D). The electrochemical properties of all complexes were studied by using cyclic voltammetry techniques.

3.4.1 Elemental analysis

Elemental analysis was used to confirmed composition in complexes (%C, %N and %H). Results are given in Table 14.

Table 14 Elemental analysis data of the $[Ru(diazpy)Cl_2]$ complex

Complex	%C		%N		%H	
	Calc.	Found	Calc.	Found	Calc.	Found
$[Ru(diazpy)Cl_2]$	44.46	44.05	15.31	15.67	2.85	2.99

3.4.2 Fast-atom bombardment (FAB) mass spectrometry

The FAB mass spectrum of $[Ru(diazpy)Cl_2]$ complex is shown in Figure 30. The results of this technique are shown in the Table 15.

Table 15 FAB mass spectroscopic data of $[Ru(diazpy)Cl_2]$ complex

m/z	Stoichiometry	Equivalent species	Rel. Abun. (%)
423	$[Ru(diazpy)Cl_2]$ -Cl$]^+$	$[M\text{-}Cl]^+$	100
389	$[Ru(diazpy)Cl_2]$ -2Cl$]^+$	$[M\text{-}2Cl]^{2+}$	99
458	$[Ru(diazpy)Cl_2]$	[M]	60

M = molecular weight (MW) of $[Ru(diazpy)Cl_2]$ complex

MW of $[Ru(diazpy)Cl_2]$ = 459.25 g/mol

From the data, the parent peak, which gave 100% relative abundance at m/z 423 corresponded to the molecular weight of $[Ru(diazpy)Cl_2]$ minus one Cl atom. Moreover, the parent peaks at m/z 389 (99%) and 458 (60%) corresponded to molecular weight of $[Ru(diazpy)Cl_2]$ minus two Cl atoms and $[Ru(diazpy)Cl_2]$, respectively. So expected structure will be confirmed by this method.

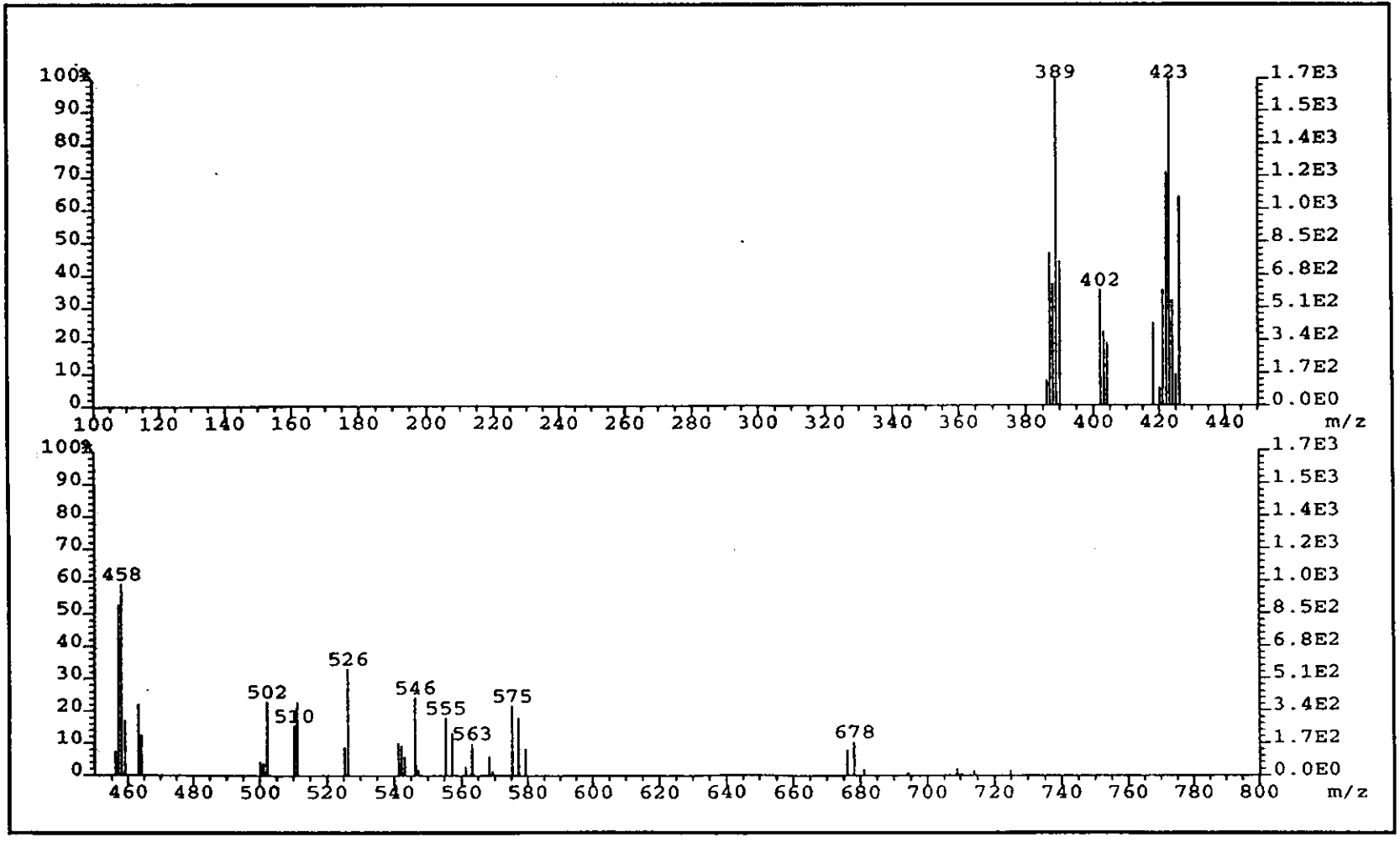

Figure 30 FAB mass spectrum of [Ru(diazpy)Cl_2].

3.4.3 UV-Visible absorption spectroscopy

The electronic transitions property of the [Ru(diazpy)Cl_2] complex was studied by UV-Visible absorption spectroscopy technique. The UV-Visible absorption spectra data of this complex exhibited in the range 200-800 nm in CH_3CN, EtOH, MtOH, DMF, DMSO and CH_2Cl_2 solvents. In addition, the absorption spectra of this [Ru(diazpy)Cl_2] complex in CH_3CN solution are shown in Figure 31. The spectroscopic data is summarized in Table 16.

Table 16 UV-visible absorption spectroscopic data of [Ru(diazpy)Cl_2] complex

Complex	λ_{max} nm, ($\varepsilon^a \times 10^{-4}$ M^{-1} cm^{-1})					
	CH_2Cl_2	CH_3CN	DMF	DMSO	EtOH	MeOH
[Ru(diazpy)Cl_2]	294 (1.50)	287 (2.80)	298 (1.40)	296 (1.10)	299 (1.70)	298 (1.62)
	428 (0.72)	426 (0.92)	430 (0.53)	433 (0.64)	423 (0.79)	425 (0.68)
	523 (0.21)	522 (0.26)	-	-	519 (0.19)	-
	612 (0.14)	610 (0.16)	-	-	608 (0.12)	621 (0.13)

[a]Molar Extinction coefficient

The absorption spectra of [Ru(diazpy)Cl_2] complex displayed the bands in both UV and visible region (200-800 nm). The absorption occurring in UV region ($\varepsilon \sim$ 10000 – 28000 $M^{-1}cm^{-1}$) were assigned to $\pi \rightarrow \pi^*$ transitions in ligand.

In visible region (400-800 nm), this complex showed intense one absorption band ($\varepsilon \sim$ 5000 – 9500 $M^{-1}cm^{-1}$) near 400 nm and two weak bands near 500 nm and 600 nm (Figure 31). The absorption bands occurring in visible region were assigned to

metal-to-ligand charge-transfer transition (MLCT) due to transfer of an electron from d orbitals of metal to empty π^* orbitals of ligand.

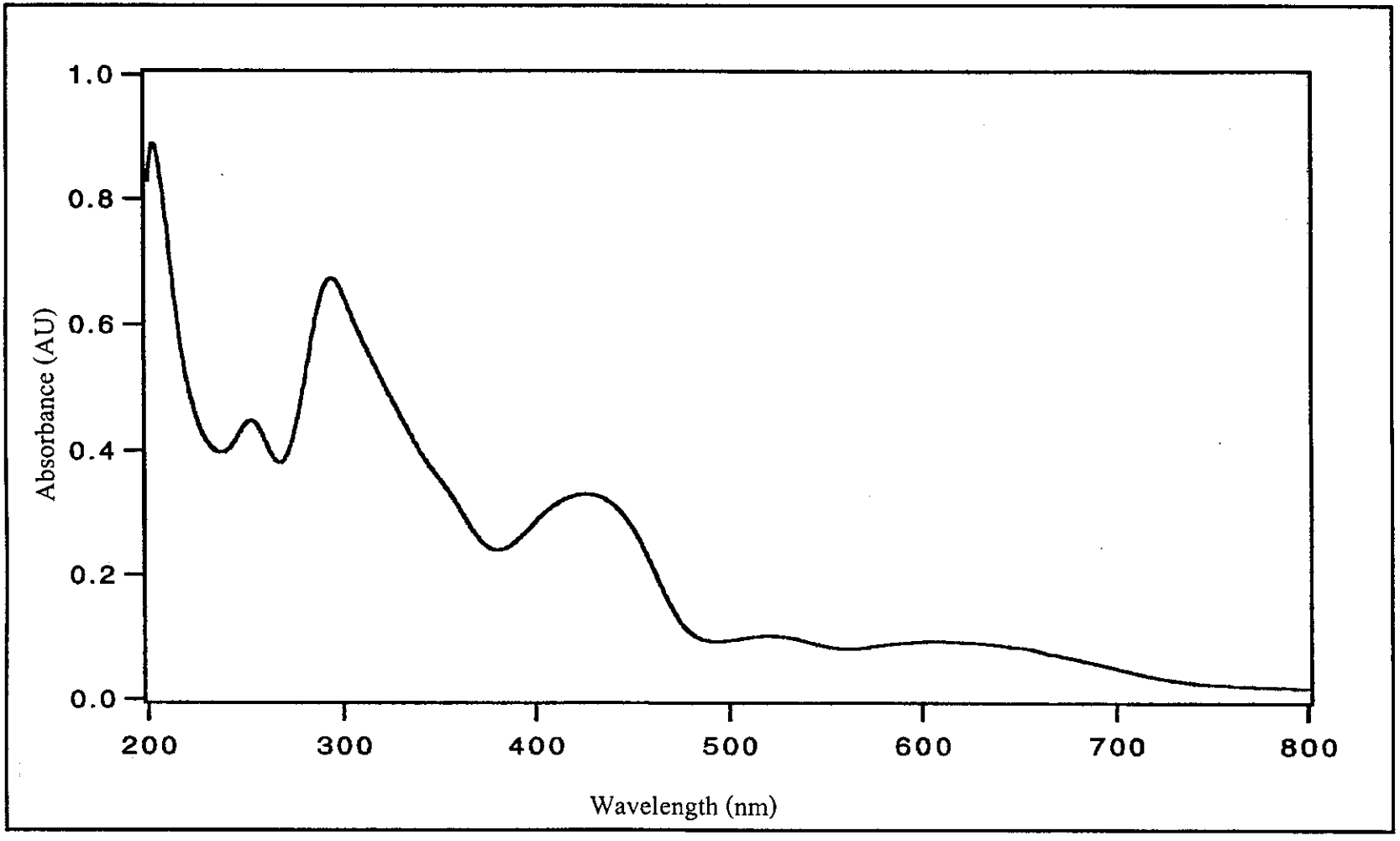

Figure 31 UV-Visible absorption spectrum of $[Ru(diazpy)Cl_2]$ in CH_3CN.

3.4.4 Infrared spectroscopy

The vibrational spectra in the range 4000-370 cm^{-1} could be used to give information about ligands coordinated to the ruthenium center. Infrared spectrum of [Ru(diazpy)Cl_2] complex was recorded in a KBr disc and is shown in Figure 32. The interesting intense vibration frequencies of this complex were C=C, C=N, N=N (azo) stretching vibration and C-H bending of monosubstituted benzene. The infrared spectroscopic data of this are shown in Table 17.

Table 17 Infrared spectroscopic data of the [Ru(diazpy)Cl_2] complex

Vibration modes	Frequencies (cm^{-1})
	[Ru(diazpy)Cl_2]
C=N, C=C stretching	1583(w) 1480(w) 1456(m)
N=N stretching	1246 (s) 1229 (s)
C-H bending of monosubstituted benzene	803(s) 769(s) 687(s)

s = strong, m = medium, w = weak,

Infrared spectrum of [Ru(diazpy)Cl_2] complex showed many vibrations of different intensities below 1,600 cm^{-1} and two intense peaks of N=N stretching similar to in free diazpy ligand. But the N=N stretching modes in this complex (1246 cm^{-1} and 1229 cm^{-1}) was shifted to lower frequencies from the free diazpy ligand (1447 cm^{-1} and 1420 cm^{-1}).

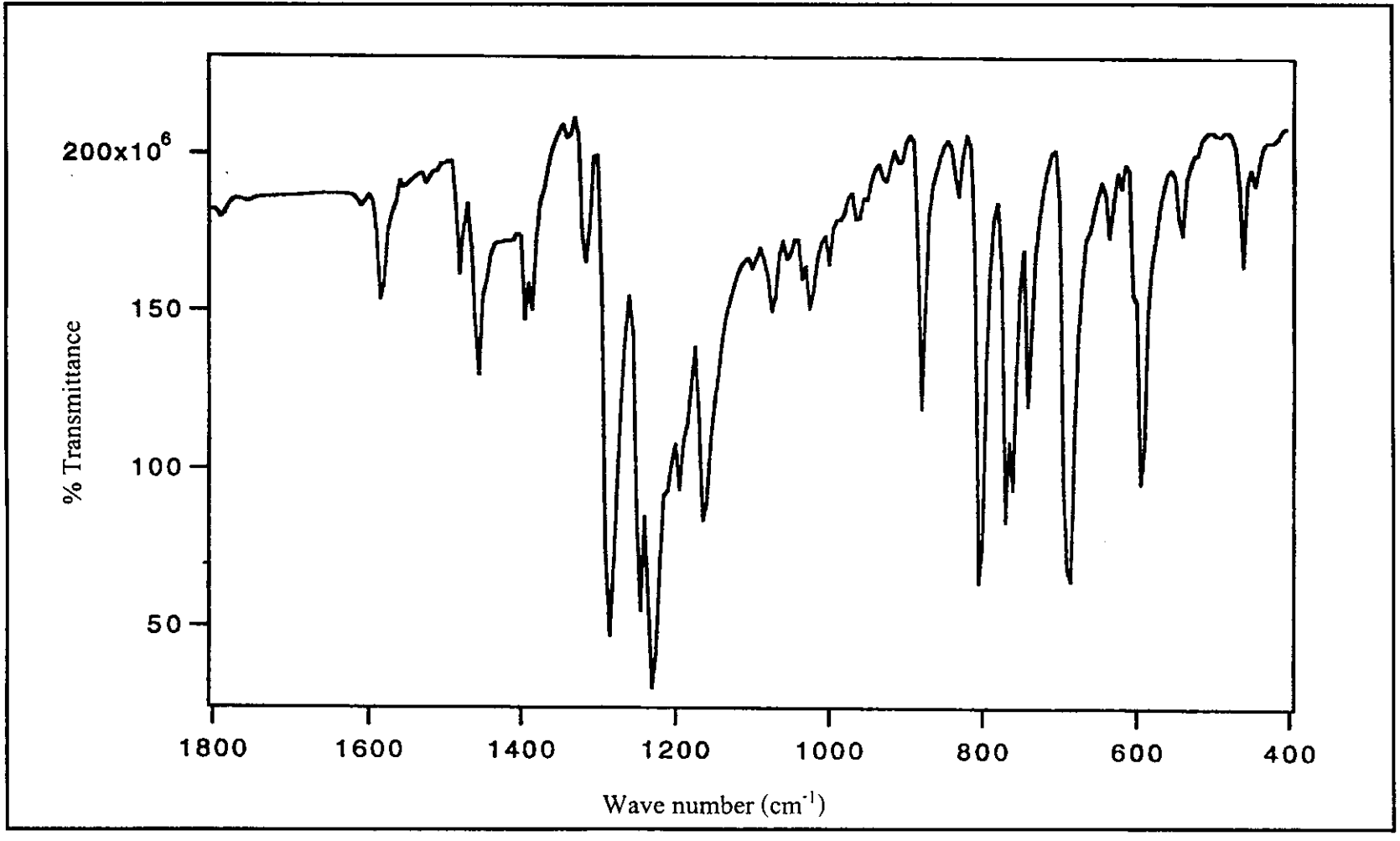

Figure 32 IR spectrum of [Ru(diazpy)Cl_2].

3.4.5 Nuclear Magnetic Resonance spectroscopy

Both 1D and 2D NMR techniques were used to determine molecular structure of the [Ru(diazpy)Cl_2] complex. All NMR spectra of this complex were recorded in $CDCl_3$. The tetramethylsilane (TMS, $(CH_3)_4Si$) was used as an internal reference. The ^1H NMR, ^1H-^1H COSY, ^{13}C NMR, DEPT, ^1H-^{13}C HMQC spectrum of [Ru(diazpy)Cl_2] complex are shown in Figure 33, 34, 35, 36 and 37, respectively. The ^1H and ^{13}C NMR spectral data of [Ru(diazpy)Cl_2] complex are listed in Table 18.

Table 18 ^1H and ^{13}C NMR spectroscopic data of the [Ru(diazpy)Cl_2] complex

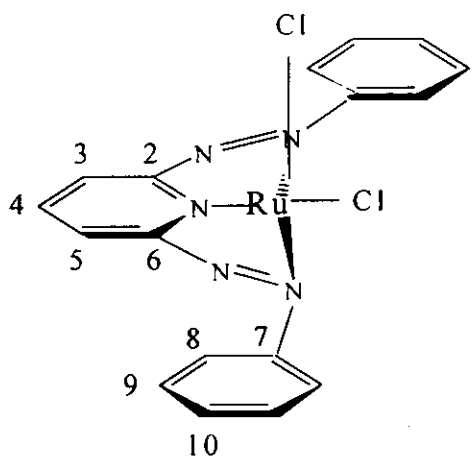

H-Position	^1H NMR			^{13}C NMR
	δ (ppm)	*J* (Hz)	Number of H	δ (ppm)
3 (5)	8.58 (d)	8.1	2	120.69
8	8.29 (d)	7.5	4	128.94
4	8.08 (t)	8.1, 8.1	1	132.68

Table 18 (continued)

H-Position	^{1}H NMR			^{13}C NMR
	δ (ppm)	*J* (Hz)	Number of H	δ (ppm)
10	7.56 (m)	-	6	131.99
9				123.31
Quaternary carbon				168.37 154.65

m = multiplet, d = doublet, dd = doublet of doublet, t = triplet

The ^{1}H NMR spectrum of [Ru(diazpy)Cl_2] complex appeared five signals as same as free ligand, but some protons in molecule showed different chemical shifts.

The signal of proton H3 (H5) exhibited at lower field than proton H4 due to decreasing electron density induced by positive ruthenium center. Therefore, the proton H3 (5), which located next to azo nitrogen occurred at the most downfield. The signal was splitted by proton H4 (J = 8.1 Hz). The signal appeared as doublet peak at 8.58 ppm. The triplet peak of proton H4 occurred at 8.08 ppm. It was splitted by proton H3 and H5 (J = 8.1, 8.1 Hz).

The signals of proton H8, H9 and H10 on both phenyl rings appeared at similar position to free ligand. The doublet peak of proton H8 appeared at 8.29 ppm. It was splitted by proton H9 (J = 7.5 Hz), but it did not show any coupling with proton H10. The signal of proton H9 showed multiplet peaks, which resonated at the same position of proton H10 at 7.56 ppm.

Furthermore, The ^{13}C NMR (Figure 35) results corresponded to the DEPT signals (Figure 36) as same as these results of free ligand, but each signal slightly shifted to lower field than free ligand. The downfield resonances at 168.37 and 154.65 ppm were assigned to two equivalent quaternary carbons (C2 and C6) on pyridine ring

and two equivalent quaternary carbons (C7 of both phenyl rings), respectively. The methine carbons occurring at 120.69, 128.94, 132.68, 131.99 and 123.31 ppm were assigned to two equivalent carbons (C3 and C5), four equivalent carbons C8, C4, two equivalent carbons C10 and C9, respectively.

In addition, the ^{13}C NMR signals assignments were based on the ^{1}H-^{13}C HMQC spectrum (Figure 37), which exhibited correlation between ^{1}H NMR spectrum and ^{13}C NMR spectrum.

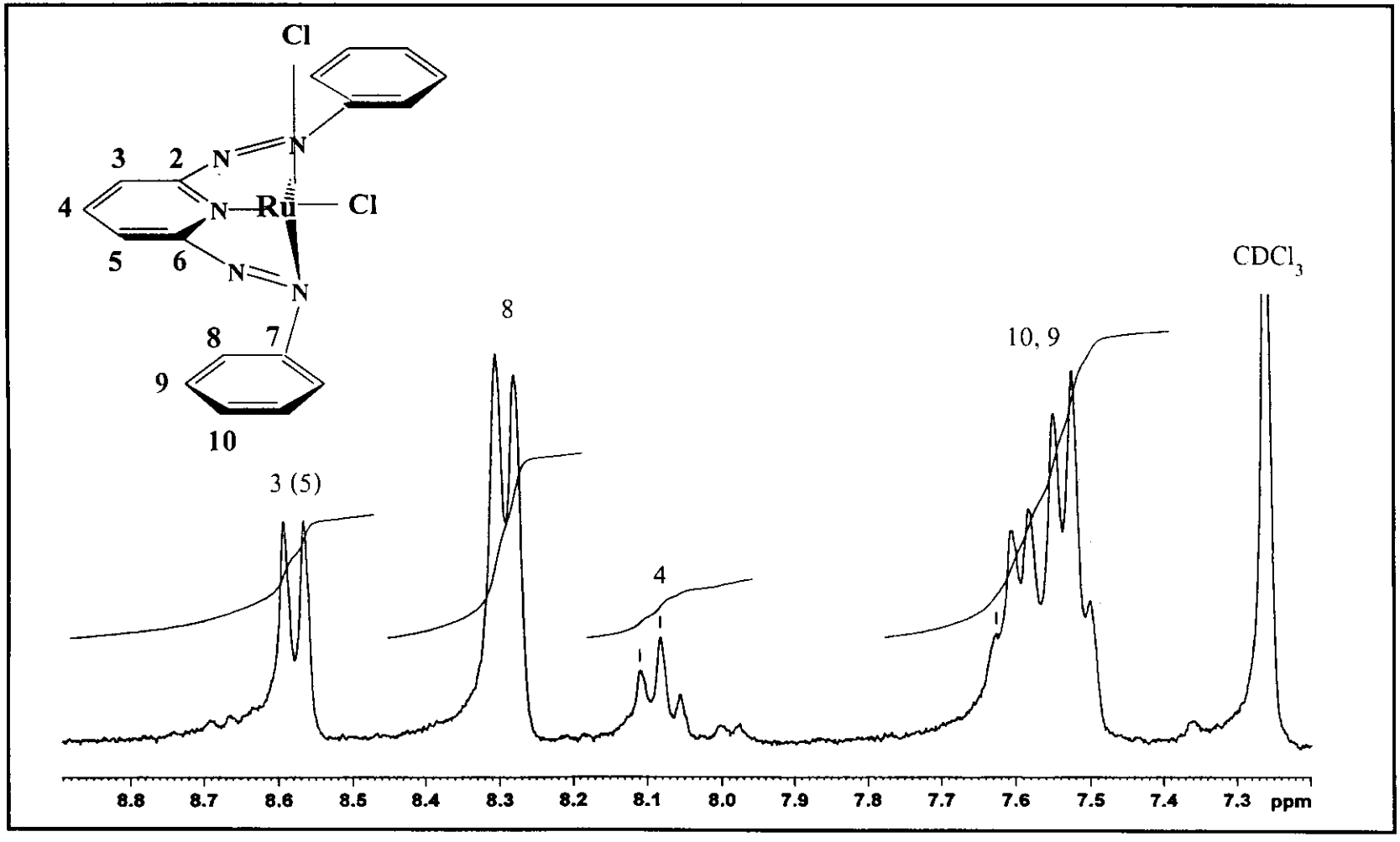

Figure 33 ^{1}H NMR spectrum of [Ru(diazpy)Cl_2] in $CDCl_3$.

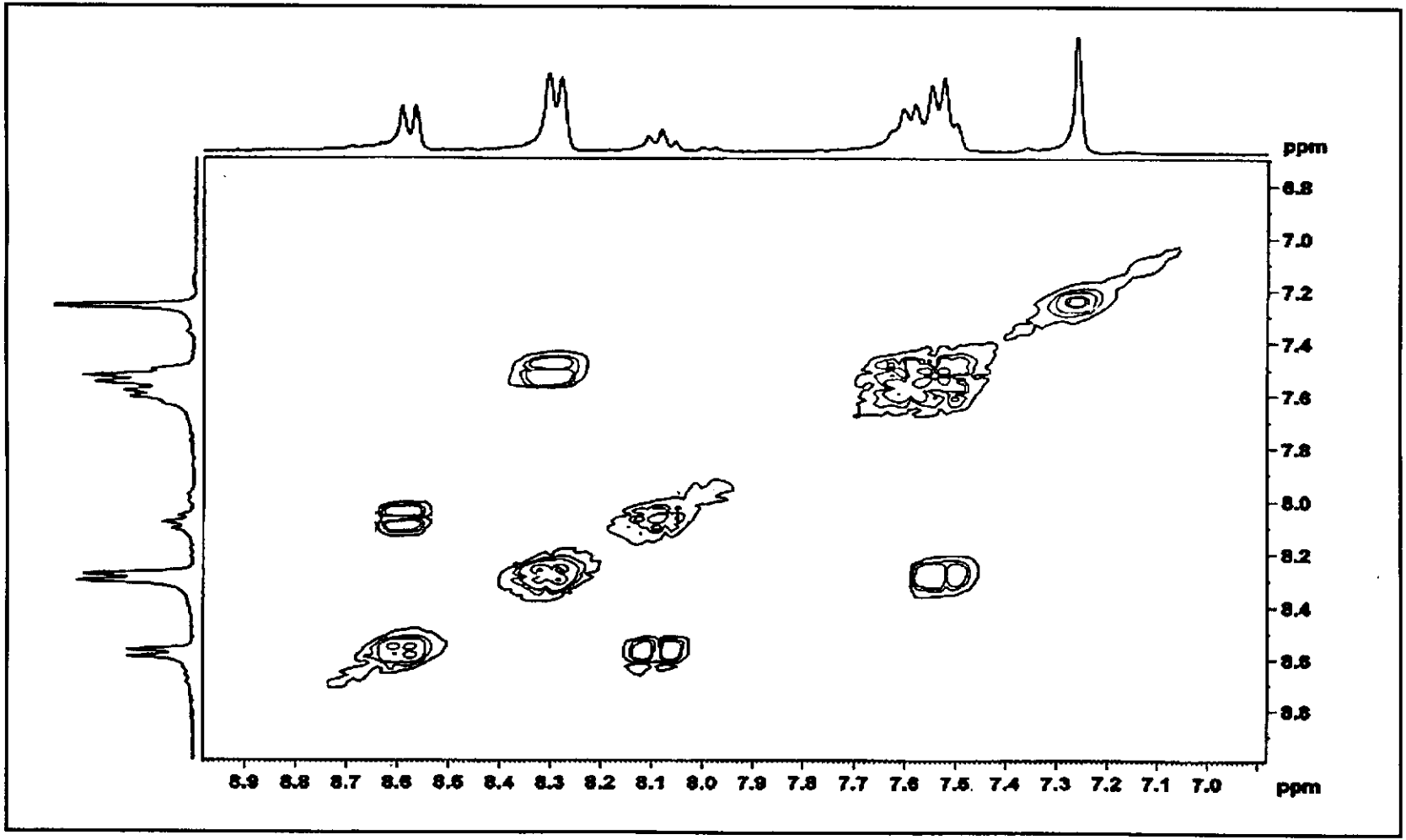

Figure 34 ^{1}H- ^{1}H COSY NMR spectrum of $[Ru(diazpy)Cl_2]$ in $CDCl_3$.

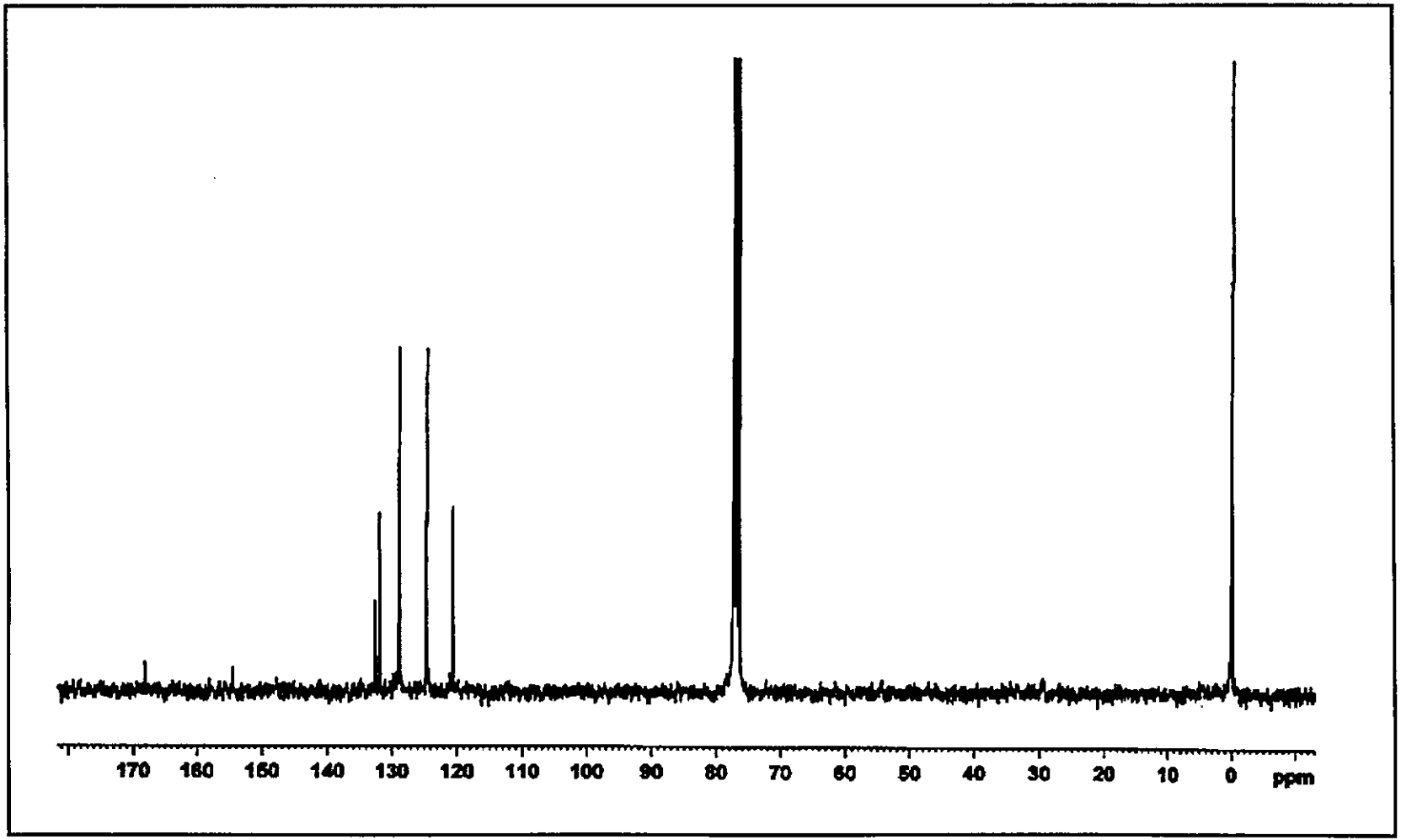

Figure 35 ^{13}C NMR spectrum of $[Ru(diazpy)Cl_2]$ in $CDCl_3$.

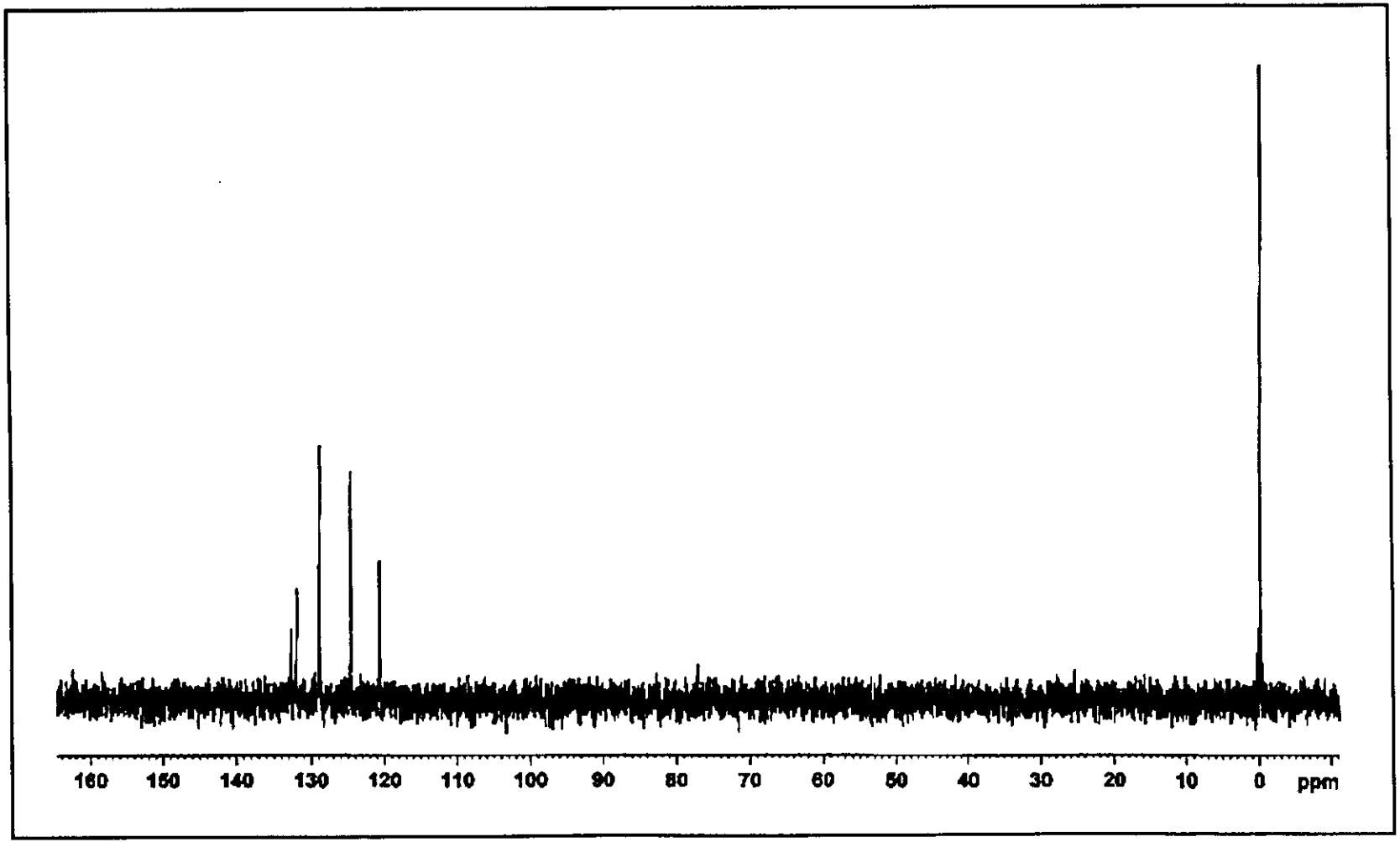

Figure 36 DEPT NMR spectrum of [Ru(diazpy)Cl_2] in $CDCl_3$.

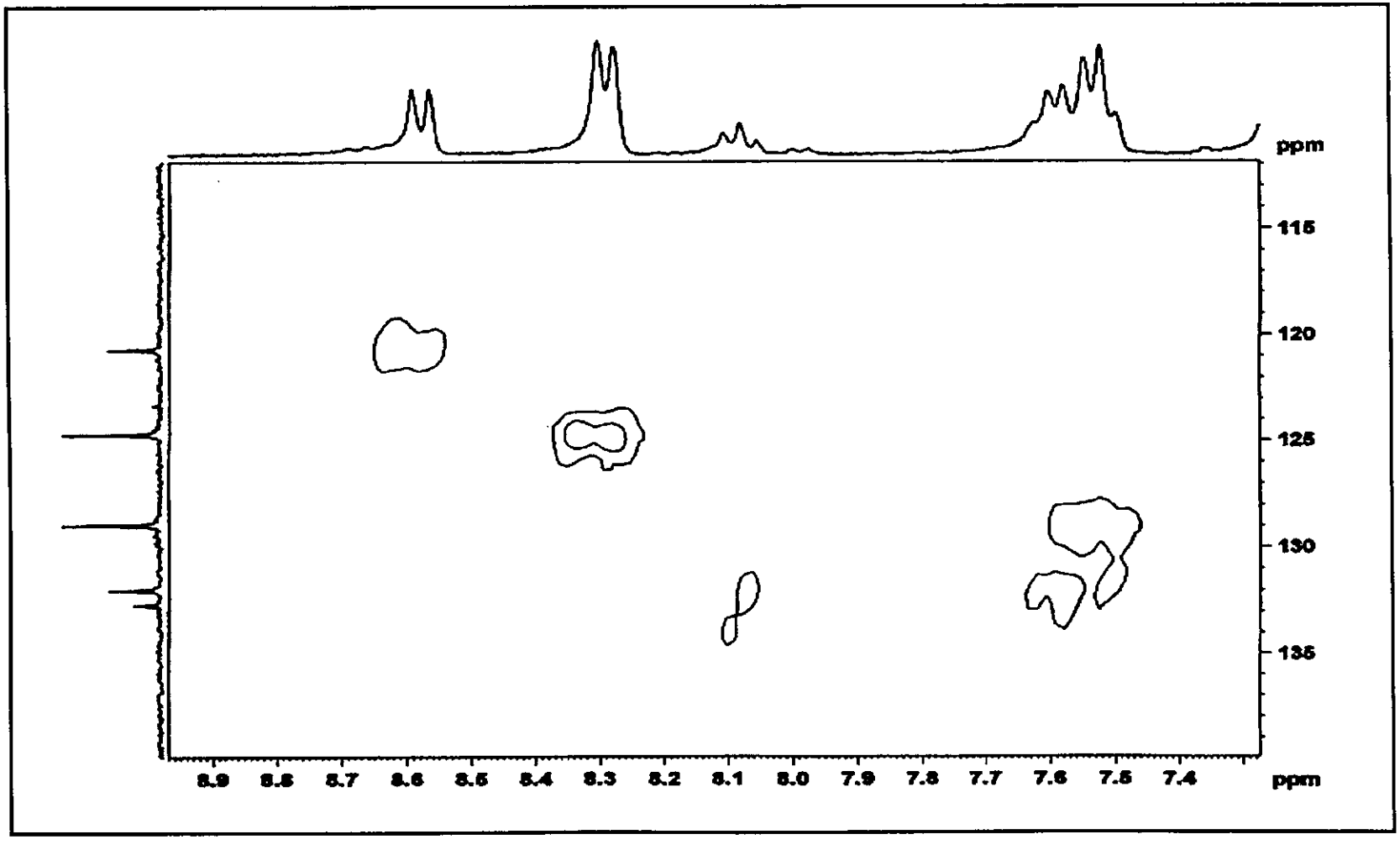

Figure 37 ^{1}H-^{13}C HMQC NMR spectrum of $[Ru(diazpy)Cl_2]$ in $CDCl_3$.

3.4.6 Cyclic Voltammetry

Cyclic voltammetry is a technique to study the redox properties of the [Ru(diazpy)Cl_2] complex. The electron transfer properties of this complex are shown in Figure 38 with corresponding half-wave potentials. The cyclic voltammogram of complex showed metal oxidation in oxidation range and ligand reduction in the reduction range. Furthermore, the potentials were compared to the potential of ferrocence couple ($E_{1/2}$ = 0 V, ΔE_p 80 mV). The cyclic voltammetric data of this complex is listed in Table 19.

Table 19 Cyclic voltammetric data of [Ru(diazpy)Cl_2] in 0.1 M TBAH acetonitrile at scan rate 50 mV/s (ferrocene as an internal standard, ΔE_p 80 mV)

Complex	$E_{1/2}$, V, (ΔE, mV)	
	Oxidation	Reduction
[Ru(diazpy)Cl_2]	+0.76 (110)	-0.79 (85) -1.12[c] -1.68 (120)

[c]cathodic peak

Oxidation Potential

The potential of the [Ru(diazpy)Cl_2] complex was studied in the range 0.00 to +1.45 V. One reversible couple of Ru(II)/Ru(III) was observed at +0.76 V. This couple corresponded to one electron transfer in comparison with ferrocene couple.

Reduction Potential

In the potential range from 0.00 to –1.60 V, three couples occurred. The peak at –0.79 and –1.68 V were reversible couple at higher scan rates. Whereas, the peak at –1.12 V was irreversible (Figure 38).

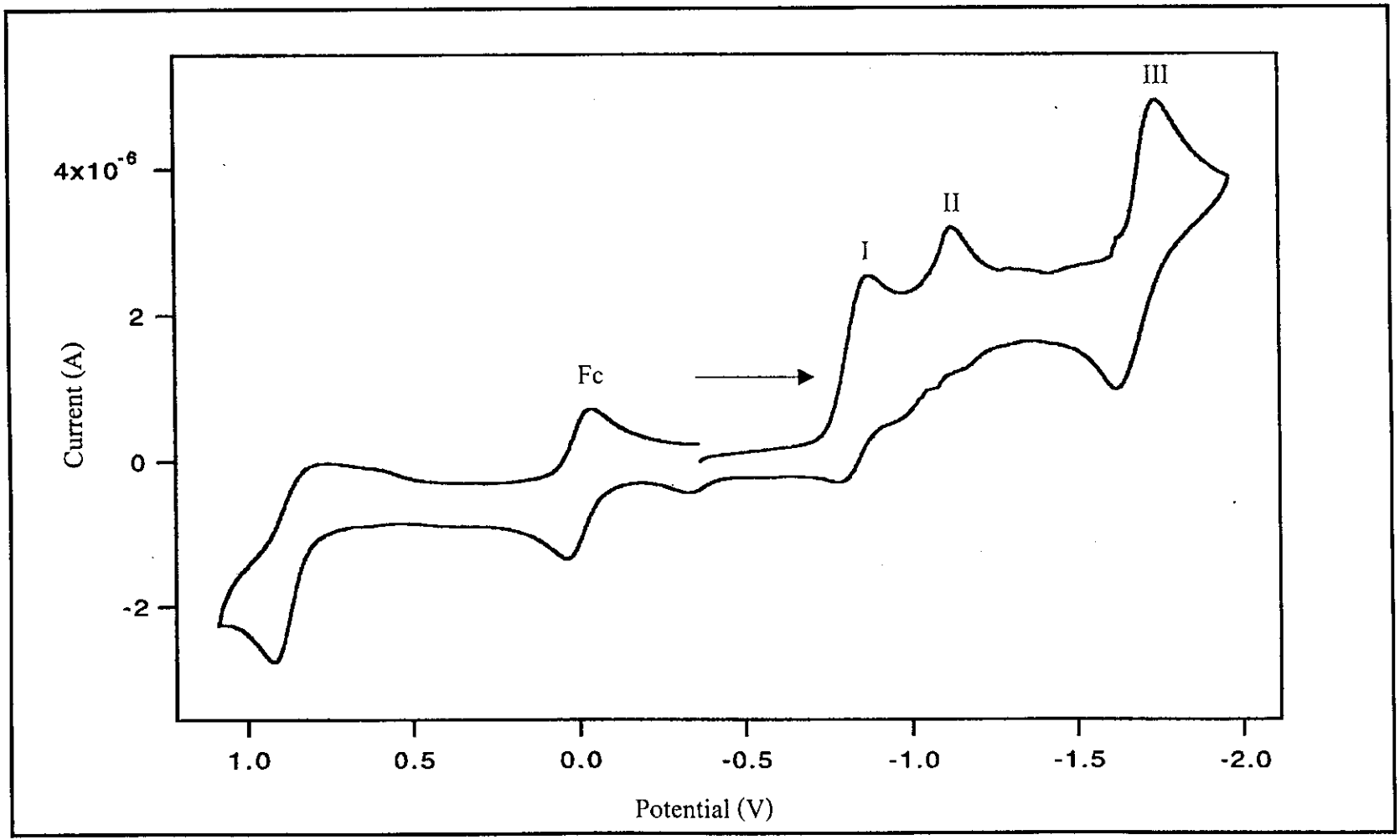

Figure 38 Cyclic voltammogram of [Ru(diazpy)Cl_2] in 0.1 M TBAH CH_3CN at scan rate 50 mV/s.

3.5 Syntheses of the $[Ru(diazpy)(L)_2]^{2+}$ (L = azpy, bpy and phen) complexes

The $[Ru(diazpy)(L)_2]^{2+}$ complexes (where L = azpy, bpy and phen) were synthesized by reaction of $[Ru(diazpy)Cl_2]$ and excess L ligands in refluxing methanol in a presence of NEt_3. Whereas, the $[Ru(diazpy)(L)_2]^{2+}$ (where L = azpy) was obtained when $AgNO_3$ was added in refluxing methanol. However, all complexes were precipitated by BF_4^- salt. The physical properties of all complexes are summarized in Table 20.

Table 20 The physical properties of the $[Ru(diazpy)(L)_2]^{2+}$ complexes (L = azpy, bpy and phen)

Complexes	Physical properties		
	Appearance	Color	Melting point (^oC)
$[Ru(diazpy)(azpy)_2](BF_4)_2$	Solid	Dark red	248-249
$[Ru(diazpy)(bpy)_2](BF_4)_2$	Solid	Dark red	285-286
$[Ru(diazpy)(phen)_2](BF_4)_2$	Solid	Red	260-261

The complexes were highly soluble in polar aprotic solvents such as acetonitrile, acetone, dimethylsulfoxide (DMSO), *N,N*-dimethylformamide (DMF). They were moderately soluble in methanol, ethanol, dichloromethane and insoluble in hexane ethyl acetate and benzene.

3.6 Characterization of the $[Ru(diazpy)(L)_2]^{2+}$ complexes

Chemistry of the $[Ru(diazpy)(L)_2]^{2+}$ complexes were characterized by using Elemental analysis, Electrospray mass spectrometry, Infrared spectroscopy, UV-Visible absorption spectroscopy, Nuclear Magnetic Resonance spectroscopy (1D and 2D techniques). The electrochemical properties of all complexes were studied by using cyclic voltammetry technique.

3.6.1 Elemental analysis

Elemental analysis was used to confirm composition in complexes (%C, %N and %H). Results are given in Table 21.

Table 21 Elemental analysis data of the $[Ru(diazpy)(L)_2]^{2+}$ complexes (L = azpy, bpy and phen)

Complexes	%C		%N		%H	
	Calc.	Found	Calc.	Found	Calc.	Found
$[Ru(diazpy)(azpy)_2](BF_4)_2$	50.45	50.02	16.59	16.53	3.36	3.31
$[Ru(diazpy)(bpy)_2](BF_4)_2$	50.82	50.98	14.47	14.49	3.32	3.32
$[Ru(diazpy)(phen)_2](BF_4)_2$	53.38	52.14	13.66	13.38	3.17	3.16

3.6.2 FAB mass spectrometry

The FAB mass spectra of $[Ru(diazpy)(L)_2](BF_4)_2$ complexes, where L = azpy, bpy and phen are displayed in Figure 39 to 41. The important FAB mass spectroscopic data of complexes with the corresponding relative abundance are listed in Table 22.

Table 22 FAB mass spectroscopic data of $[Ru(diazpy)(L)_2](BF_4)_2$ complexes (L = azpy, bpy and phen)

m/z	Stoichiometry	Equivalent species	Rel. Abun. (%)
$[Ru(diazpy)(azpy)_2](BF_4)_2$			
755	$[Ru(diazpy)(azpy)_2]^{2+}$	$[M-2(BF_4)]^{2+}$	100
$[Ru(diazpy)(bpy)_2](BF_4)_2$			
788	$[Ru(diazpy)(bpy)_2]^{+}(BF_4)$	$[M-BF_4]^{+}$	100
701	$[Ru(diazpy)(azpy)_2]^{2+}$	$[M-2(BF_4)]^{2+}$	42
$[Ru(diazpy)(phen)_2](BF_4)_2$			
836	$[Ru(diazpy)(phen)_2]^{+}(BF_4)$	$[M-BF_4]^{+}$	100
749	$[Ru(diazpy)(azpy)_2]^{2+}$	$[M-2(BF_4)]^{2+}$	90

M = molecular weight (MW) of each complexes

MW of $[Ru(diazpy)(azpy)_2](BF_4)_2$ = 928.25 g/mol

MW of $[Ru(diazpy)(bpy)_2](BF_4)_2$ = 874.37 g/mol

MW of $[Ru(diazpy)(phen)_2](BF_4)_2$ = 922.44 g/mol

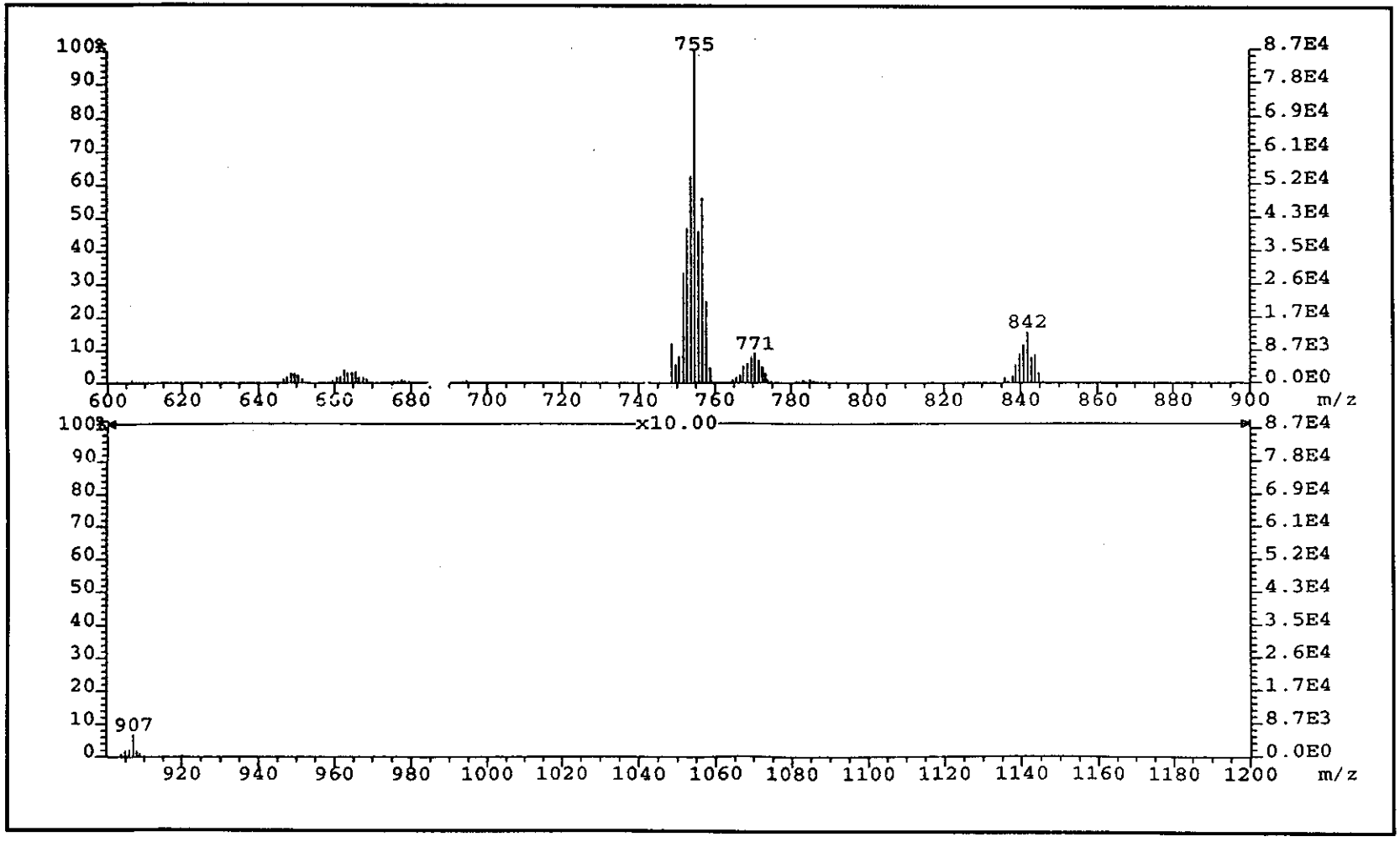

Figure 39 FAB mass spectrum of $[Ru(diazpy)(azpy)_2](BF_4)_2$.

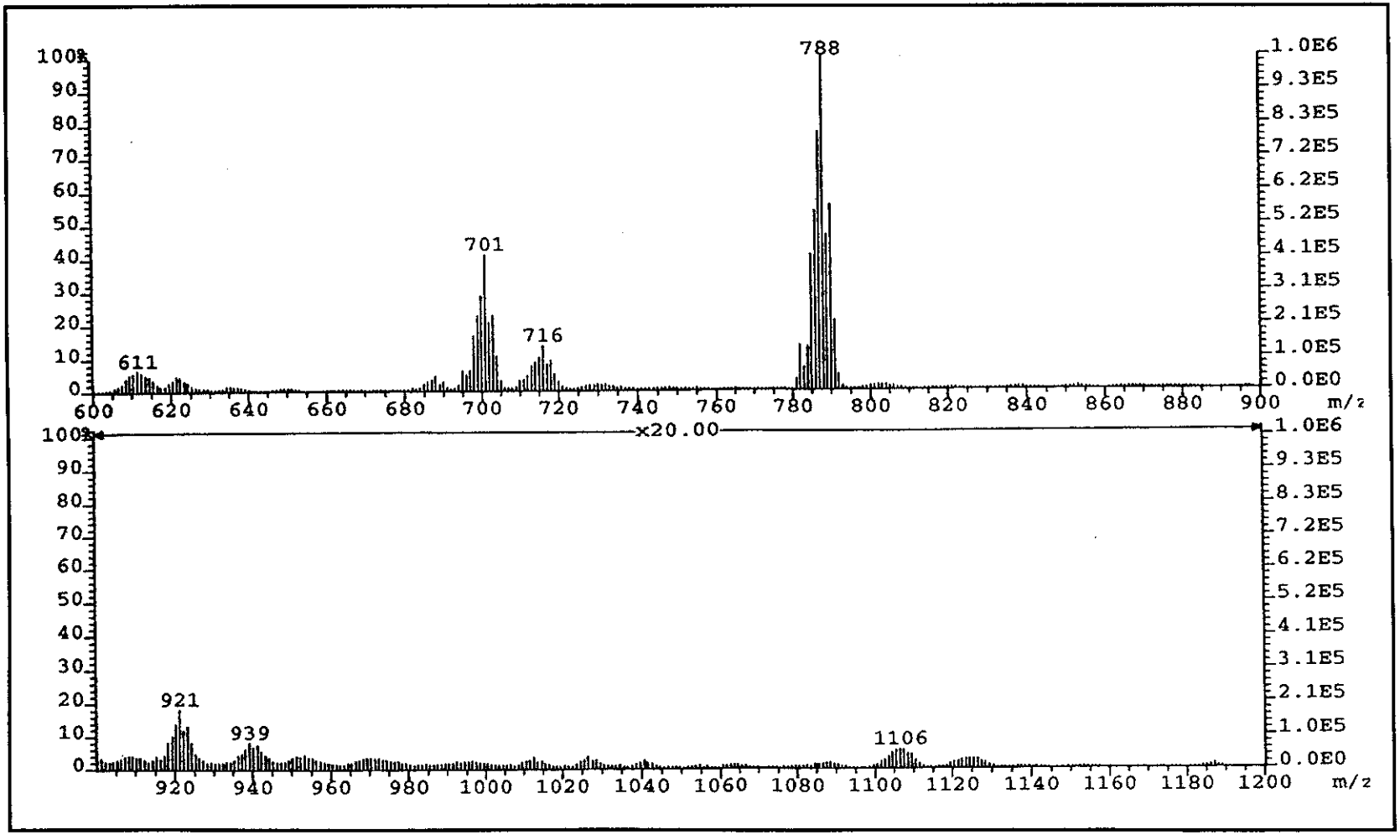

Figure 40 FAB mass spectrum of $[Ru(diazpy)(bpy)_2](BF_4)_2$.

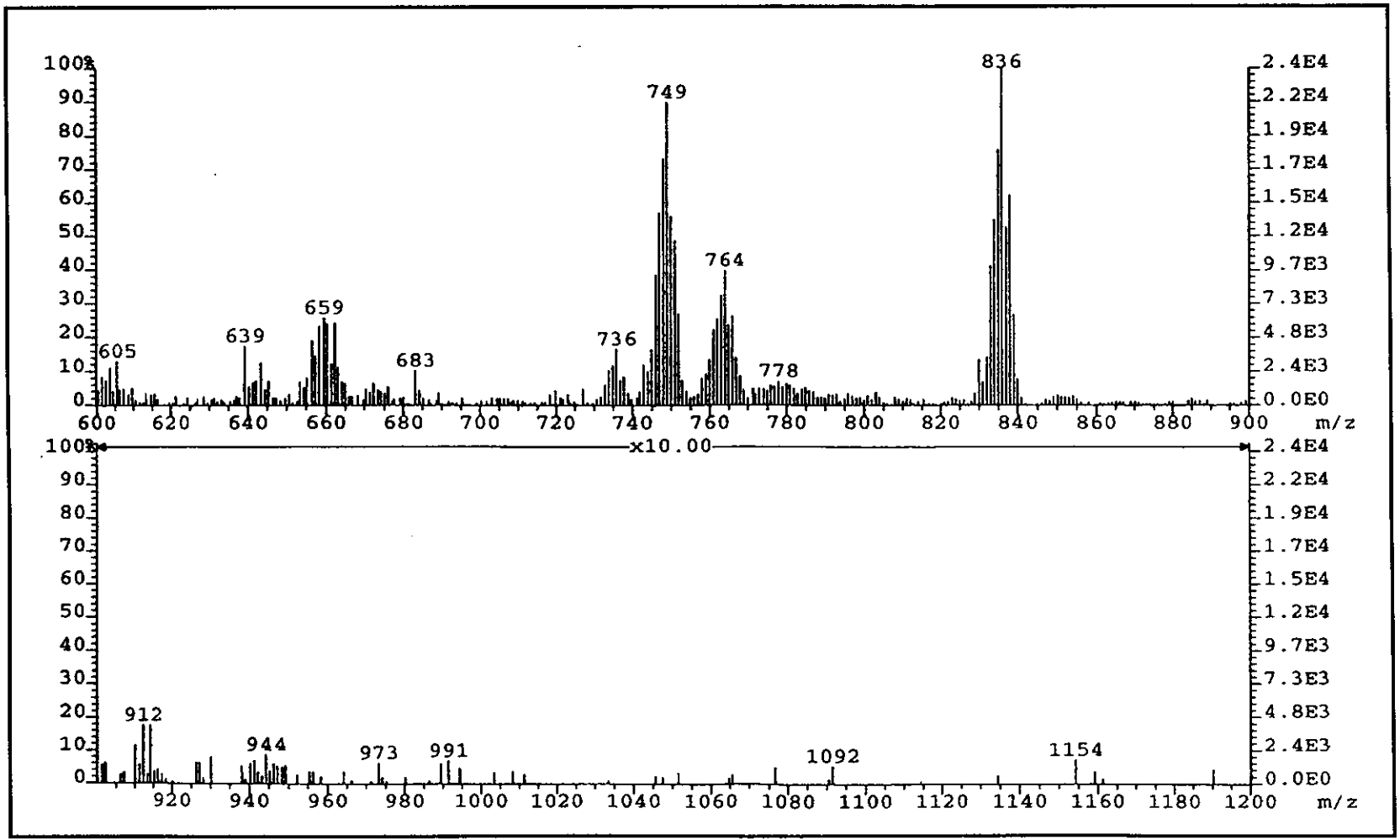

Figure 41 FAB mass spectrum of $[Ru(diazpy)(phen)_2](BF_4)_2$.

3.6.3 UV-Visible absorption spectroscopy

The UV-Visible absorption spectra of $[Ru(diazpy)(L)_2](BF_4)_2$ complexes, where L = azpy, bpy and phen in acetonitrile solution are shown in Figure 42-44. Electronic spectra of these complexes were recorded in six solvents; dimethylsulfoxide (DMSO), *N,N*-dimethylformamide (DMF), dichloromethane, ethanol and methanol.

Table 23 UV-Visible absorption spectroscopic data of the $[Ru(diazpy)(L)_2](BF_4)_2$ complexes (L = azpy, bpy and phen) in various solvents

Complexes	λ_{max} nm, ($\varepsilon^a \times 10^{-4}$ M^{-1} cm^{-1})					
	CH_2Cl_2	CH_3CN	DMF	DMSO	EtOH	MeOH
$[Ru(diazpy)(azpy)_2]^{2+}$	282 (2.1)	280 (2.3)		280 (2.3)	285 (2.0)	281 (1.9)
	375 (3.4)	367 (3.1)	362 (3.6)	368 (3.0)	368 (3.4)	367 (3.5)
	489 (0.6)	491 (0.8)	487 (0.4)	492 (0.7)	493 (0.8)	490 (0.7)
$[Ru(diazpy)(bpy)_2]^{2+}$	277 (4.2)	278 (4.0)		277 (3.9)	273 (4.1)	278 (4.1)
	375 (2.3)	364 (1.7)	366 (2.1)	366 (1.9)	368 (2.0)	365 (1.8)
	504 (0.6)	502 (0.6)	503 (0.8)	502 (0.8)	500 (0.7)	500 (0.6)
$[Ru(diazpy)(phen)_2]^{2+}$	263 (6.2)	264 (7.1)			263 (6.8)	265 (8.9)
	360 (1.9)	352 (1.9)	352 (2.0)	350 (2.7)	351 (2.3)	353 (1.5)
	500 (0.6)	502 (0.5)	506 (0.7)	506 (1.0)	502 (0.9)	506 (0.6)

[a]Molar Extinction coefficient

The absorption spectra in UV region (200-400 nm) were assigned to $\pi \rightarrow \pi^*$ transitions of ligand ($\varepsilon \sim 10000 - 90000$ $M^{-1}cm^{-1}$). While, the absorption bands in visible region (400-800 nm) were assigned to metal-to-ligand charge-transfer

transition (MLCT) ($\varepsilon \sim 4000 - 10000\ M^{-1}cm^{-1}$). The absorption bands of all complexes were not shifted when polarity of solvents was increased.

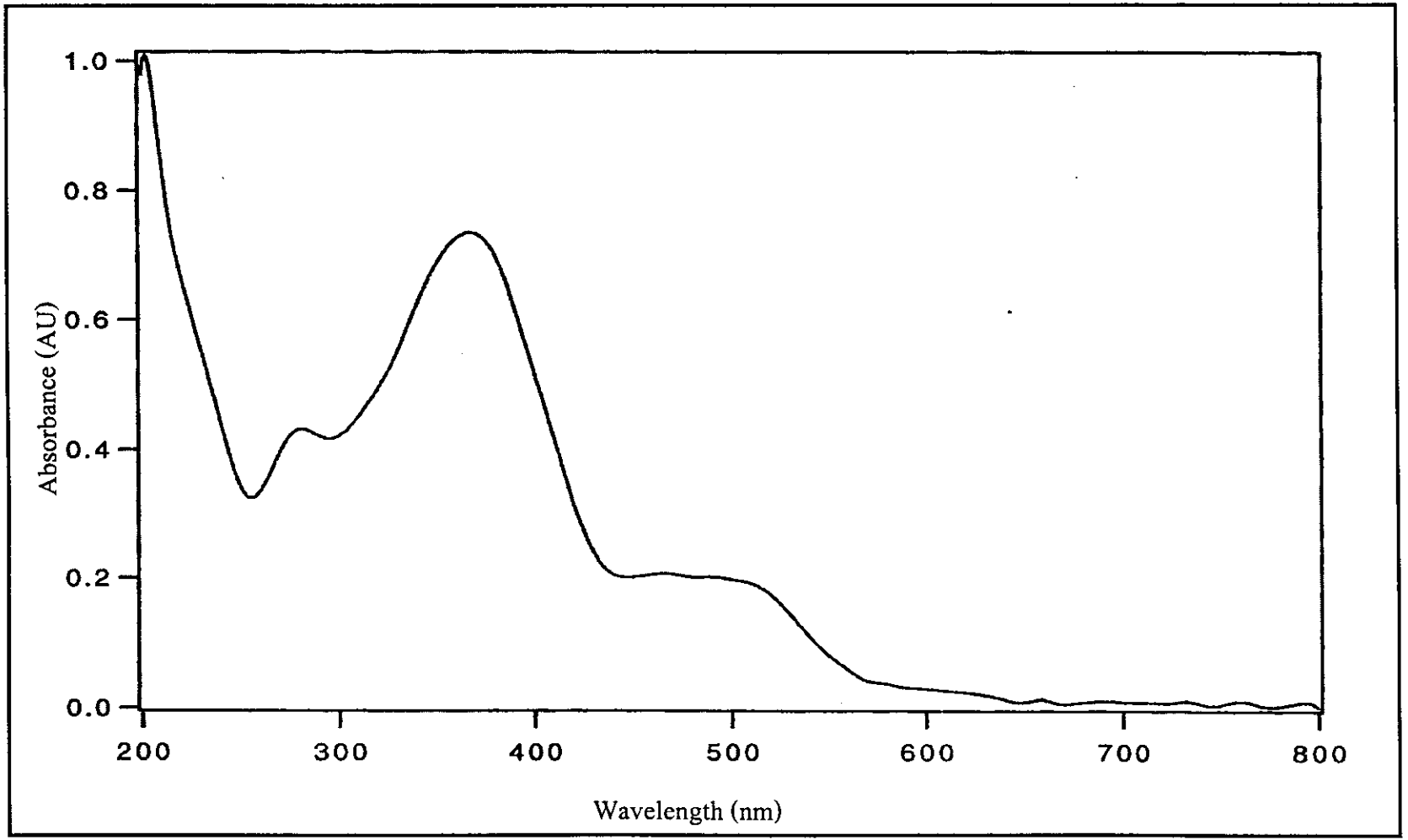

Figure 42 UV-Visible absorption spectrum of $[Ru(diazpy)(azpy)_2](BF_4)_2$ in CH_3CN.

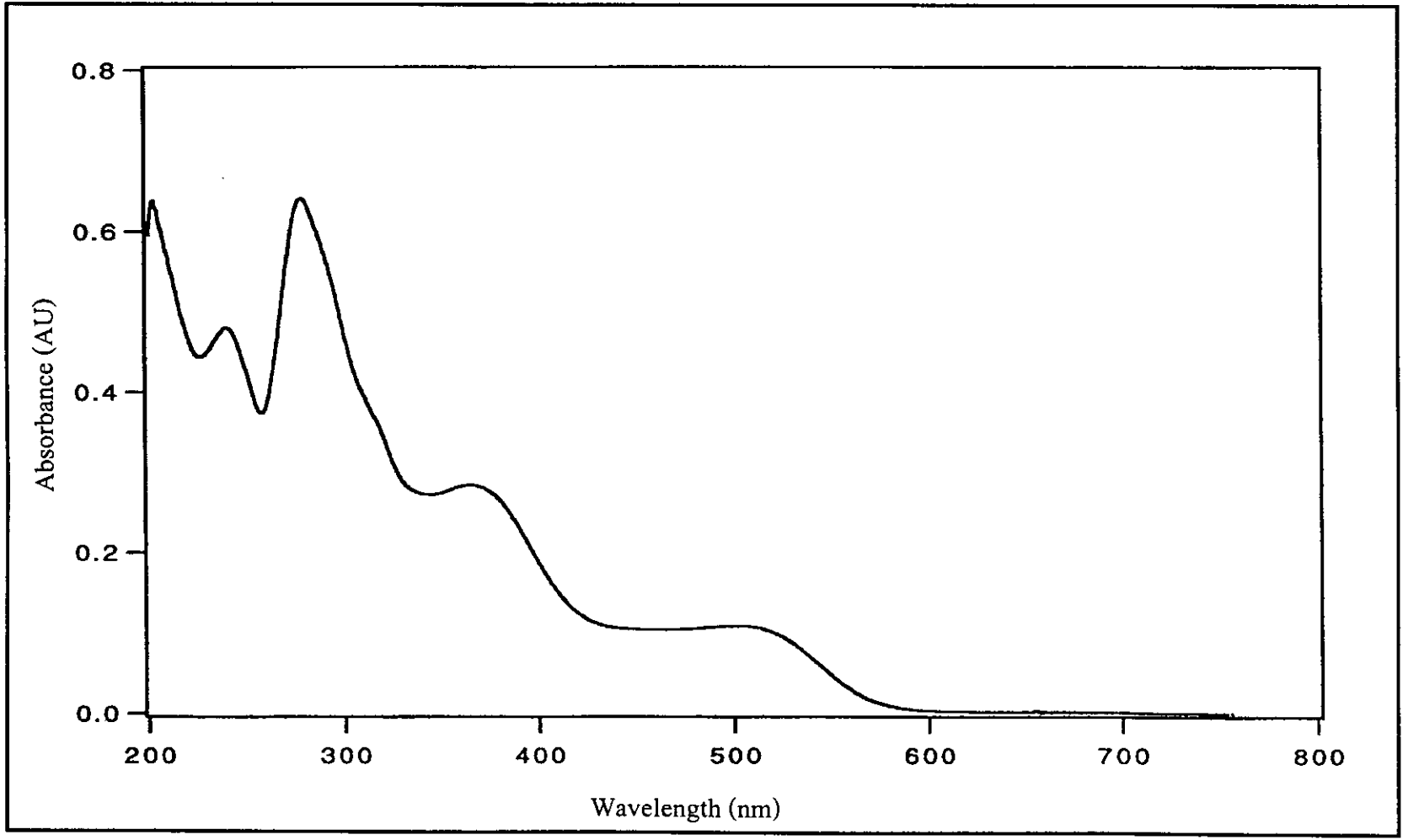

Figure 43 UV-Visible absorption spectrum of $[Ru(diazpy)(bpy)_2](BF_4)_2$ in CH_3CN.

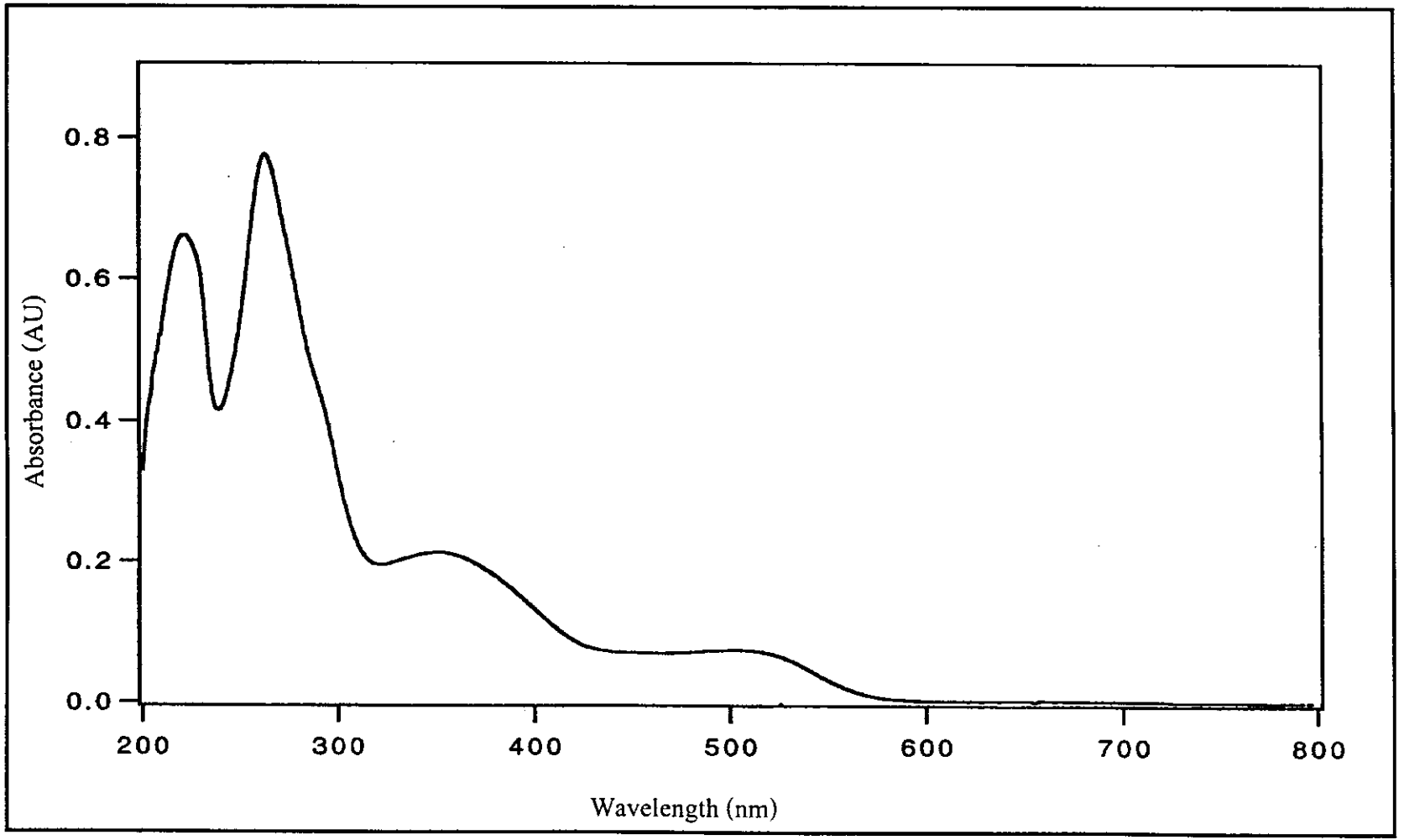

Figure 44 UV-Visible absorption spectrum of $[Ru(diazpy)(phen)_2](BF_4)_2$ in CH_3CN.

3.6.4 Infrared spctroscopy

Vibrational spectra in the region 4000-370 cm^{-1} could be used to give information about ligands coordination to the ruthenium center. Infrared spectroscopic data of $[Ru(diazpy)(L)_2](BF_4)_2$ complexes, where L = azpy, bpy and phen, were important in the range 1800-370 cm^{-1} with KBr disc. The infrared spectra of complexes are shown in Figure 45-47. The summaries of the infrared spectroscopic data are listed in Table 24.

Table 24 Infrared spectroscopic data of $[Ru(diazpy)(L)_2]^{2+}$ complexes (L = azpy, bpy and phen)

Vibrational modes	Wave number (cm^{-1}) of $[Ru(diazpy)(L)_2](BF_4)_2$ complexes (L = ligand)		
	azpy	bpy	phen
N=N (azo) stretching	1365(s) 1432(m)	1341(s) 1410(m)	1340(s) 1409(m)
C=N, C=C stretching	1600(m) 1585(m) 1485(w) 1455(s)	1616(m) 1590(m) 1455(w) 1428(s)	1627(m) 1594(m) 1455(w) 1428(s)

Table 24 (continued)

Vibrational modes	Wave number (cm^{-1}) of $[Ru(diazpy)(L)_2](BF_4)_2$ complexes (L = ligand)		
	azpy	bpy	phen
C-H out of plane bending	814(w)	842(s)	846(s)
	769(s)	776(s)	772(s)
	736(m)	720(s)	720(s)
	695(s)	702(s)	698(s)

m = medium, s = strong, w = weak

Infrared spectra of all $[Ru(diazpy)(L)_2]^{2+}$ complexes showed characteristic peaks of different intensities below 1,600 cm^{-1}. The band near 1,600 cm^{-1} was assigned to the stretching vibration of monosubstituted benzene ring (Santra and Lahiri, 1998). The N=N stretching frequencies of free diazpy exhibited two sharp bands at 1447 cm^{-1} and 1420 cm^{-1}. The N=N stretching frequencies of $[Ru(diazpy)(azpy)_2]^{2+}$ complex showed peaks at 1365 and 1432 cm^{-1} corresponded to coordinated N=N azo stretching frequency and free N=N azo stretching frequency of diazpy, respectively. Since, the $[Ru(diazpy)(bpy)_2]^{2+}$ and $[Ru(diazpy)(phen)_2]^{2+}$ complexes had just two N=N of diazpy. Therefore, both complexes showed N=N stretching frequencies of coordinated N=N of diazpy and free N=N at 1341 and 1410 cm^{-1} for bpy complex and 1340 and 1409 cm^{-1} for phen complex, respectively.

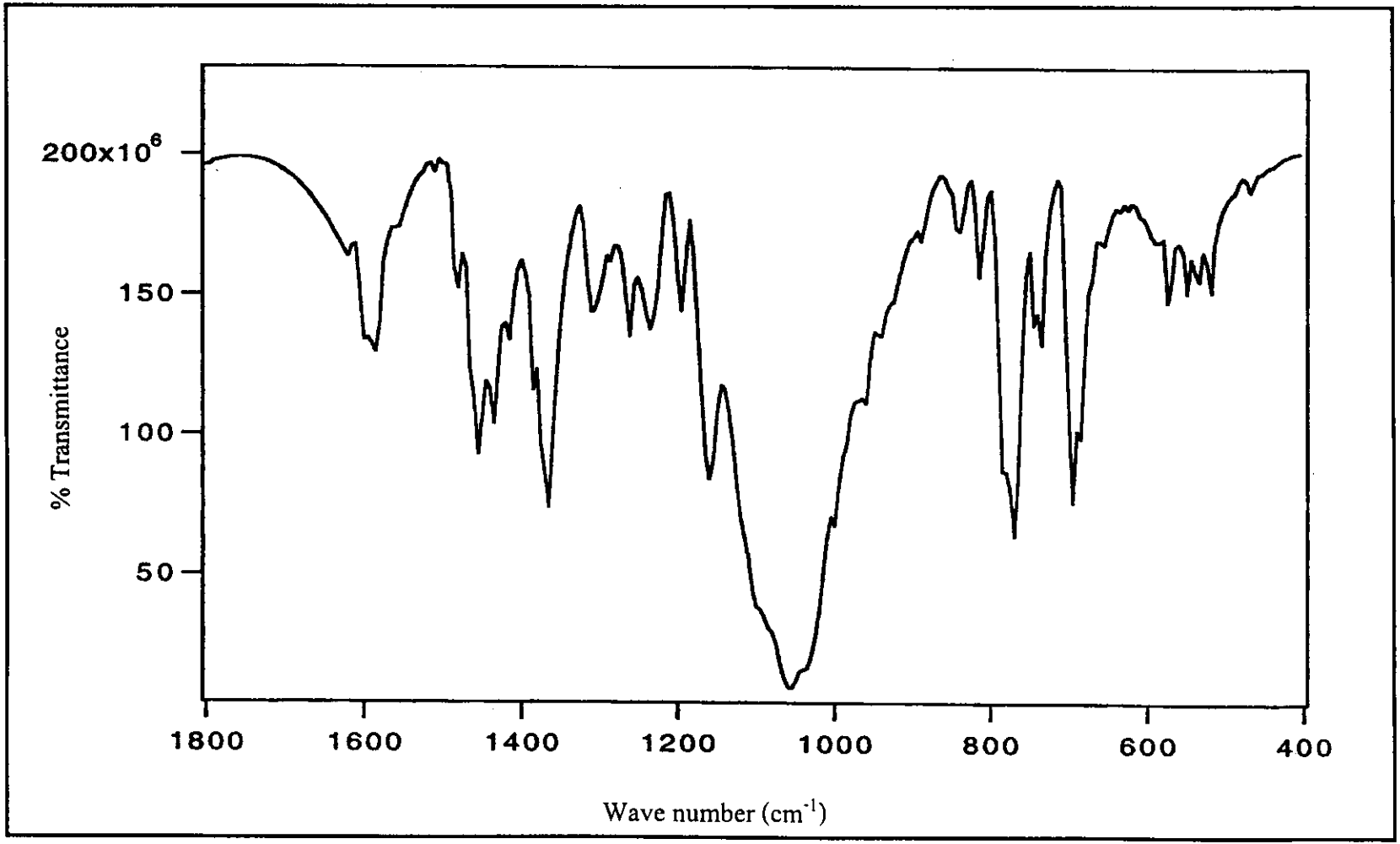

Figure 45 IR spectrum of $[Ru(diazpy)(azpy)_2](BF_4)_2$.

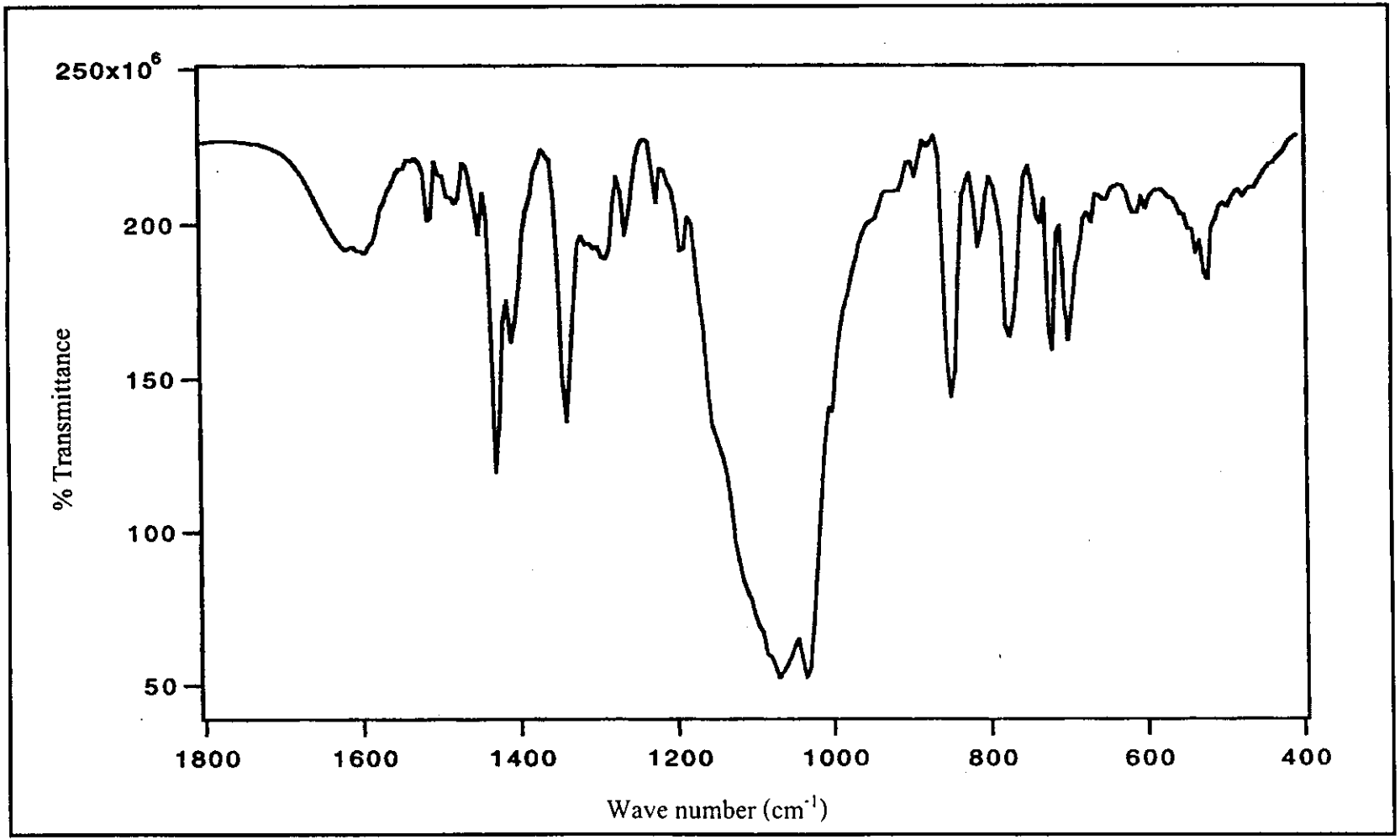

Figure 46 IR spectrum of $[Ru(diazpy)(bpy)_2](BF_4)_2$.

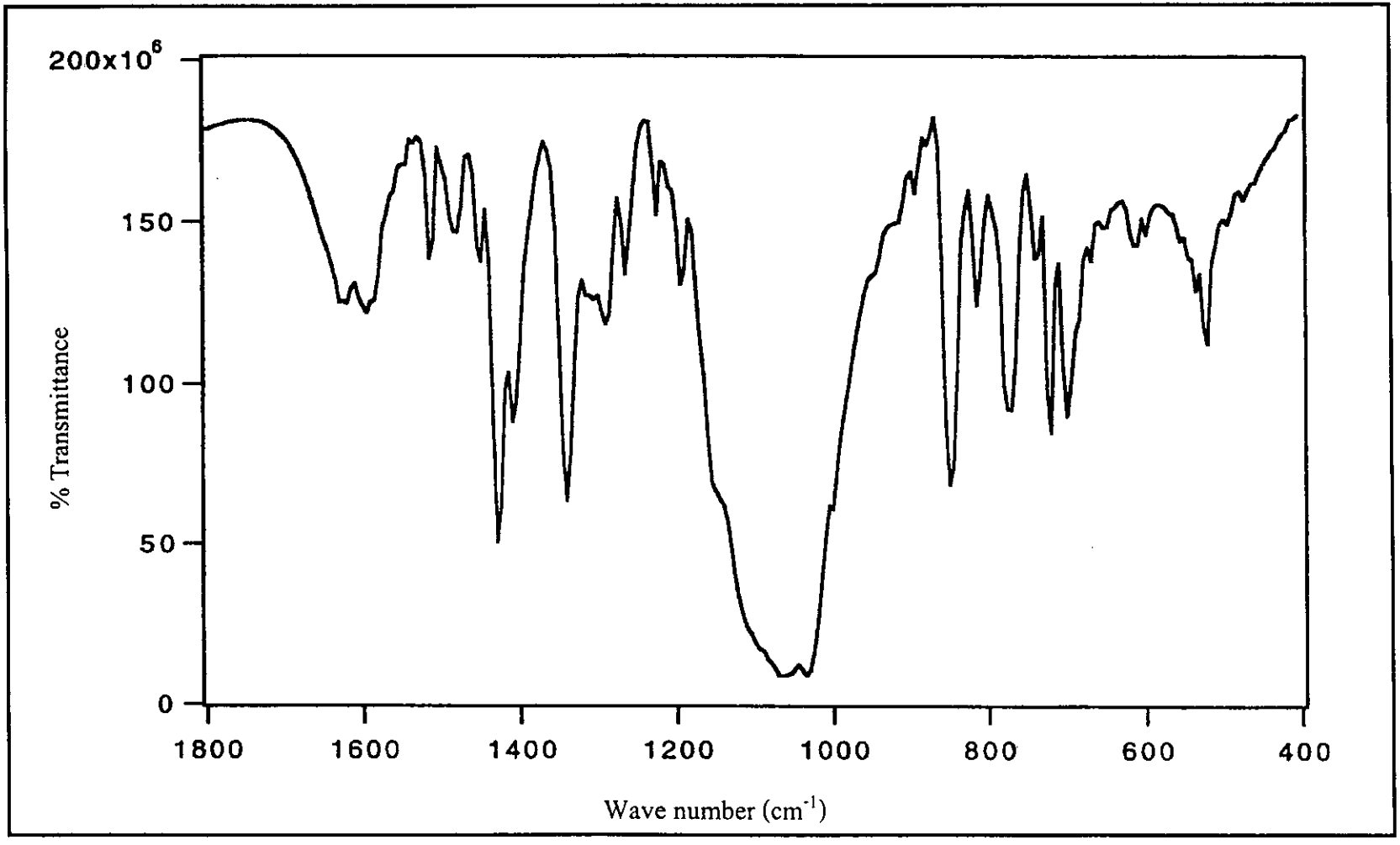

Figure 47 IR spectrum of $[Ru(diazpy)(phen)_2](BF_4)_2$.

3.6.5 Nuclear Magnetic Resonance spectroscopy

The NMR spectra of each complexes were studied in acetone-d_6. Tetramethylsilane (TMS, $(CH_3)_4Si$) was used as an internal reference. The individual proton resonance was assigned on the basis of its relative intensity, spin-spin structure and ^1H-^1H COSY NMR spectroscopy. The ^{13}C NMR assignments were based on the ^1H-^{13}C HMQC NMR spectra. The NMR spectroscopic data of all complexes are presented in Table 25-27.

(a) $[Ru(diazpy)(azpy)_2](BF_4)_2$ complex

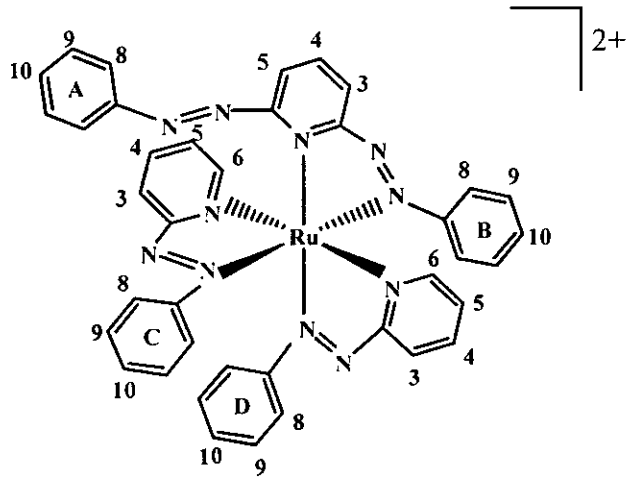

The ^1H NMR spectrum (Figure 48) of the $[Ru(diazpy)(azpy)_2](BF_4)_2$ complex showed seventeen resonances, eight from diazpy ligand and nine from azpy ligand. This result indicated that the diazpy ligand was unsymmetrical molecule. Besides, the ^1H NMR signals of both azpy showed no equivalent. The protons on pyridine rings appeared at lower field than phenyl ring. In addition, the first signal exhibited at the lowest field was H3 on pyridine ring of diazpy ligand. Figure 49 showed ^1H-^1H COSY NMR spectrum of this complex.

The ^{13}C NMR signal assignments (Figure 50) were based on the ^{1}H-^{13}C HMQC NMR spectrum (Figure 52). The ^{13}C NMR spectrum showed seventeen methine carbons, and six quaternary carbons (δ163.28, 151.91, 149.52, 133.11, 128.73, 126.31 ppm). Furthermore, The ^{13}C NMR results corresponded to the DEPT signals (Figure 51). The chemical shift data and proton, carbon assignments of this complex are shown in Table 25.

Table 25 The NMR spectroscopic data of $[Ru(diazpy)(azpy)_2](BF_4)_2$ in acetone-d_6 solution (500 MHz)

H-Position	^{1}H NMR			^{13}C NMR
	δ (ppm)	J (Hz)	Number of H	δ (ppm)
3 (diazpy)	8.87 (d)	7.5	1	134.62
3 (azpy)	8.70 (d)	7.5	2	145.43
6 (azpy)	8.47 (d)	5	1	153.23
6 (azpy)	8.41 (d)	5	1	153.23
4 (azpy)	8.33 (dd)	7.5, 5	2	143.11
4 (diazpy)	7.95 (t)	7.5, 8	1	141.45
10 (B, C)	7.73 (dt)	8, 7.5, 1.2	2	135.50
8 (C)	7.68 (dd)	7.5	2	134.43
9 (B, C)	7.62 (dd)	8.5, 7.5	4	130.41
9 (D)	7.57 (dd)	8.5, 7.5	2	131.13
8 (B)	7.57 (dd)	7.5	2	131.13
9 (A)	7.48 (d)	8	2	130.41
5 (azpy)	7.43 (d)	5	1	130.25
5 (azpy)	7.41 (d)	5	1	130.25

Table 25 (continued)

H-Position	^{1}H NMR			^{13}C NMR
	δ (ppm)	*J* (Hz)	Number of H	δ (ppm)
5 (diazpy)	7.38 (d)	8	1	129.13
8 (A, D)	7.34 (dd)	8.5, 1.2	4	124.60
10 (A, D)	7.34 (dd)	8.5	2	124.09
Quaternary carbon				163.28, 151.91 149.52, 133.11 128.73, 126.31

d = doublet, dd = doublet of doublet, t = triplet

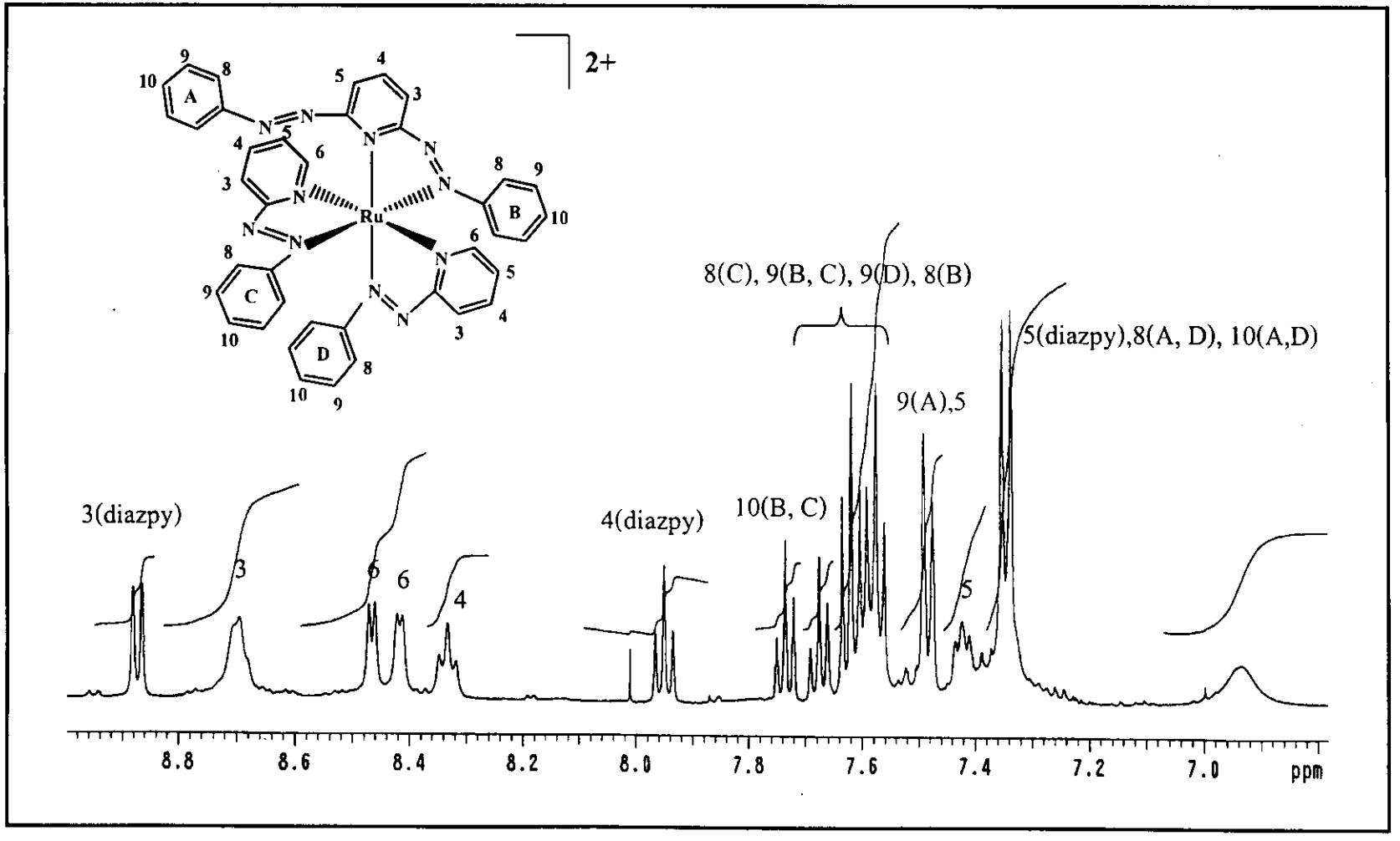

Figure 48 ^{1}H NMR spectrum of $[Ru(diazpy)(azpy)_2](BF_4)_2$.

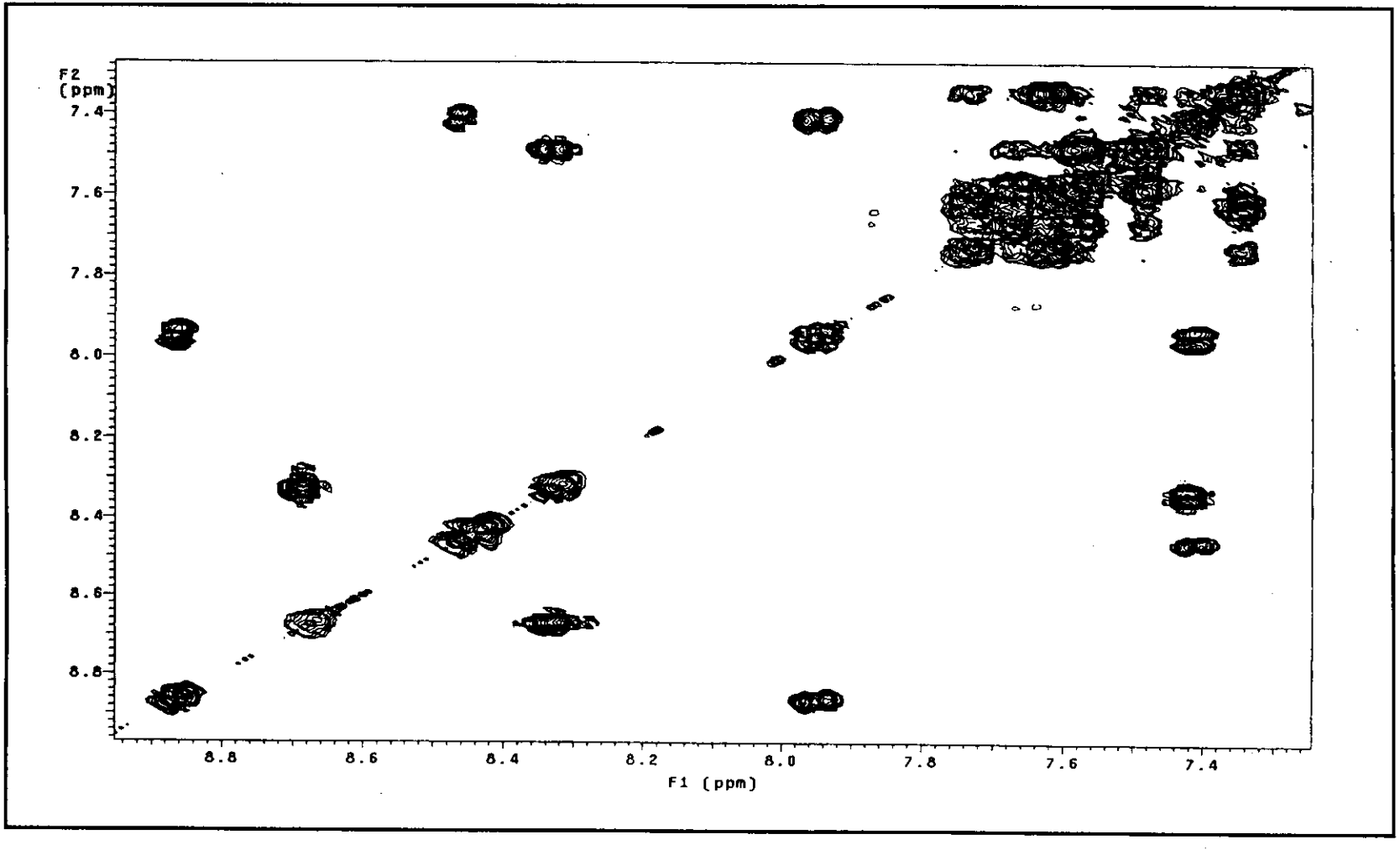

Figure 49 ^{1}H- ^{1}H COSY NMR spectrum of $[Ru(diazpy)(azpy)_2]^{2+}$ in acetone-d_6.

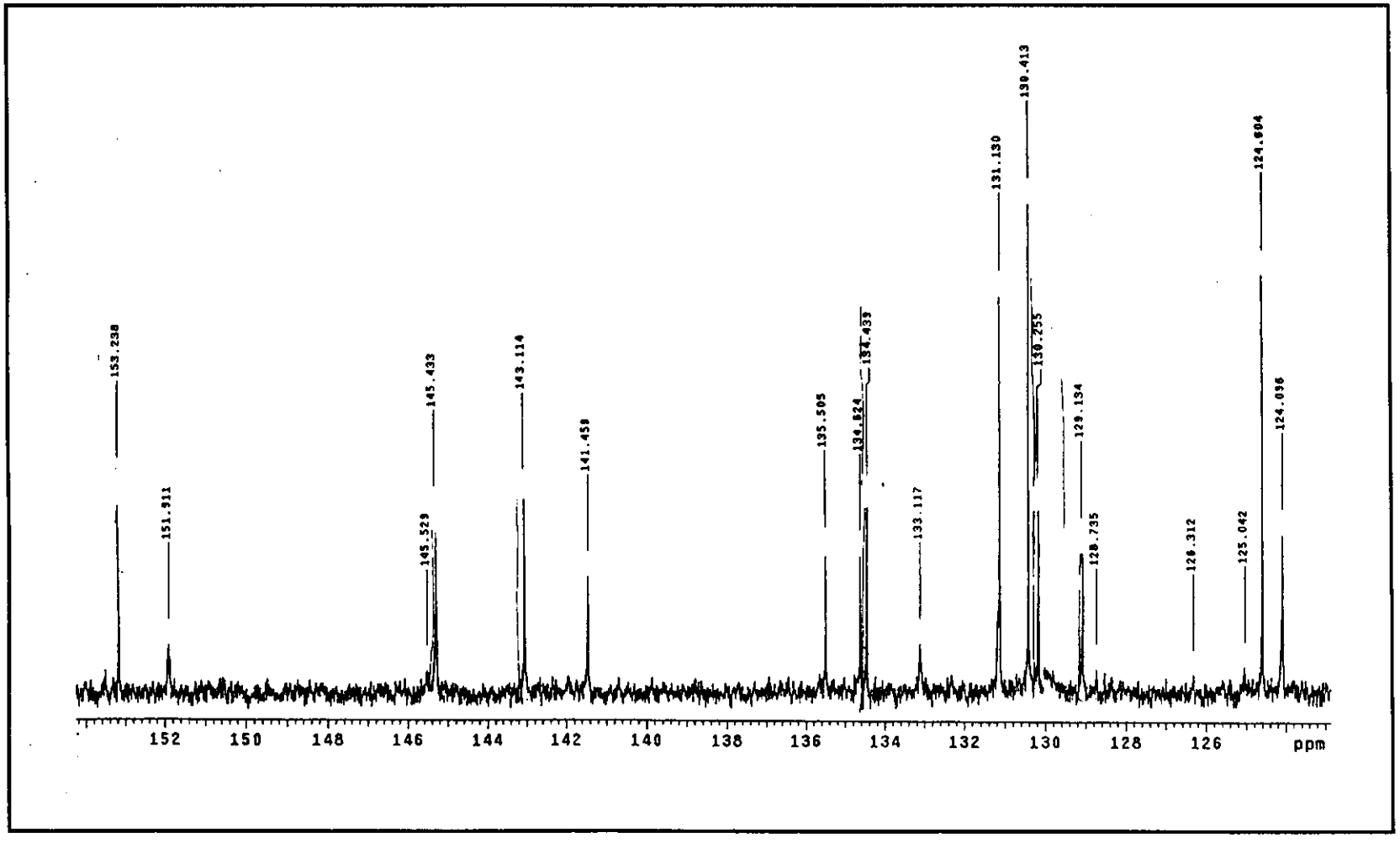

Figure 30 ^{13}C NMR spectrum of $[Ru(diazpy)(azpy)_2]^{2+}$ in acetone-d_6.

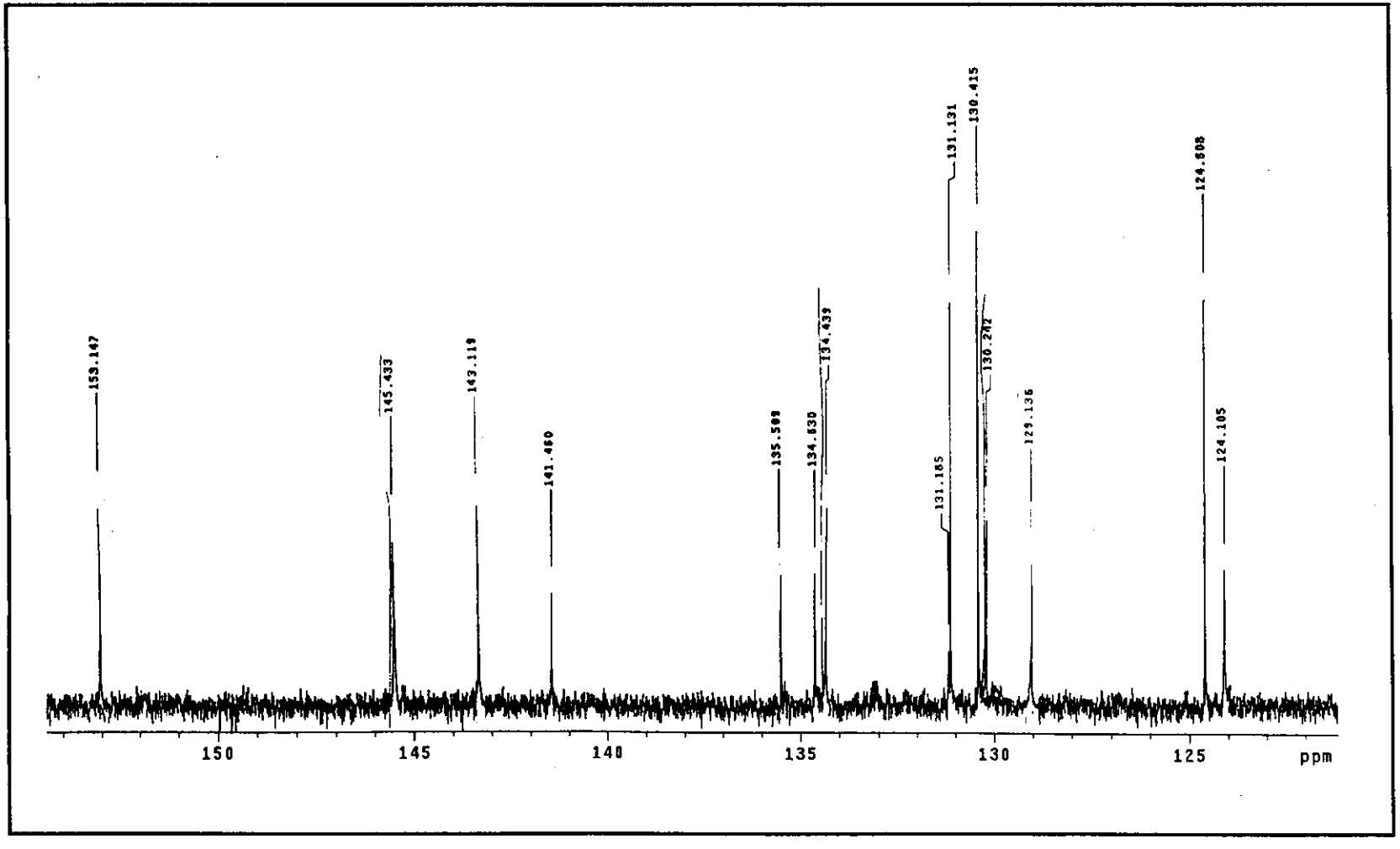

Figure 31 DEPT NMR spectrum of $[Ru(diazpy)(azpy)_2]^{2+}$ in acetone-d_6.

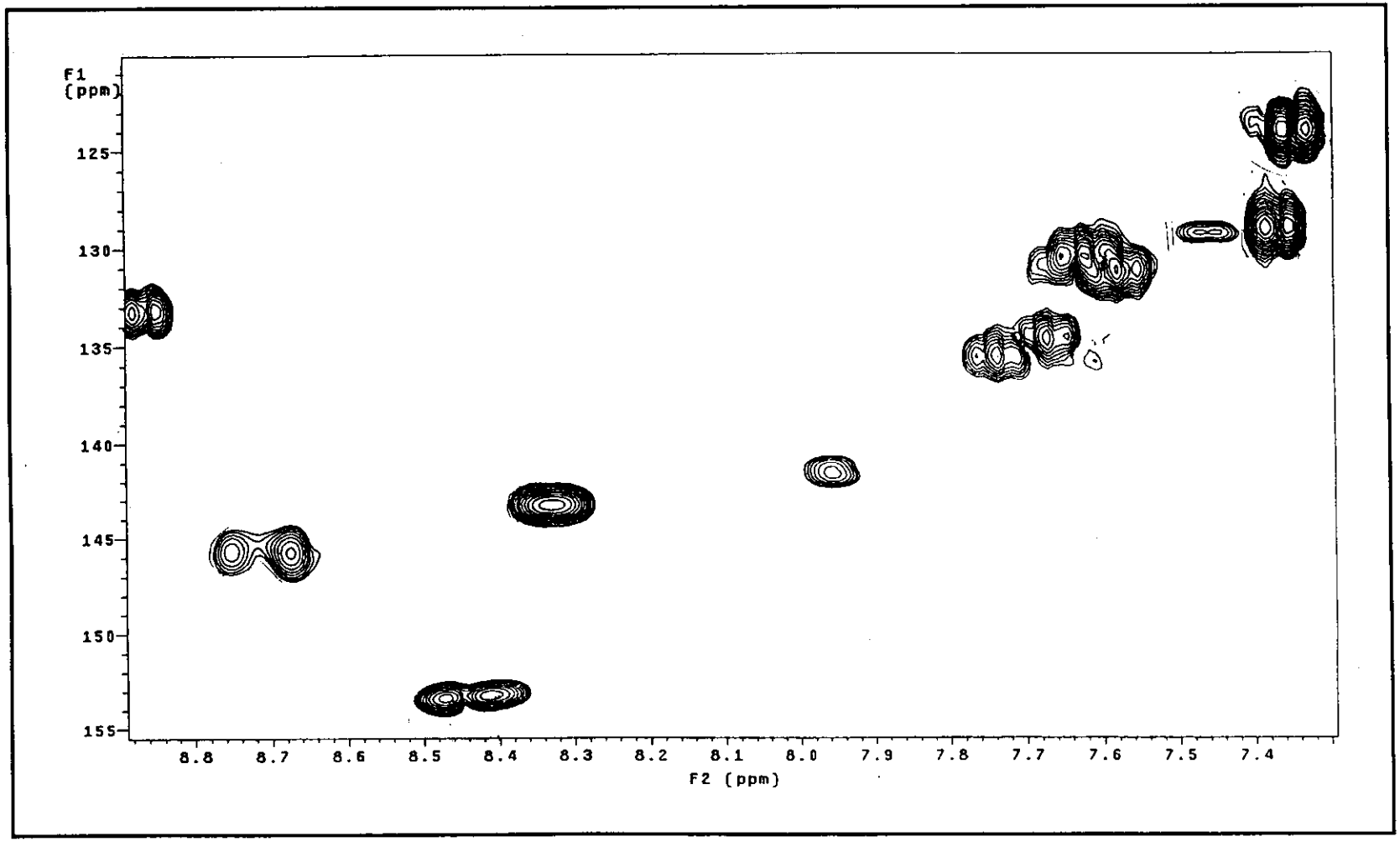

Figure 32 ^{1}H-^{13}C HMQC NMR spectrum of $[Ru(diazpy)(azpy)_2]^{2+}$ in acetone-d_6.

(b) $[Ru(diazpy)(bpy)_2](BF_4)_2$ complex

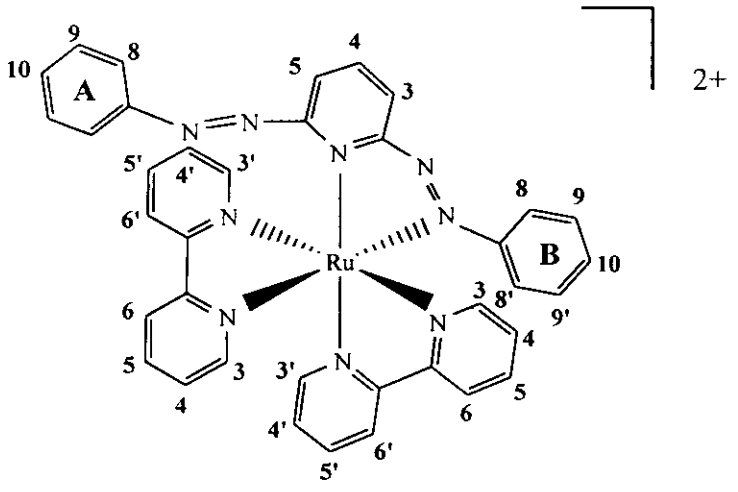

The ^{1}H NMR spectrum (Figure 53) of the $[Ru(diazpy)(bpy)_2](BF_4)_2$ complex showed 26 resonances for 29 protons. The spectrum displayed distinct chemical shift of each bpy ligand. This result indicated that both bpy ligands in this complex were not equivalent. A chemical shift of proton on pyridine ring in diazpy ligand exhibited at lower field than phenyl rings because of inductive effect of N atom in pyridine ring. The H3 on pyridine ring of diazpy ligand appeared at the lowest field, at 9.08 ppm. Figure 54 showed ^{1}H-^{1}H COSY NMR spectrum of this complex.

The ^{13}C NMR spectrum (Figure 55) showed 25 methine carbons, and 8 quaternary carbons (δ166.98, 166.63, 157.66, 157.32, 156.91, 155.85, 154.70, 153.10 ppm). In addition, the result of ^{13}C NMR corresponded to the DEPT signals (Figure 56). The chemical shift data and proton, carbon assignments of this complex are summarized in Table 26.

Table 26 The NMR spectroscopic data of $[Ru(diazpy)(bpy)_2](BF_4)_2$ in acetone-d_6 solution (300 MHz)

H-Position	^{1}H NMR			^{13}C NMR
	δ (ppm)	*J* (Hz)	Number of H	δ (ppm)
3 (diazpy)	9.08 (dd)	8.1, 1.2	1	128.69
3 (bpy)	8.78 (d)	7.8	1	125.74
3 (bpy)	8.65 (d)	7.8	1	125.51
4 (diazpy)	8.62 (t)	7.8, 8.1	1	143.57
3 (bpy)	8.55 (d)	7.8	1	125.11
4 (bpy)	8.40 (dd)	7.8, 1.2	1	141.53
3 (bpy)	8.39 (d)	7.8	1	125.04
6 (bpy)	8.38 (dd)	5.4, 1.2	1	154.60
4 (bpy)	8.31 (dd)	7.8, 1.2	1	140.77
6 (bpy)	8.17 (dd)	5.4, 1.2	1	154.60
4 (bpy)	7.99 (dd)	7.8, 1.2	1	140.16
6 (bpy)	7.81 (dd)	5.4, 1.2	1	152.44
5 (bpy)	7.80 (dd)	5.4, 1.5	1	129.85
5 (diazpy)	7.74 (dd)	7.8, 1.2	1	117.34
6 (bpy)	7.71 (dd)	5.4, 1.2	1	150.55
5 (bpy)	7.70 (d)	5.4, 1.5	1	129.26
9 (B)	7.62 (dd)	7, 8	1	134.49
4 (bpy)	7.58 (dd)	7.8, 1.2	1	139.02
8 (B)	7.49 (dd)	7, 1.5	2	129.93
5 (bpy)	7.40 (dd)	5.4, 1.5	1	129.36
8 (A)	7.38 (dd)	7.5, 1.5	1	131.37

Table 26 (continued)

H-Position	^{1}H NMR			^{13}C NMR
	δ (ppm)	*J* (Hz)	Number of H	δ (ppm)
9 (A)	7.23 (dd)	7.5, 8	2	124.11
8 (A)	7.22 (dd)	8, 1.5	1	130.28
9 (B)	7.19 (dd)	7.5, 8	1	130.28
5 (bpy)	7.08 (dd)	5.4, 1.5	1	129.05
10 (A, B)	7.06 (dd)	8, 1.5	2	122.33
Quaternary carbon				166.98, 166.63 157.66, 157.32 156.91, 155.85 154.70, 153.10

d = doublet, dd = doublet of doublet, t = triplet

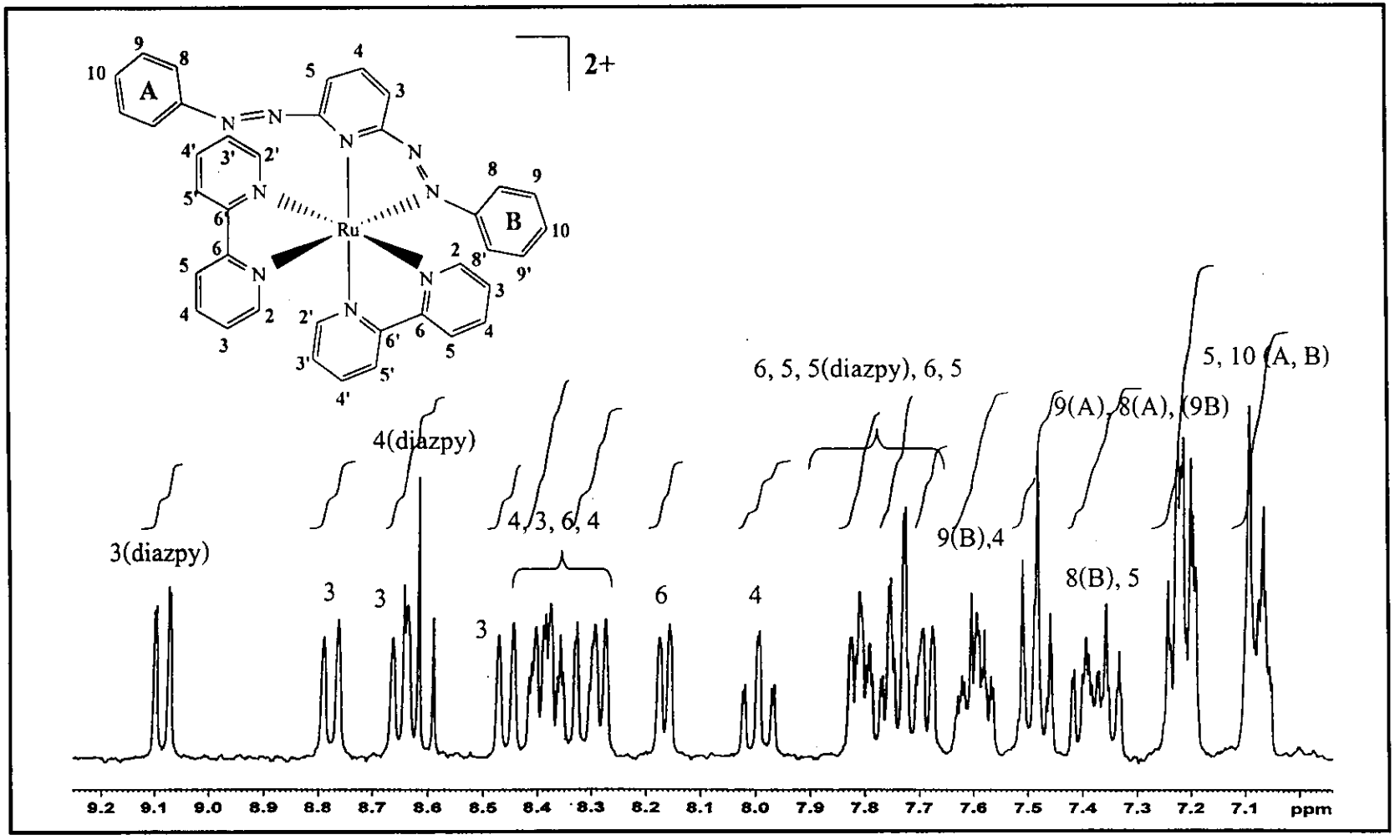

Figure 33 ^{1}H NMR spectrum of $[Ru(diazpy)(bpy)_2]^{2+}$ in acetone-d_6.

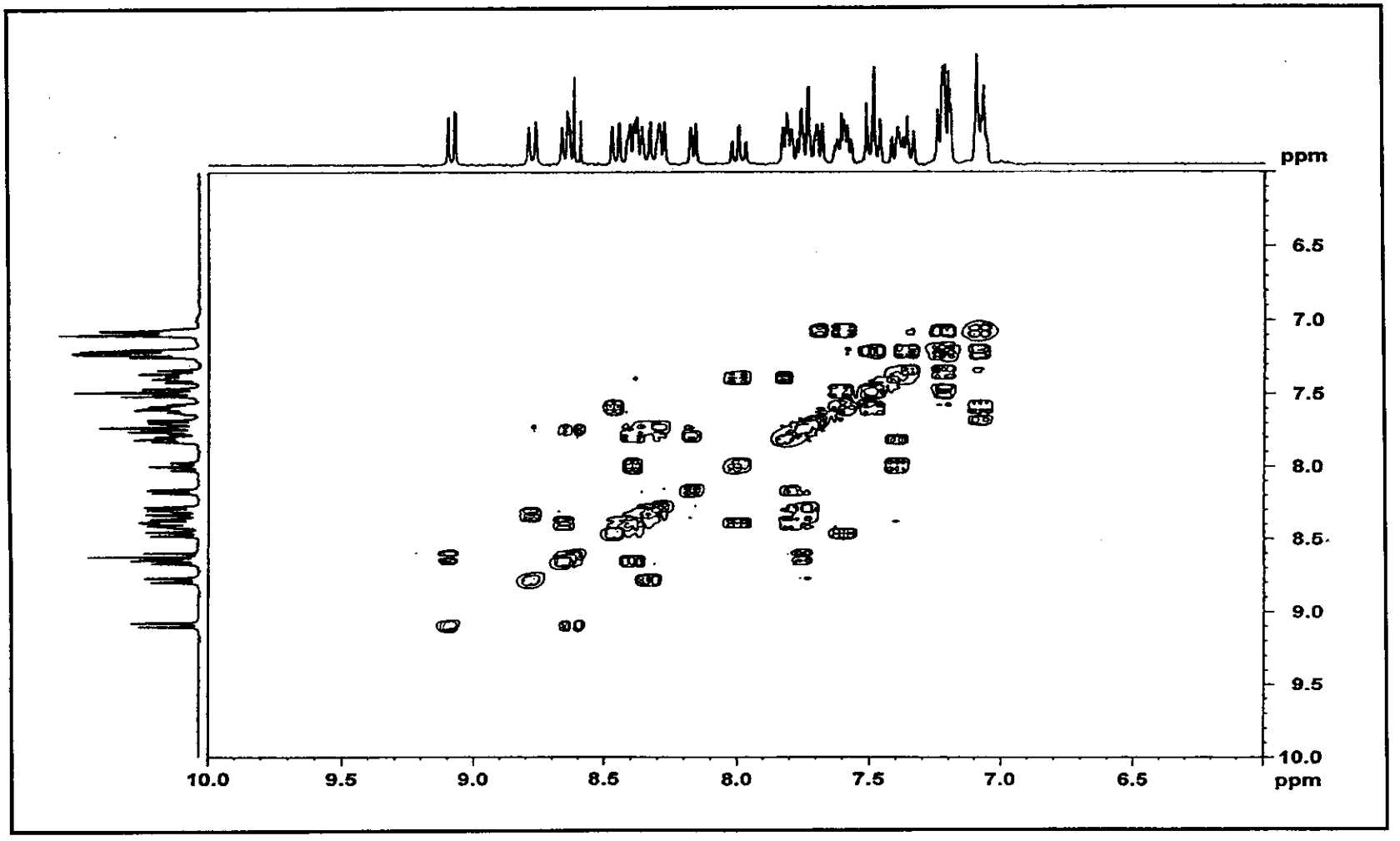

Figure 34 ^{1}H- ^{1}H COSY NMR spectrum of $[Ru(diazpy)(bpy)_2]^{2+}$ in acetone-d_6.

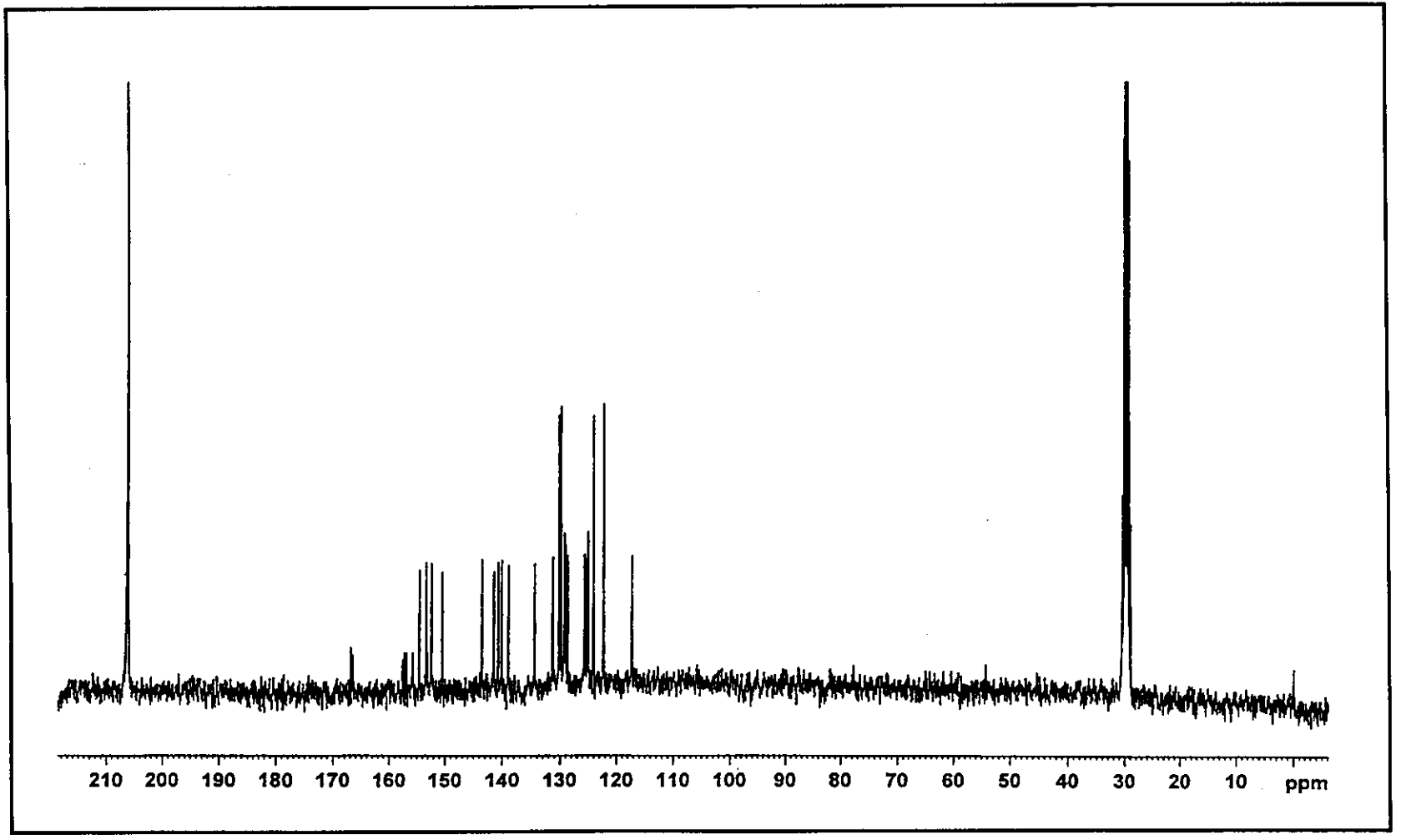

Figure 35 ^{13}C NMR spectrum of $[Ru(diazpy)(bpy)_2]^{2+}$ in acetone-d_6.

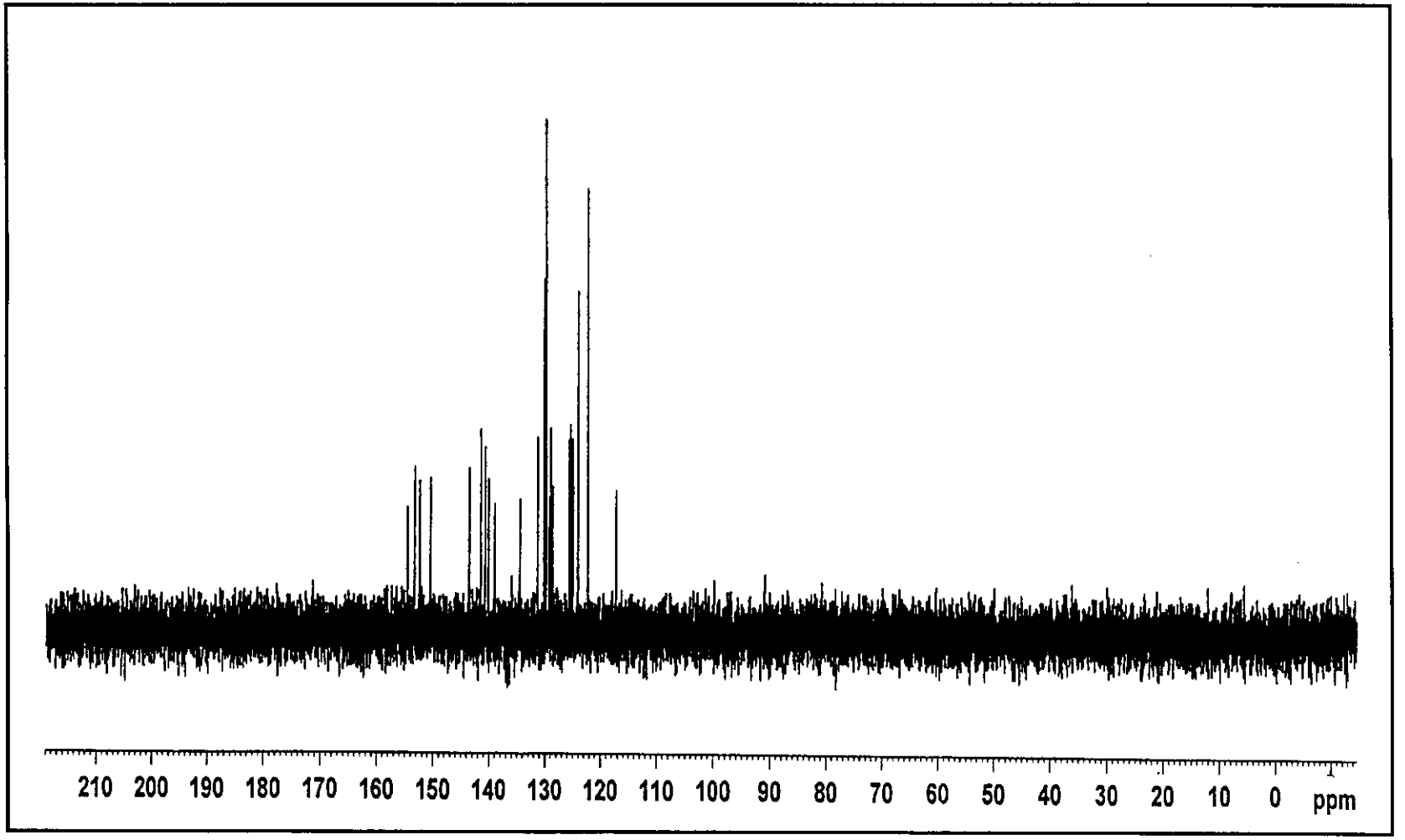

Figure 56 DEPT NMR spectrum of $[Ru(diazpy)(bpy)_2]^{2+}$ in acetone-d_6.

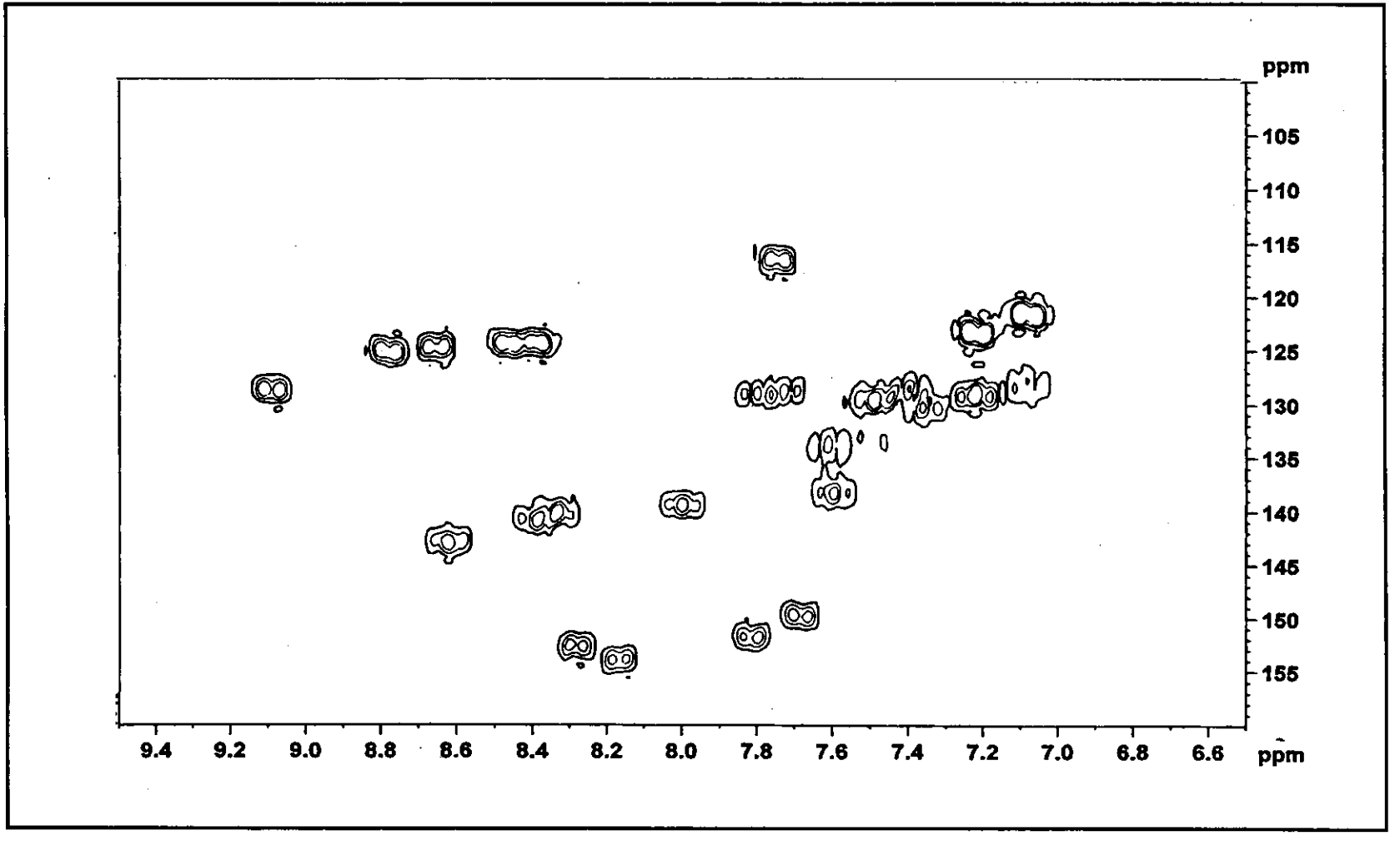

Figure 57 ^{1}H-^{13}C HMQC NMR spectrum of $[Ru(diazpy)(bpy)_2]^{2+}$ in acetone-d_6.

(c) [Ru(diazpy)(phen)$_2$](BF$_4$)$_2$ complex

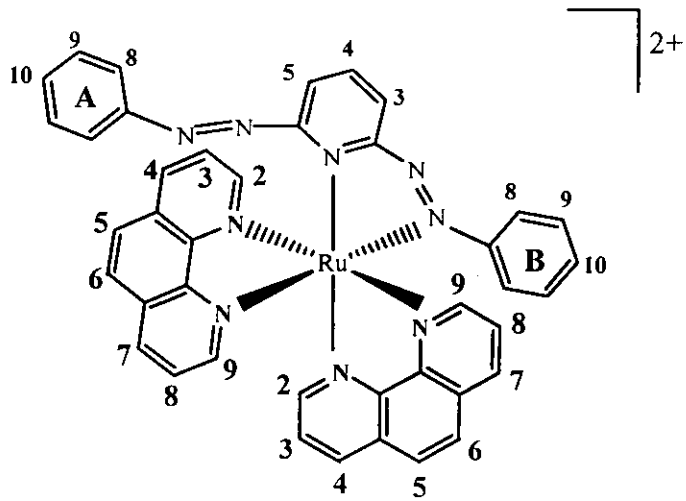

The ^{1}H NMR spectrum (Figure 58) of the [Ru(diazpy)(phen)$_2$](BF$_4$)$_2$ complex showed 25 resonances, 10 from the diazpy ligand and 15 from both phen in the region of 9.13-6.79 ppm. The spectrum showed distinct chemical shift of each phen ligand. It is indicated that both phen ligands in this complex were not equivalent. The chemical shift of proton on pyridine ring in diazpy ligand exhibited at lower field than phenyl rings because of inductive effect of N atom in pyridine ring. The H3 on pyridine ring of diazpy ligand appeared at the lowest field (9.13 ppm). Figure 59 showed ^{1}H-^{1}H COSY NMR spectrum of this complex.

The ^{13}C NMR spectrum (Figure 60) showed 25 methine carbons, and 10 quaternary carbons (δ 169.95, 163.56, 157.79, 157.33, 155.66, 155.25, 154.41, 154.23, 152.52 and 151.30 ppm). In addition, the ^{13}C NMR results corresponded to the DEPT signals (Figure 61). The chemical shift data and proton, carbon assignments of this complex are summarized in Table 27.

Table 27 The NMR spectroscopic data of $[Ru(diazpy)(phen)_2](BF_4)_2$ in acetone-d_6 solution (300 MHz)

H-Position	^{1}H NMR			^{13}C NMR
	δ (ppm)	*J* (Hz)	Number of H	δ (ppm)
3 (diazpy)	9.13 (dd)	8.1, 1.2	1	131.07
7 (phen)	9.06 (dd)	8.4, 1.2	1	140.40
7 (phen)	8.99 (dd)	8.4, 1.2	1	139.69
9 (phen)	8.95 (dd)	5.4, 1.2	1	155.14
9 (phen)	8.72 (dd)	5.4, 1.2	1	155.85
4 (diazpy)	8.62 (t)	8.1, 8.1	1	143.55
4 (phen)	8.53 (dd)	8.4, 1.2	1	138.82
5 (phen)	8.39 (d)	9	1	129.28
5 (phen)	8.35 (d)	9	1	129.28
8 (phen)	8.19 (d)	8.4, 5.4	1	127.22
6 (phen)	8.16 (d)	9	2	129.40
4 (phen)	8.15 (dd)	8.4, 1.2	1	137.77
8 (phen)	8.12 (d)	8.4, 5.4	1	127.87
2 (phen)	7.95 (dd)	5.4, 1.2	1	151.77
2 (phen)	7.90 (dd)	5.4, 1.2	1	153.45
5 (diazpy)	7.67 (dd)	8.1, 1.2	1	117.38
10 (B)	7.58 (dd)	7.5, 1.2	1	134.40
3 (phen)	7.51 (dd)	8.4, 5.4	1	128.13
9 (B)	7.38 (dd)	7.5, 1.2	2	130.07
3 (phen)	7.14 (dd)	8.4, 5.4	1	128.76
10 (A)	7.11 (dd)	8.1	1	126.82

Table 27 (continued)

H-Position	^{1}H NMR			^{13}C NMR
	δ (ppm)	*J* (Hz)	Number of H	δ (ppm)
8 (B)	6.95 (dd)	8.4	2	121.81
9 (A)	6.95 (dd)	8.4	1	129.04
9 (A)	6.95 (dd)	8.4	1	128.87
8 (A)	6.79 (dd)	8.4, 1.2	2	123.74
Quaternary carbon				169.95, 163.56 157.79, 157.33 155.66, 155.25 154.41, 154.23 152.52, 151.30

d = doublet, dd = doublet of doublet, t = triplet

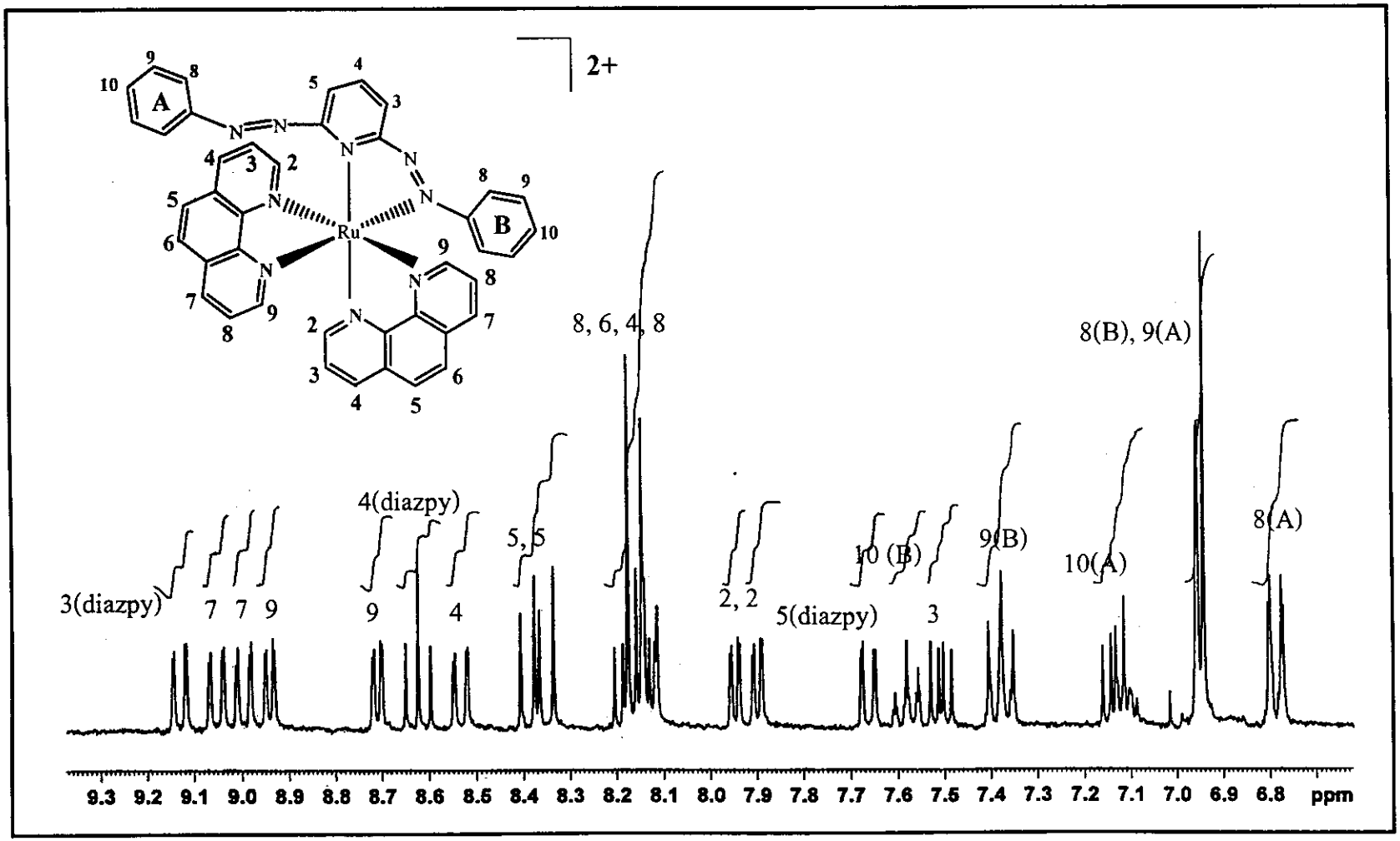

Figure 58 ^{1}H NMR spectrum of $[Ru(diazpy)(phen)_2]^{2+}$ in acetone-d_6.

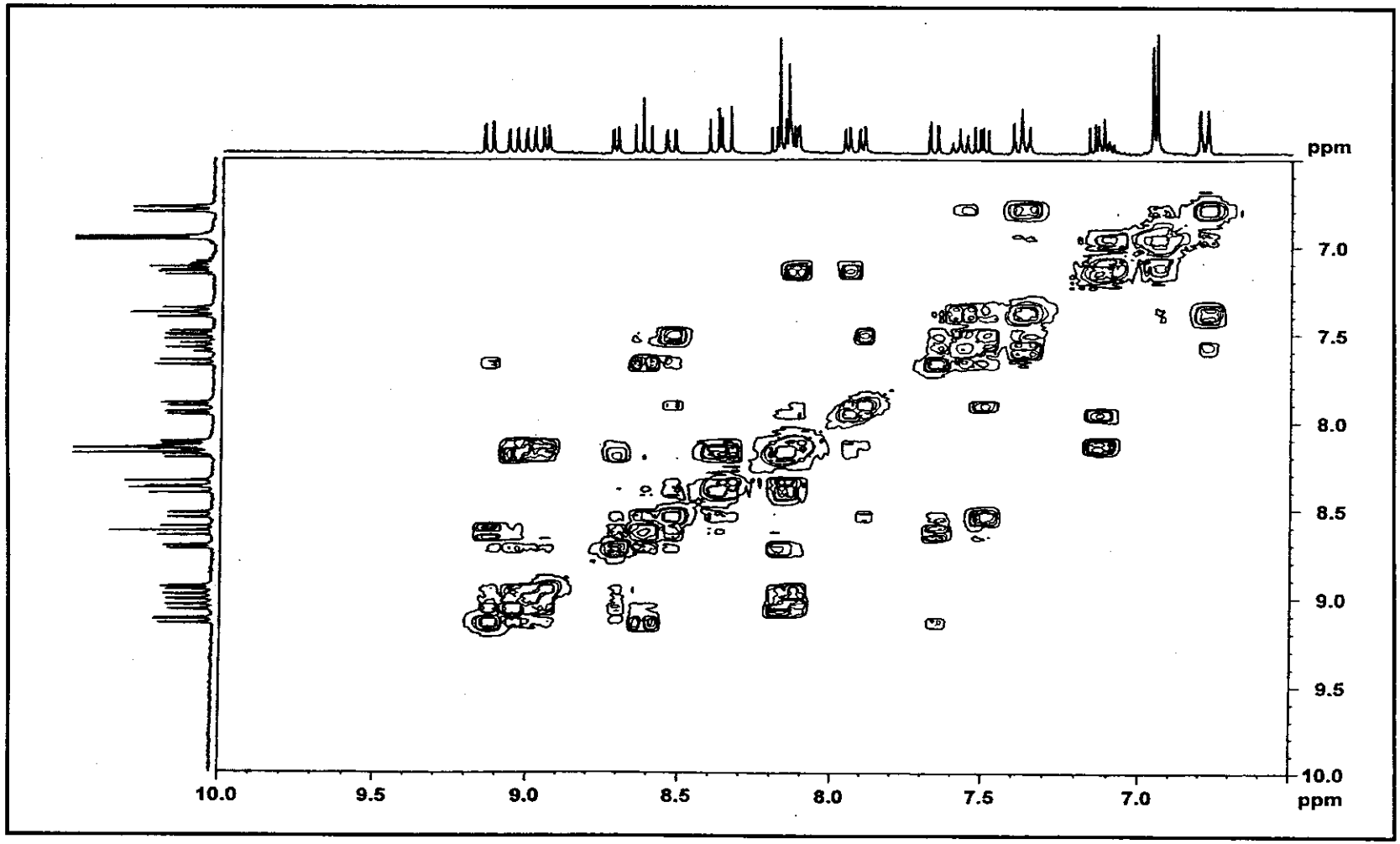

Figure 59 ^{1}H- ^{1}H COSY NMR spectrum of $[Ru(diazpy)(phen)_2]^{2+}$ in acetone-d_6.

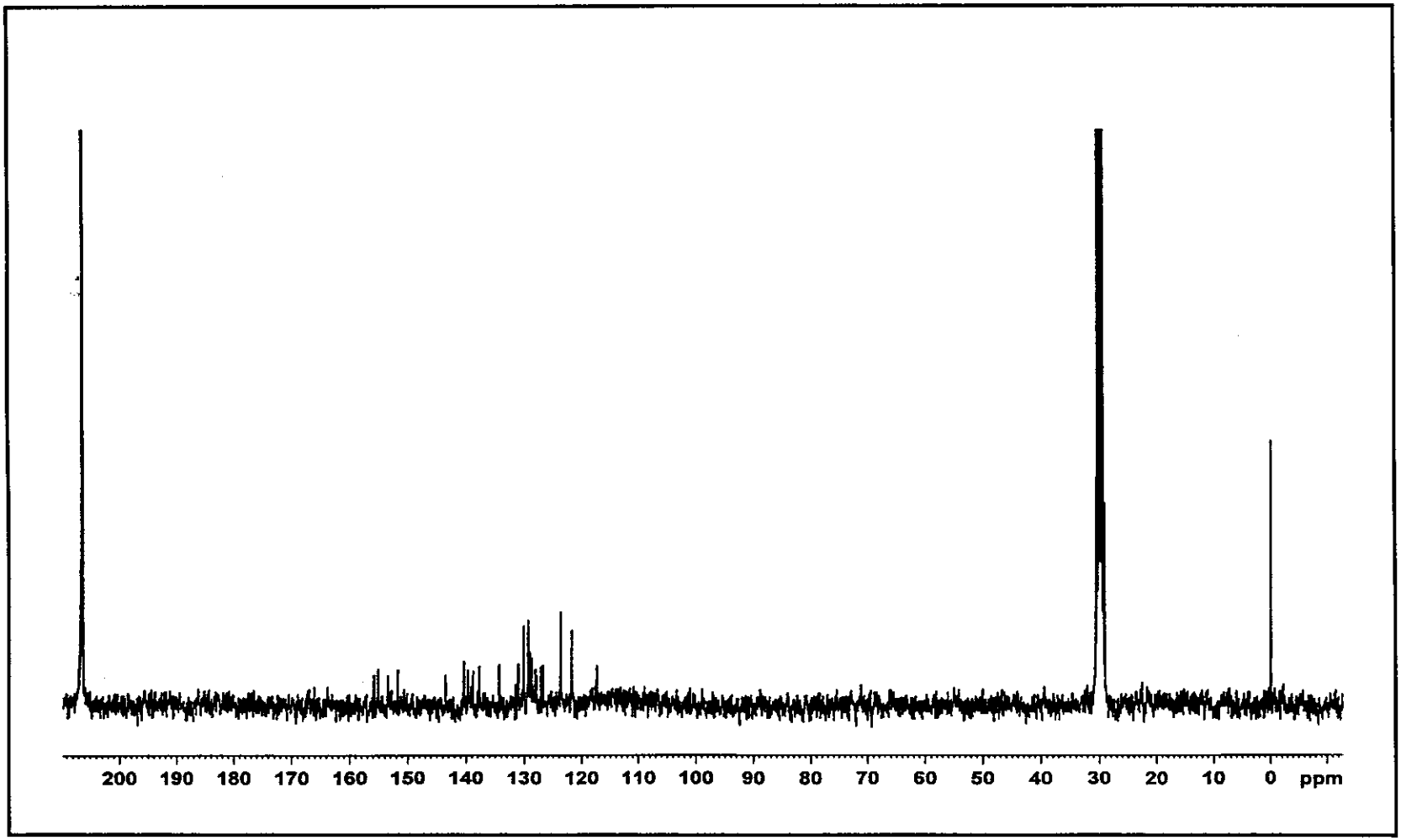

Figure 60 ^{13}C NMR spectrum of $[Ru(diazpy)(phen)_2]^{2+}$ in acetone-d_6.

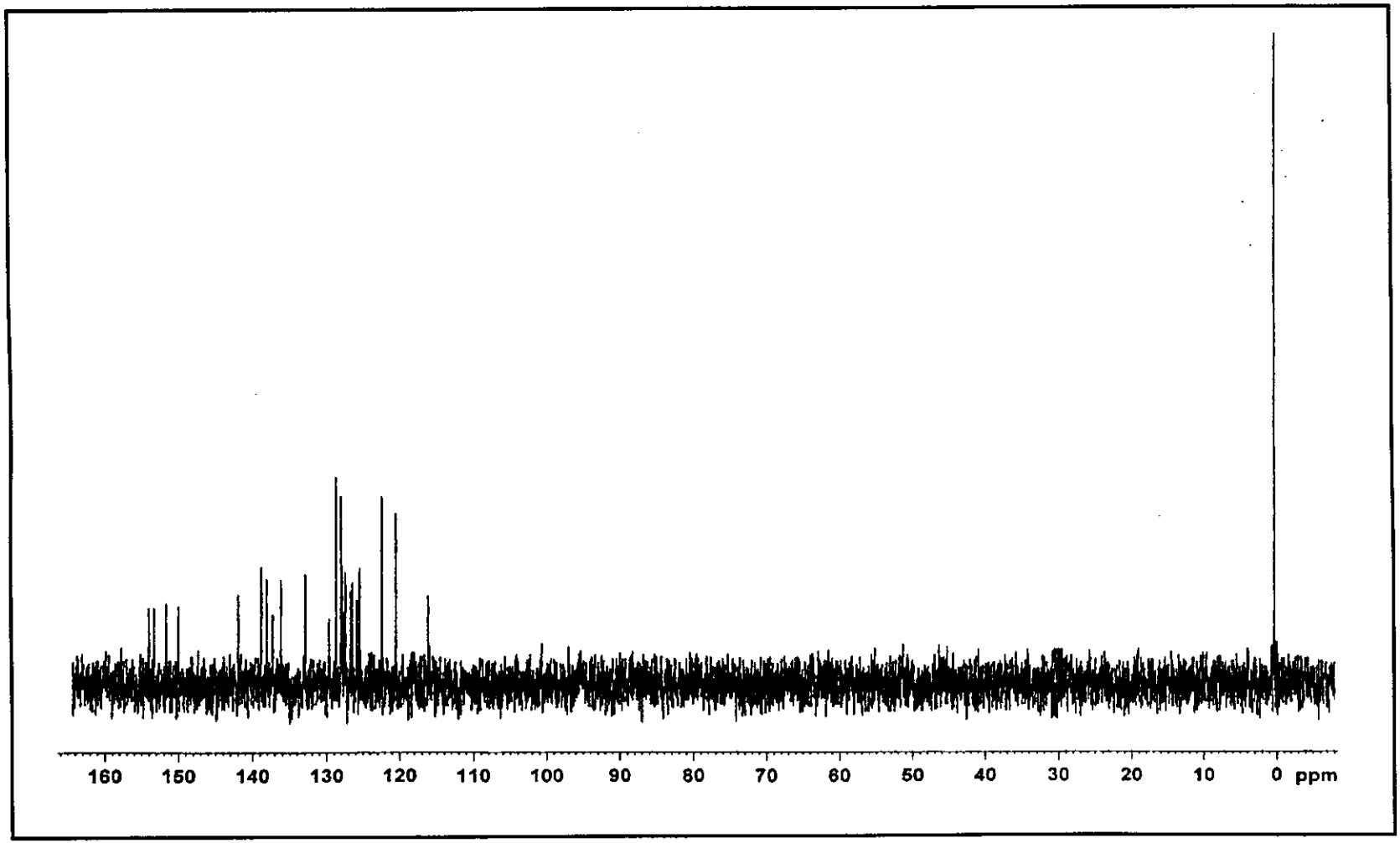

Figure 61 DEPT NMR spectrum of $[Ru(diazpy)(phen)_2]^{2+}$ in acetone-d_6.

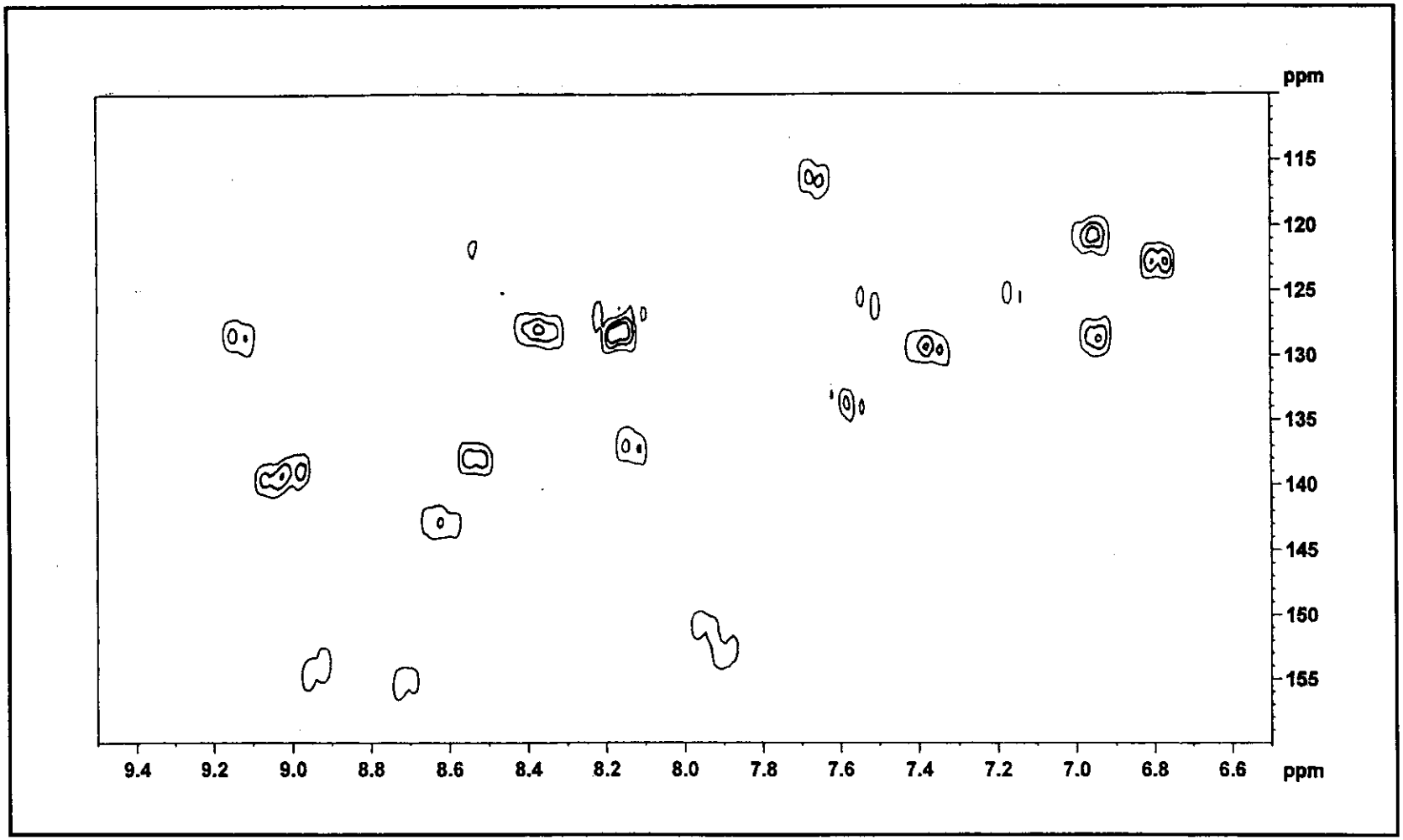

Figure 62 ^{1}H-^{13}C HMQC NMR spectrum of $[Ru(diazpy)(phen)_2]^{2+}$ in acetone-d_6.

3.6.6 Cyclic Voltammetry

Cyclic voltammetry of the $[Ru(diazpy)(L)_2]^{2+}$ complexes (L = azpy, bpy and phen) were carried out in 0.1 M TBAH using acetonitrile as the solvent. The cyclic voltammetric data of all complexes are listed in Table 28 and cyclic voltammograms of all complexes are shown in Figure 63 to 65.

Table 28 Cyclic voltammetric data of $[Ru(diazpy)(L)_2]^{2+}$ where L =azpy, bpy and phen in 0.1 M TBAH acetonitrile at scan rate 50 mV/s (ferrocene as an internal standard, ΔE_p 75 mV)

$[Ru(diazpy)(L)_2]^{2+}$ L =	$E_{1/2}$, V, (ΔE, mV)						
	Oxidation range	Reduction range					
	Ru(II)/Ru(III)	I	II	III	IV	V	VI
azpy	n	-0.38 (72)	-0.78 (70)	-1.22 (90)	-1.72 (145)	-1.81 (68)	-2.13 (120)
bpy	n	-0.83 (80)	-0.98[a]	-1.45 (60)	-1.62 (65)	-1.97 (80)	-2.21 (110)
phen	n	-0.82 (75)	-0.95[a]	-1.42 (65)	-1.62 (70)	-1.93 (70)	-2.22 (105)

[a]cathodic peak, n = cannot be observed

Oxidation Potential

The cyclic voltammogram of the $[Ru(diazpy)(L)_2]^{2+}$ complexes where L =azpy, bpy and phen were studied in the range 0.00 to +2.00 V. The couples of Ru(II)/Ru(III)

in oxidation range did not occur in the range of solvent window.

Reduction Potential

The reduction potential of $[Ru(diazpy)(L)_2]^{2+}$ complexes where L =azpy, bpy and phen were studied in the range 0.00 to –2.25 V. Cyclic voltammogram of all complexes appeared six couples. In the case of of $[Ru(diazpy)(bpy)_2]^{2+}$ and $[Ru(diazpy)(phen)_2]^{2+}$, first and the second cathodic peaks were displayed electron reduction of diazpy (Figure 63 and 64). Whereas, they were the fourth and fifth cathodic peaks in $[Ru(diazpy)(azpy)_2]^{2+}$ (Figure 65).

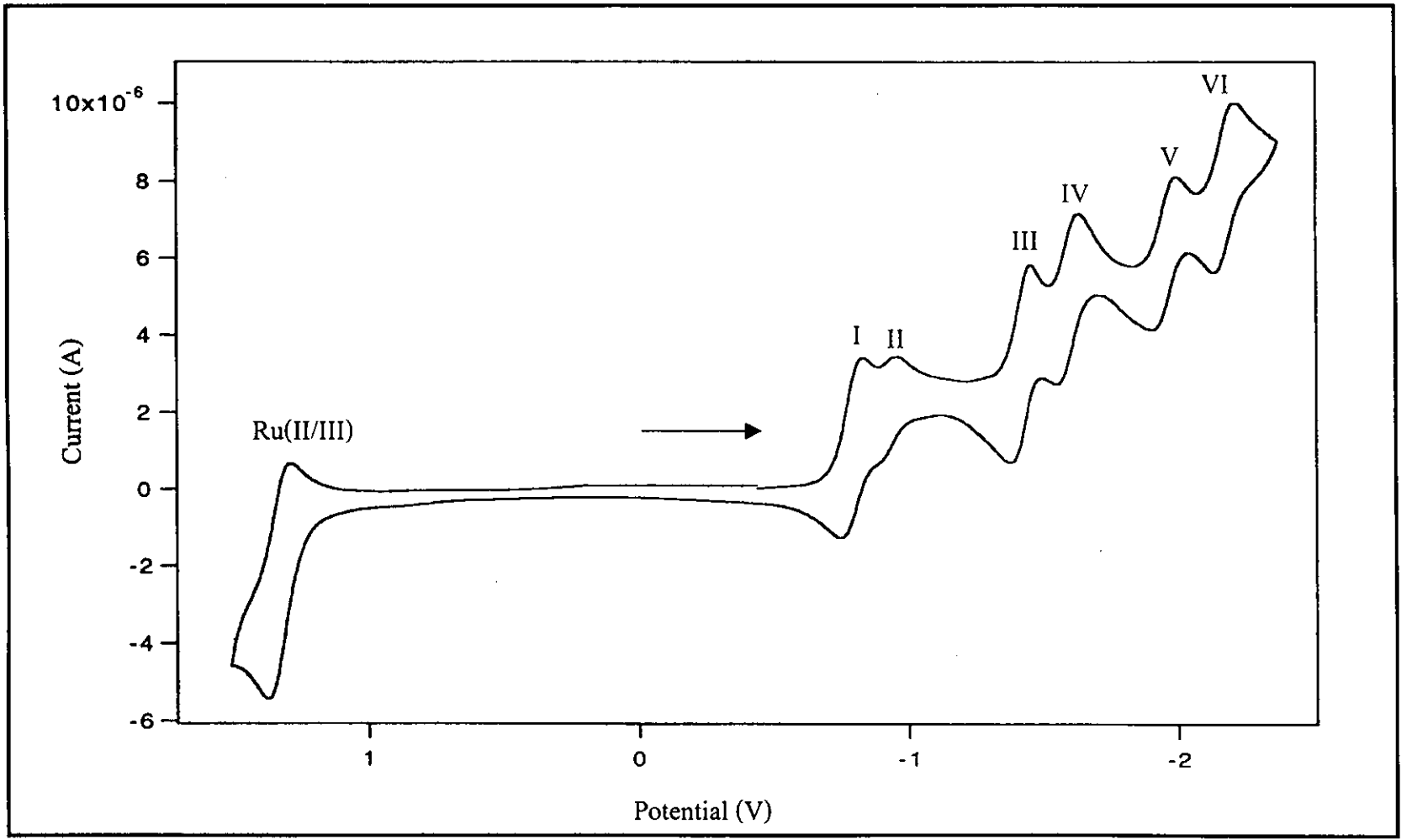

Figure 63 Cyclic voltammogram of $[Ru(diazpy)(bpy)_2]^{2+}$ in 0.1 M TBAH CH_3CN at scan rate 50 mV/s.

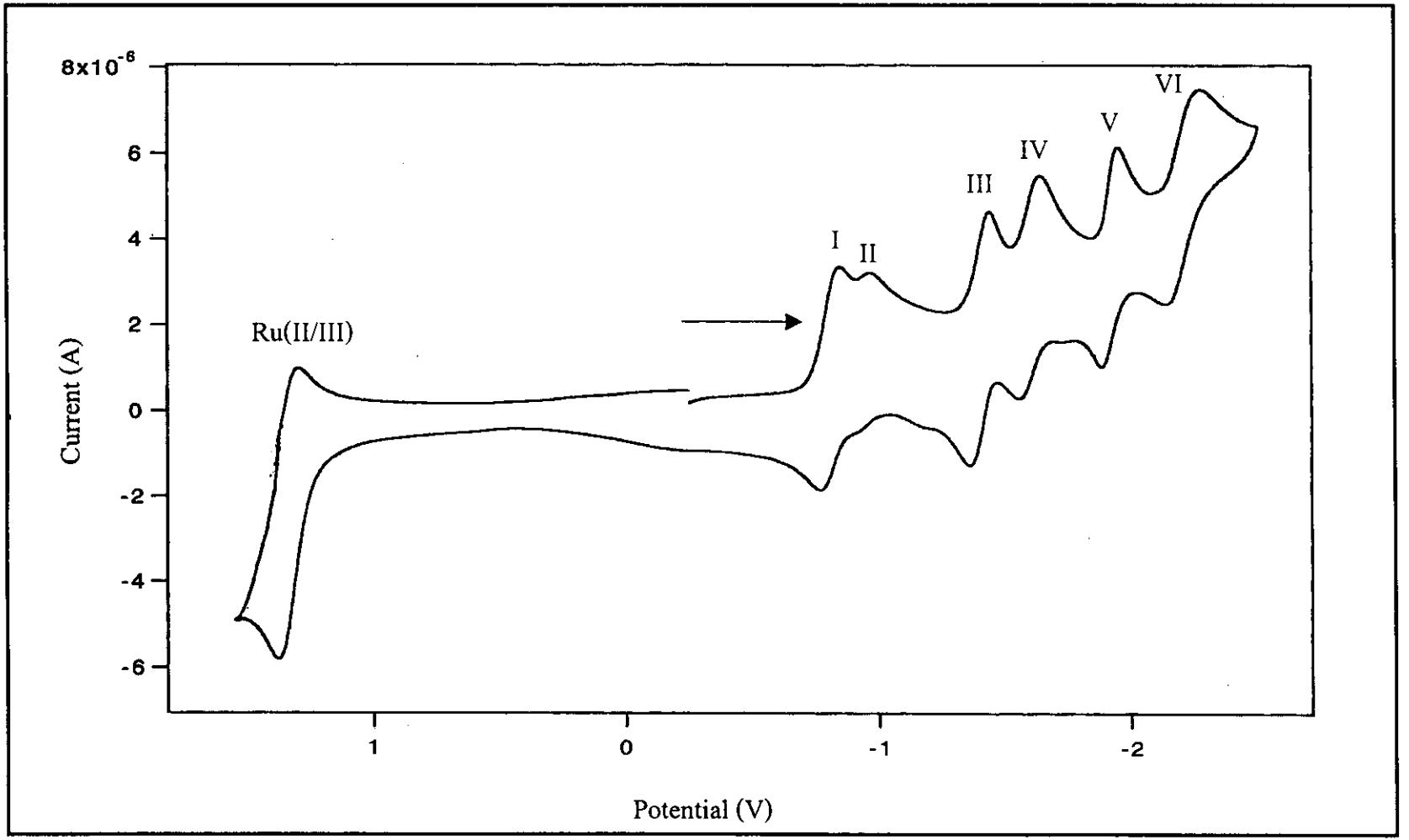

Figure 64 Cyclic voltammogram of $[Ru(diazpy)(phen)_2]^{2+}$ in 0.1 M TBAH CH_3CN at scan rate 50 mV/s.

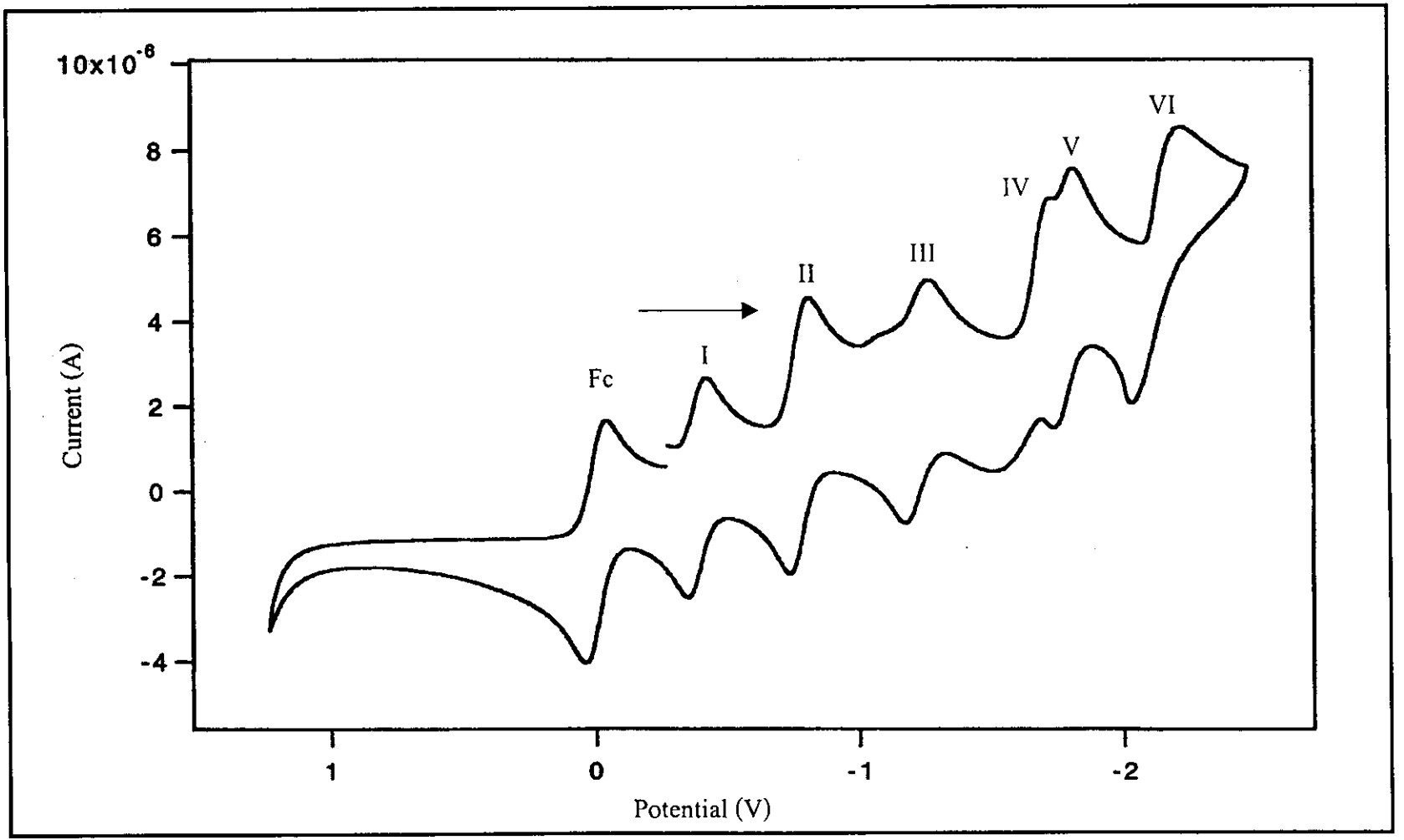

Figure 65 Cyclic voltammogram of $[Ru(diazpy)(azpy)_2]^{2+}$ in 0.1 M TBAH CH_3CN at scan rate 50 mV/s.

3.6.7 X-ray Diffractometer

The X-ray crystallography is the most important technique to identify the geometry of complex. The structure of complex showed six coordination around the ruthenium atom.

X-ray structure of $[Ru(diazpy)(bpy)_2](BF_4)_2$

X-ray quality crystal was obtained by slowly precipitate in mixture solvents EtOH : CH_2Cl_2 at room temperature. The crystal structure of the $[Ru(diazpy)(bpy)_2](BF_4)_2$ complex is shown in Figure 66. The bond lengths and angles within the coordination sphere of the ruthenium ion are listed in Table 29. The coordination sphere around ruthenium was approximately octahedral involving the diazpy bidentate ligand and the two bpy ligands.

Table 29 Crystal and experimental data of the $[Ru(diazpy)(bpy)_2](BF_4)_2$ complex

Empirical formular	$C_{37}H_{29}N_9B_2F_8Ru$
Formular weight	874.37
Crystal system	Triclinic
Space group	P1
Unit cell dimention	$a = 12.255(3), \alpha = 108.05(3)^\circ$
	$b = 12.907(3), \beta = 107.13(3)^\circ$
	$c = 13.236(3), \gamma = 98.66(3)^\circ$

Table 29 (continued)

Volume	1833.5(6) $Å^3$
Z	2
Temperature	293(2) K
Wavelength	0.71073
Density	1.584 mg/m^3
Absorption coefficient	0.511 nm^{-1}
Goodness-of-fit on F2	1.021
Final R indices [$I>2\sigma(I)$]	$R1$ = 0.0560, $wR2$ = 0.1042
R indices (all data)	$R1$ = 0.0745, $wR2$ = 0.1143

Table 30 The selected bond distances (Å) and angles (°) and their estimated standard deviations for the $[Ru(diazpy)(bpy)_2](BF_4)_2$ complex

	Distances		
Ru(1A)-N(1A)	2.109(9)	Ru(1B)-N(1B)	1.993(9)
Ru(1A)-N(2A)	2.081(8)	Ru(1B)-N(2B)	2.046(9)
Ru(1A)-N(3A)	2.092(11)	Ru(1B)-C(3B)	2.059(8)
Ru(1A)-N(4A)	2.092(9)	Ru(1A)-N(4B)	2.125(9)
Ru(1A)-N(5A)	1.910(11)	Ru(1B)-N(5B)	2.007(8)
Ru(1A)-N(7A)	2.060(10)	Ru(1B)-N(7B)	2.093(8)
N(5A)-N(6A)	1.362(13)	N(5B)-N(6B)	1.236(12)
N(8A)-N(9A)	1.287(13)	N(8B)-N(9B)	1.219(11)

Table 30 (continued)

		Angles	
N(1A)-Ru(1A)-N(7A)	169.6(4)	N(1B)-Ru(1B)-N(7B)	104.7(4)
N(2A)-Ru(1A)-N(4A)	167.0(3)	N(2B)-Ru(1B)-N(4B)	90.8(4)
N(3A)-Ru(1A)-N(5A)	174.4(4)	N(3B)-Ru(1B)-N(5B)	94.9(4)
N(1A)-Ru(1A)-N(2A)	79.4(4)	N(1B)-Ru(1B)-N(2B)	78.5(3)
N(3A)-Ru(1A)-N(5A)	79.7(4)	N(3B)-Ru(1B)-N(5B)	75.7(4)
N(5A)-Ru(1A)-N(7A)	77.6(4)	N(5B)-Ru(1B)-N(7B)	73.7(3)

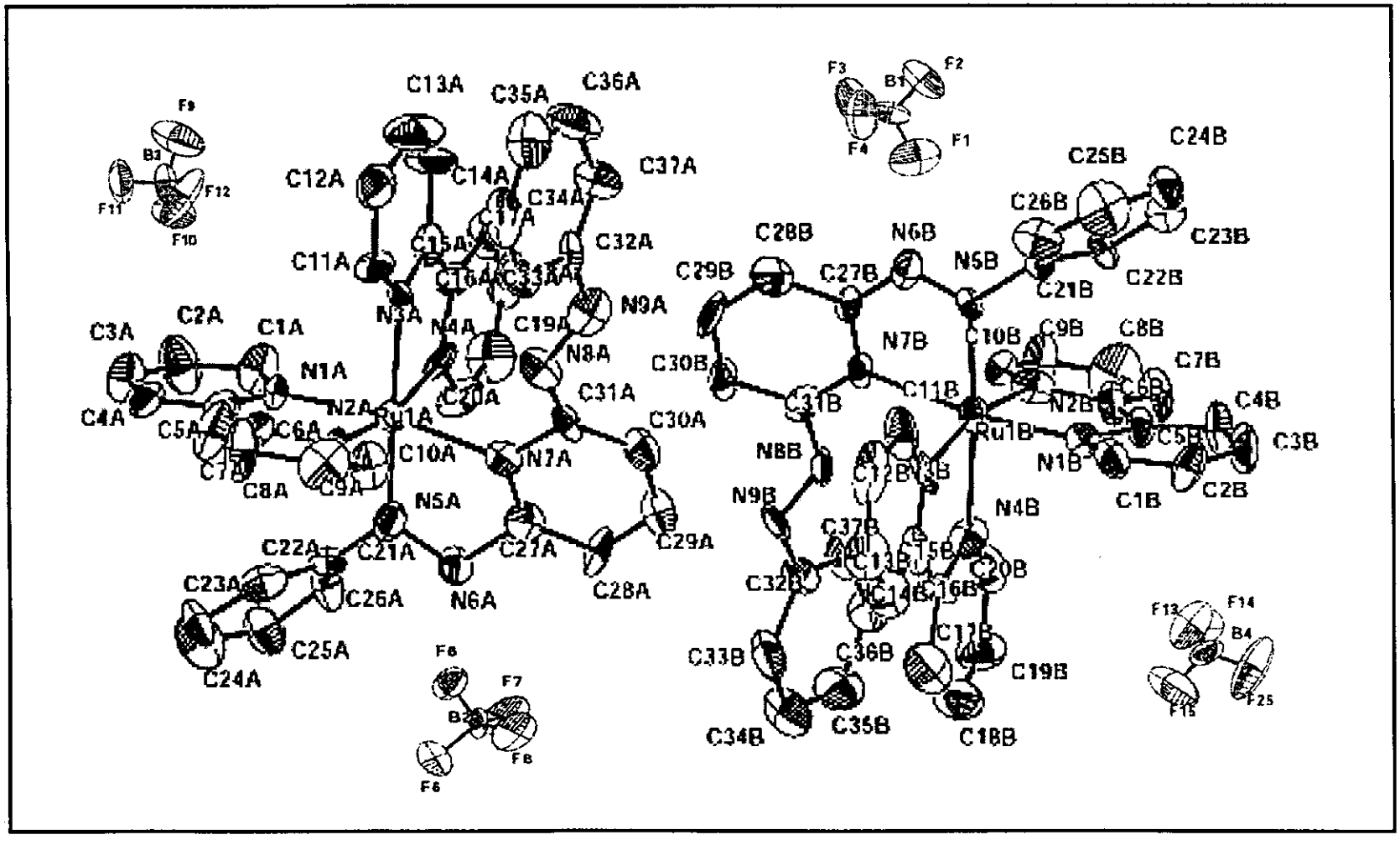

Figure 66 The structure of $[Ru(diazpy)(bpy)_2](BF_4)_2$ (H-atom omitted0.